
Site U1366¹

Expedition 329 Scientists²

Chapter contents

Background and objectives	1
Operations	2
Igneous lithostratigraphy, petrology, alteration, and structural geology	7
Physical properties	8
Paleomagnetism	10
Biogeochemistry	10
Microbiology	14
References	16
Figures	17
Tables	55

Background and objectives

Integrated Ocean Drilling Program (IODP) Site U1366 (proposed Site SPG-2A) was selected as a drilling target because

- Its microbial activities and cell counts were expected to be characteristic of a setting midway between the western gyre edge and the gyre center and
- Its basement age rendered it a reasonable location for testing the extent of basalt alteration and openness to flow in a thinly sedimented region of ancient (~95 Ma) basaltic basement.

The principal objectives at Site U1366 were

- To document the habitats, metabolic activities, genetic composition, and biomass of microbial communities in subsea-floor sediment with very low total activity;
- To test how oceanographic factors (such as surface ocean productivity, sedimentation rate, and distance from shore) control variation in sedimentary habitats, activities, and communities from gyre center to gyre margin;
- To quantify the extent to which these sedimentary microbial communities may be supplied with electron donors by water radiolysis; and
- To assess how basement habitats and potential activities vary with basement age and sediment thickness (from ridge crest to abyssal plain).

Site U1366 (~5129 meters below sea level) is in the western portion of the South Pacific Gyre within a region of abyssal hill topography trending roughly northeast–southwest (065°) (D'Hondt et al., 2010) (Fig. F1). Two populations of abyssal hill topography are present. The larger hills' relief ranges from 300 to 400 m with a spacing of ~20 km. The smaller hills are superimposed on the larger abyssal hills and have a relief of ~50–100 m and a spacing of ~5–6 km. Several small seamounts (2 km wide; 300 m high) are scattered throughout the region. The largest seamount is ~3–4 km south of the coring site. The closest previous drilling site is Deep Sea Drilling Project (DSDP) Leg 91 Site 596, 500 nmi away.

Site U1366 is within magnetic polarity Chron 34n, so the crustal age could range from 84 to 124.6 Ma (Gradstein et al., 2004). Based on tectonic reconstruction of the region by Larson et al. (2002), the crust was accreted along the Pacific-Phoenix spreading

¹Expedition 329 Scientists, 2011. Site U1366. In D'Hondt, S., Inagaki, F., Alvarez Zarikian, C.A., and the Expedition 329 Scientists, *Proc. IODP, 329*: Tokyo (Integrated Ocean Drilling Program Management International, Inc.).
doi:10.2204/iodp.proc.329.104.2011
²Expedition 329 Scientists' addresses.



center at ~95 Ma at ultrafast spreading rates (~90 km/m.y., half rate).

Many geological and geophysical characteristics of the target site were characterized by the 2006/2007 KNOX-02RR survey expedition (D'Hondt et al., 2011) (Figs. F1, F2, F3, F4, F5, F6). The sediment is brown clay capped by manganese nodules (D'Hondt et al., 2009). Manganese oxide and cosmic debris occur throughout the upper 8.2 m of sediment (D'Hondt et al., 2009).

D'Hondt et al. (2009) documented the presence of microbial cells and oxic respiration throughout the uppermost 8.2 m of sediment at Site U1366. Cell concentrations were approximately three orders of magnitude lower than at similar depths in previously drilled marine sediment of other regions. Net respiration was similarly much lower than at previously drilled sites. From extrapolation of dissolved oxygen content in the uppermost 8 m of sediment, Fischer et al. (2009) predicted that dissolved oxygen penetrates the entire sediment column, from seafloor to basement.

Operations

Transit to Site U1366

After a 48.85 h transit from Site U1365, covering 494 nmi and averaging 10.1 kt, the speed was reduced and thrusters and hydrophones were lowered. Speed was less than expected because two of the propulsion motors on the starboard shaft were offline with failed field coils. Dynamic positioning was initiated over Site U1366 at 2215 h on 29 October 2010. The position reference was a combination of GPS signals. No acoustic beacon was deployed, but a beacon remained on standby in the event of loss of GPS satellite coverage. Although automatic input into the dynamic positioning system was not possible, it was possible to manually hold the vessel in position to clear the seafloor with the bottom-hole assembly, if necessary.

All times in this section are given in local ship time unless otherwise noted. For most of the expedition, local time was Universal Time Coordinated -10 h.

Site U1366

Six holes were drilled or cored at this site (Table T1). The first hole was a washdown hole drilled with the center bit in order to establish the sediment depth. The next five holes were cored and drilled with the advanced piston corer (APC) system. Perfluorocarbon tracer (PFT) was continuously injected into the drilling fluid for all coring of Holes U1366B–U1366F. The advanced piston corer temperature tool was not

deployed because the sediment thickness was only ~20 m. APC system recovery for Site U1366 was 100.6%. Extended core barrel (XCB) recovery was 0%. A total of 14 cores were attempted after coring 97.9 m. The total length of core recovered from this site was 96.45 m, for a recovery of 98.5%.

Hole U1366A

Rig floor operations commenced at 2215 h on 29 October 2010. The trip to the seafloor was uneventful. The top drive was picked up, and the drill string was spaced out and spudded at 0815 h. The PFT pump was turned on to distribute PFT evenly throughout the fluid in the drill string. The washdown hole was drilled to determine depth of basement. Mudline was established at 5146.0 meters below rig floor (mbrf) by tagging with the bit. After drilling down, basement was established at 17.8 meters below seafloor (mbsf). The bit was pulled back, clearing the seafloor at 0845 h and ending Hole U1366A.

Hole U1366B

After clearing the seafloor, the center bit was pulled by wireline, the vessel was offset 20 m west, and the drill string was spaced out to spud Hole U1366B. After making up the first APC core barrel, the core barrel was run to bottom on the wireline and Hole U1366B was spudded at 1045 h on 30 October. Seafloor depth was established with a mudline core at 5141.8 mbrf. APC coring continued to 17.2 mbsf. Two cores were taken with a total recovery of 17.31 m (100.6% recovery). After Core 329-U1366B-2H, the bit was tripped back to just above the seafloor, ending Hole U1366B at 1300 h on 30 October.

Hole U1366C

Hole U1366C began at 1300 h when the APC assembly cleared the seafloor after completing Hole U1366B. After offsetting the vessel 20 m north, Hole U1366C was spudded at 1345 h on 30 October and advanced with the APC system to 25 mbsf before encountering basement. Seafloor was established at 5140.5 mbrf. Three cores were taken with a total recovery of 25.42 m (101.7% recovery). The drill string was then tripped to just above the mudline, clearing the seafloor at 1715 h on 30 October and ending Hole U1366C.

Hole U1366D

Hole U1366D began at 1715 h when the APC assembly cleared the seafloor after completing Hole U1366C. After offsetting the vessel 20 m east, Hole U1366D was spudded at 1800 h on 30 October and advanced with the APC system for three cores to

18.9 mbsf, with an 18.86 m recovery (99.8% recovery). Seafloor was established at 5137.1 mbrf. After APC refusal, an XCB system was deployed and advanced 2 m into the formation without any recovery. After the last core, the drill string was tripped to just above the mudline, clearing the seafloor at 2330 h on 30 October and ending Hole U1366D.

Hole U1366E

After clearing the seafloor, the vessel was offset 40 m west and the drill string was spaced out to spud Hole U1366E. After making up the first APC core barrel, the core barrel was run to bottom on the wireline and Hole U1366E was spudded at 0015 h on 31 October. Seafloor depth was established with a mudline core at 5138.8 mbrf. APC coring consisted of a single mudline core to 4.7 mbsf. One core was taken with a total recovery of 4.71 m (100.2% recovery). Core 329-U1366E-1H was recovered with a shattered liner and was not acceptable for microbiology. Hole U1366E ended with the first APC core at 0015 h on 31 October.

Hole U1366F

Hole U1366F began at 0015 h after the mudline core of Hole U1366E was completed. After offsetting the vessel 20 m west, Hole U1366F was spudded at 0130 h on 31 October and advanced with the APC coring system for four cores to 30.1 mbsf with a 30.15 m recovery. Overall recovery in Hole U1366F was 100.2%. After the last core, the drill string was tripped to surface and all drilling equipment was secured at 1815 h on 31 October, ending Hole U1366F and beginning the 1019 nmi transit to the next site.

Lithostratigraphy

The sediment at Site U1366 is primarily clay. The principal components of the clay are smectite and mica-group members, phillipsite (a zeolite), and red-brown to yellow-brown semiopaque oxide (RSO) (see Site U1366 smear slides in “[Core descriptions](#)”; Fig. [F7](#)). Although clay and zeolite abundance rises and falls within the sediment column, they both exhibit overall trends of decreasing abundance with increasing depth. RSO, an iron manganese hydrated material found frequently in the southwestern Pacific (Graham et al., 1997), is the most common constituent of the clay. RSO gives the sediment a range of colors, including dark brown (7.5 Y 3/3, 3/4) to very dark brown (7.5YR 2.5/2, 2.5/3) to black (N2.5), that vary with changes in its abundance.

Subdivisions of the sediment at Site U1366 are based on RSO and zeolite distributions. Unit I includes metalliferous to zeolitic metalliferous pelagic clay.

Subunit IA contains equal portions of RSO, zeolite, and clay minerals. The modal RSO concentration increases in Subunit IB as zeolite abundance decreases proportionately. The upper boundary of Subunit IC is defined by an increase in zeolite, whereas its base coincides with the absence of zeolite. RSO dominates the composition of Unit II and gives this metalliferous clay a distinctly black color.

Lithostratigraphic correlation shows that thickness and composition of units are variable among the five holes cored at Site U1366 (Fig. [F8](#)). The total thickness of Unit I, for example, is 2.6 m thinner in Hole U1366F than it is in the other holes at this site. Correlative sediment has variable composition. For example, manganese nodules found in Subunit IB in Holes U1366C and U1366D are not found in the equivalent sediment of Holes U1366B and U1366F. Similarly, lithic silt beds recovered in Hole U1366F are altogether absent from the other holes. Given these irregularities, the description of units that follows represents a composite stratigraphic section based on observations of cores from all holes at Site U1366.

Description of units

Unit I

Subunit IA

Intervals: 329-U1366B-1H-1, 0 cm, to 1H-CC, 23 cm; 329-U1366C-1H-1, 0 cm, to 2H-1, 150 cm; 329-U1366D-1H-1, 0 cm, to 2H-1, 130 cm; 329-U1366E-1H-1, 0 cm, to 1H-CC, 12 cm; 329-U1366F-1H-1, 0 cm, to 2H-3, 150 cm

Depths: Hole U1366B = 0–7.7 mbsf, Hole U1366C = 0–7.5 mbsf, Hole U1366D = 0–10.7 m, Hole U1366E = 0–4.7 mbsf, Hole U1366F = 0–10.0 mbsf

Lithology: zeolitic metalliferous pelagic clay

Subunit IA is a uniform dark brown (7.5YR 3/3) (Fig. [F9A](#)) that gradually changes to very dark brown. The lower interval is unevenly colored with irregularly shaped areas of interwoven shades of very dark brown (7.5YR 2.5/2 and 7.5YR 2.5/3). The transition to Subunit IB is clearly observed in Holes U1366B and U1366C, partially expressed in Holes U1366D and U1366F, and is not observed in Hole U1366E because that hole was not deep enough to reach the Subunit IA–IB transition.

RSO, zeolite, and clay minerals (Fig. [F7](#)) are found in Subunit IA in abundances of 30%, 30%, and 20%, respectively. The color change noted in the lower part of the subunit corresponds to slightly higher abundance of RSO and a corresponding reduction in zeolite. The RSO forms 30%–40% of the sediment and consists of grains that are rounded to irregularly

shaped and range in size from 1 to 80 μm . X-ray diffraction (XRD) results of representative pelagic clay taken from Subunit IA at interval 329-U1366C-1H-1, 30–32 cm, contain diffraction peaks that correspond to smectite, chlorite, quartz, and phillipsite. The zeolite crystals observed in smear slides are euhedral and prismatic. A majority of the crystals have long axes that are $<20 \mu\text{m}$ (Fig. F10A). Cobble-sized manganese nodules are present at the top of Subunit IA in Holes U1366C, U1366E, and U1366F (Fig. F9A). Smaller nodules were observed at varying depths within Subunit IA in Holes U1366B and U1366C.

Consolidation of Subunit IA sediment transitions from very poorly consolidated near the mudline to poorly consolidated at the base of the subunit. Most samples of this unit are sticky.

The upper two-thirds of Subunit IA are homogeneous and without bedding features. Burrows are evident throughout the lower 40 cm of the subunit in Holes U1366B and U1366D. Several individual burrows were noted for their large diameter (1 cm) and length (10 cm).

Subunit IB

Intervals: 329-U1366B-2H-1, 0 cm, to 2H-2, 30–70 cm; 329-U1366C-2H-2, 0 cm, to 2H-4, 68–94 cm; 329-U1366D-2H-1, 130 cm, to 2H-3, 130 cm; 329-U1366F-2H-4, 0 cm, to 2H-5, 54–90 cm

Depths: Hole U1366B = 7.7 to 9.5–9.9 mbsf, Hole U1366C = 7.5 to 11.2–11.4 mbsf, Hole U1366D = 10.7–13.7 mbsf, Hole U1366F = 10.0 to 12.0–12.4 mbsf

Lithology: metalliferous pelagic clay

Subunit IB is exclusively dark brown (7.5YR 3/3) in Holes U1366B, U1366C, and U1366F. In Hole U1366D, the dark brown sediment includes an intervening very thick (1.5 m) bed of very dark brown (7.5YR 2.5/2) clay. Within each interval, the color is nearly uniform with only subtle variations that are detectable on the Section Half Multisensor Logger (SHMSL) spectrometric imaging of core section halves (see “Physical properties”).

Zeolite is present in very low abundance or altogether absent in Subunit IB (Fig. F7). Although the interval is thin (2–4 m), proportions of clays and RSO in the interval fluctuate between ratios of 20%/80% and 35%/62%. In Hole U1366D, RSO concentration is sustained at 75%–80% and forms a very thick (1 m) bed of very dark brown clay within Subunit IB. Manganese nodules are present in Holes U1366C and U1366D.

Consolidation in the subunit is uniformly moderately indurated (firm).

The majority of Subunit IB is homogeneous and lacks any discernible structure (Figs. F9B, F10B). Occasional burrows are visible in the lowermost meter of Subunit IB in Holes U1366C and U1366F. Faint mottling occurs in the stratigraphically equivalent interval in Hole U1366D.

Subunit IC

Intervals: 329-U1366B-2H-2, 30–70 cm, to 2H-CC, 23 cm; 329-U1366C-2H-4, 68–94 cm, to 3H-1, 25 cm; 329-U1365D-2H-3, 130 cm, to 2H-CC, 20 cm; 329-U1365F-2H-5, 54–90 cm, to 2H-CC, 10 cm

Depths: Hole U1366B = 9.5–9.9 to 17.3 mbsf, Hole U1366C = 11.2–11.4 to 15.7 mbsf, Hole U1366D = 13.7–18.8 mbsf, Hole U1366F = 12.0–12.4 to 14.0 mbsf

Lithology: zeolitic metalliferous pelagic clay

Subunit IC has two distinctly colored intervals. The sediment in the uppermost 1 m (Hole U1366F) to 6 m (Hole U1366B) of the subunit is uniform very dark brown (7.5YR 2.5/2) with occasional flecks of very pale brown (10YR 8/4). Below this interval, the very dark brown sediment is punctuated by very pale brown and red-brown laminations, diffuse beds, and rounded to subangular lenses. Where the pale brown sediment blends with the dark brown sediment, the resulting color is brown (7.5YR 5/4) (Fig. F9C; see core photograph of Section 329-U1366B-2H-5 in “Core descriptions”). Other brown beds appear in granular, thin beds of varying thickness in Holes U1366B–U1366D.

The very dark brown intervals of Subunit IC consist of RSO mixed with lesser amounts of smectite-group clay and very small amounts of zeolite (Fig. F7). The abundance of RSO varies without an obvious trend between 25% and 80% of the grains observed in smear slides. XRD analysis of a sample from Section 329-U1366C-2H-6 suggests that (1) the smectite minerals include montmorillonite, (2) the zeolite crystals are likely phillipsite, and (3) fluorapatite could be present. Zeolite is visible in smear slides and consists of small bladed crystals that are present in small amounts ($<5\%$) in the very dark brown clay. The crystals are slightly more abundant (15%) in the very pale brown laminations. Among Holes U1366B–U1366D, 2–5 thin beds (1–2 cm) of porcellaneous clay were observed. A single, very thin (1 cm) bed of chert was encountered in the bottom of Hole U1366D. One manganese nodule was found in the middle of Subunit IC in Core 329-U1366B-3H. A 1.5 cm long ichthyolith was found in Sample 329-U1366C-2H-CC (Fig. F11).

The entire interval is moderately well indurated. The porcellaneous clay is marked by granular disturbances in the clay that are attributable to its brittle-

ness. The chert is very well indurated and breaks along flattened blades with conchoidal fractures.

Subunit IC comprises two intervals with distinctive structure. The uppermost 1–6 m of clay is homogeneous and faintly mottled. Burrowed, very pale brown to red-brown laminations are present in the lower interval. The frequency of the laminations and beds is ~3–5 per 10 cm of core (e.g., see photographs of Section 329-U1366B-2H-7 in “[Core descriptions](#)”). Porcellaneous clay forms as many as five thin beds (3–5 cm) in Hole U1366B and as few as two in Hole U1366C.

Unit II

Interval: 329-U1366F-3H-1, 0 cm, to 4H-5, 116 cm

Depth: Hole U1366F = 14.0–30.0 mbsf

Lithology: metalliferous clay

Unit II consists of very dark sediment intercalated with laminations and thin beds of a wide variety of colors. The dominant colors of the unit are brown-black (7.5YR 2.5/1, 2.5/2, and 2.5/3) and black (5Y 2.5/1 and GLEY1 2.5/N). Individual beds and laminations have various colors that were interpreted as shades of white (7.5YR 8/1), pale yellow (7Y 8/4), olive-gray (5Y 4/2), brown (7.5YR 4/6), very pale brown (10YR 8/4), and reddish brown (2.5YR 3/4).

Smear slide analyses indicate Unit II is predominantly composed of RSO (Figs. [F7](#), [F10C](#), [F10D](#)). Most intervals contain 80%–100% RSO. The unit also contains at least one thick (10 cm) bed of ~60% smectite and numerous other thinner beds of porcellaneous clay, lithic grains, and volcanic ash/ altered ash. Zeolite minerals are absent. Seven thin (<5 cm) beds of porcellaneous clay were recovered from the upper half of Unit II. Three distinctive ash/ altered ash layers are found in Sections 329-U1366F-3H-4 and 3H-5. The upper layer was partially removed by whole-round sampling prior to sedimentary description. The upper layer is >10 cm thick and consists of brown and black clay. No distinguishing crystals were observed during smear slide analysis. The second ash/ altered ash layer contains a core of very soft white clay surrounded by olive-green clay (Fig. [F9D](#)). The third bed is 4 cm thick and similar to the overlying white and olive-green ash layer. Olivine and feldspar crystals were identified in lithic silt and sand found in Sections 329-U1366F-3H-1, 3H-7, and 4H-5. Both silt beds also contain numerous radiolarians (Fig. [F10D](#)).

The brown- and red-black metalliferous clays that make up most of Unit II are moderately well consolidated (i.e., stiff clay). Porcellaneous clay beds are

similarly consolidated and break into granules when cores are sectioned and split. Ash/ altered ash layers are soft but consolidated. Lithic silt and sand layers are made of loose grains.

In contrast to Unit I, Unit II contains numerous bedding features. Very pale brown layers are laminated to very thinly bedded and commonly show gaps, offsets, and other irregularities associated with burrows. Porcellaneous clay forms beds that are 3–10 cm thick. Lower in the section, several ash/ altered ash layers are thickly (10+ cm) bedded. The lithic silt and sand are thin, 1 and 3 cm, respectively, with distinct upper and lower contacts.

Sediment/Basalt contact

Because of coring difficulties in Holes U1366B–U1366D, components of the sediment/basalt contact were only recovered in the lowermost core of Hole U1366F. The basalt and obsidian that were recovered consist of numerous small pieces (2 cm maximum diameter) that were packed tightly into the upper 7 cm of the core catcher of Core 329-U1366F-4H. Sediment was recovered in the lowermost part of Core 5H. Although probably representational of the basalt and sediment composition, this form of core recovery precludes our ability to observe structural relationships between the sediment and basalt. A description of the volcanic rocks is provided in “[Igneous lithostratigraphy, petrology, alteration, and structural geology](#).” A description of the interface interval is provided below.

The lowermost sediment interval at Site U1366 consists of lithic sand, nodular clay, and massive red clay. The basal interval (329-U1366F-4H-5, 113–116 cm) is black (5YR 2.5/1) clayey lithic sand that includes a firm, large (2 cm × 3 cm) nodule of dark gray (GLEY 1 3/N) clay (Fig. [F9E](#)). The composition of the sand is a mix of lithic fragments (olivine and plagioclase feldspar) and clay. Shipboard scientists concluded that the large clay nodule imbedded in the sand is made of altered basalt. The interval overlying the lithic sand contains 10.5–14.5 cm of friable, very dusky red and reddish black clay nodules. The uncertainty in thickness of this interval is due to whole-round sampling of the core sections prior to sedimentary description. Above the sampled zone, the interface is reddish brown (2.5YR 4/4) metalliferous clay. XRD analysis of the clay indicates the presence of smectite and hematite (Fig. [F12](#)). The upper limit of the red clay is an abrupt transition to black metalliferous clay at interval 329-U1366F-4H-5, 53 cm, ~63 cm above the basal lithic sand.

Discussion

Sediment composition and texture

Smear slide and XRD analyses identify smectite, mica, zeolite, and RSO as the principal components of the zeolitic, metalliferous, and pelagic clay at Site U1366. Overall, the proportion of zeolite in the sediment decreases with depth. Conversely, the portions of RSO increase with depth. In the 10 m of sediment that overlie the basement, RSO becomes the dominant (occasionally exclusive) lithologic component. These trends define the two lithologic units found at Site U1366: Unit I contains RSO, clay, and zeolite and Unit II contains RSO and clay.

Within the broad trends of changing principal components outlined above, several of the less abundant lithologies help refine the description of sedimentary units and provide insight into the depositional history of Site U1366. These features are described below.

Porcellaneous clay

The porcellaneous intervals at Site U1366 are very poorly developed. Although radiolarians occur throughout the upper half of Unit II, their volume is relatively small compared to the RSO and clay fractions of the sediment. The porcellaneous beds retain the dark color of surrounding metalliferous clay and can be easily disaggregated into granules. Thus, we identify this sediment as “porcellaneous clay” rather than by the name “porcellanite,” which carries connotations of being a well-indurated microcrystalline rock with dull luster (Keene, 1975). Sediment at the site does include chert; however, the only chert recovered during coring was one thin (<5 cm) bed in Hole U1366C. The high concentration of clay likely precluded the formation of porcellanite and chert at this site despite the numerous occurrences of radiolarians in the sediment (Kastner et al., 1977).

Volcanic ash

The ash/altered ash layers at Site U1366 show variable thicknesses and compositions. Most of these ash layers are in the lower half of Unit I and upper half of Unit II. They consist of laminated to very thinly bedded, uniformly very pale brown zeolitic clay layers. Using sediment samples from DSDP Site 597, Kastner (1986) identified these layers as altered volcanic ash layers. Although her description of the altered volcanic ash at Site 597 is similar to our observations at Site U1366, we prefer to call the altered volcanic ash by the name ash/altered ash because the thorough studies needed to assess alteration of the ash were beyond the scope of our shipboard lithologic observations.

In the lower half of Unit II, three ash/altered ash layers differ from those found in the overlying sediment. The first of these, found at interval 329-U1366F-3H-4, 40–50 cm, is brown and may have received ash from the same source as the numerous overlying ash/altered ash layers. However, this bed is at least five times thicker than any of the other very pale brown layers found at Site U1366. The lower two ash/altered ash layers (located at intervals 329-U1366F-3H-4, 96–103 cm, and 3H-5, 15–19 cm) are also thick (7 and 4 cm, respectively) and possess unique compositions as indicated by their white, pale yellow, and olive-green colors. The small size of the crystals in these ash layers makes them petrographically indeterminate. However, the unique colors of the ash layers imply they (currently) possess chemical constituencies that differ from all other ash/altered ash recovered at Site U1366. Because these layers in Unit II are the oldest and reside in sediment that is similar to numerous overlying very pale brown altered ashes, it is possible that the older ashes originated from a different volcanic source than the younger ash or that ash composition from a single source evolved over time.

Lithic silt and sand

The lithic silt beds and sand recovered in Cores 329-U1366F-3H and 4H suggest that weathering, erosion, and lateral sediment transport impacted Site U1366. Because the sand contains numerous olivine and plagioclase grains and directly overlies basement rocks, it is likely a product of basaltic seafloor weathering and short-distance sediment transport.

The origin of the lithic silt is less clear. The composition, including the presence of olivine and plagioclase grains, also implies a basaltic source. However, the silt beds are separated from the basement rocks by 10 m of metalliferous clay. Given the mean rate of sediment deposition at this site (D'Hondt et al., 2009), the silt was deposited millions of years after the basement was formed. Exposed basalt near the ridge could still be the source, however, because spreading rates along the East Pacific Ridge were generally slow between 60 and 70 Ma (Smith and Sandwell, 1997) and Site U1366 was likely within several hundred kilometers of the ridge when the silt beds were deposited. Transport of the silt grains to Site U1366 by low-density gravity flow is suspected but cannot be substantiated because the silt beds lack indicators of depositional processes (e.g., graded bedding, cross bedding, flute marks, and so on). Additional information regarding the areal distribution of the silt or paleogeography of Site U1366 is needed before the origin of the silt can be accurately interpreted.

Sedimentary structures

Sedimentary structures at Site U1366 define a continuum from thoroughly massive to thickly bedded sediment. The majority of the pelagic clay in Subunits IA and IB lacks any discernible structure. We attribute this to the uniformity of sediment composition because small burrows (2–4 mm diameter and 1–2 cm length) are evident at the compositional boundary between Subunits IA and IB. The occurrence of manganese nodules in the upper 15 m of core and RSO throughout the sedimentary succession at Site U1366 implies that sedimentation rates at Site U1366 were very low for a protracted period of time (Hein et al., 1979). Therefore, the lack of sedimentary structures in Subunits IA and IB may have resulted from prolonged exposure of uniform sediment to burrowing organisms.

The presence of massive and bedded sediment in Subunit IC provides further insight into biologic activity at Site U1366. The massive sediment found in Subunits IA and IC transitions to bedding in Subunit IC through a gradual transition zone of 10–30 cm. Through this short interval, uniform very dark brown pelagic clay grades into dark brown clay with occasional fine flecks of very pale brown sediment and then into dark brown clay with thin beds of very pale brown sediment (see core photographs of Cores 329-U1366B-1H and U1366B-2H in “[Core descriptions](#)”). The very pale sediment comprising the flecks and thin beds is interpreted to be the ash/alterated ash lithology previously described. Burrowing impacted the laminations in the lower part of Subunit IC and in the upper half of Unit II; however, the disturbance of this sediment was incomplete and numerous beds were retained in the developing strata. The loss of bedding features in the upper part of Subunit IC could correspond to an increase in biologic activity or a marked decrease in sediment accumulation rates.

Bedding is absent below the porcellaneous clay layers in Unit II. Although the massive texture of this sediment could result from bioturbation, it could be a primary feature of the sediment; 70%–100% of the sediment is RSO. Consequently, the lack of bedding in Unit II could have resulted from active burrowing through sediment that possesses insufficient contrast to record the biologic activity or it could have resulted from deposition of homogeneous sediment in an environment free of active burrowing.

Interhole correlation

- Lithostratigraphic correlation among the five APC holes at Site U1366 shows differences between the units and subunits of Site U1366.

Several of the differences are artificial, created by coring operations. They include

- Coring operations inadvertently missed 0.8 m of Subunit IA between Core 329-U1366C-1H and 2H,
- The lower 9.2 m of Core 329-U1366C-3H is flow-in and not in situ sediment, and
- Whole-round sampling created a large number of gaps in Holes U1366D and U1366F that masked unit boundaries and some beds.

Despite these challenges, we created a tentative correlation of lithostratigraphic units among the holes of Site U1366 (Fig. F8). Noteworthy observations illustrated by the correlation include

- Subunit IA thickness varies by as much as 2.6 m;
- Subunit IB varies in thickness by ~0.5 m and contains alternating composition that is not observed in the other holes;
- Manganese nodules are not evenly distributed by unit or depth; and
- Porcellaneous clay beds occur in Subunit IC in Holes U1366B–U1366D but in Unit II in Hole U1366F. This difference is an artifact of our lithostratigraphic classification system. Because the clay that envelopes the porcellaneous beds in Holes U1366B–U1366D is zeolitic, whereas the clay that over and underlies the beds in Hole U1366F is metalliferous, the beds are assigned to different units. However, given the short distances that separate holes at Site U1366, the porcellaneous beds are likely continuous across the site.

Igneous lithostratigraphy, petrology, alteration, and structural geology

Fragmented pieces of altered basalt were found in sandy sediment at the base of Core 329-U1366F-4H (Fig. F13). The small (<5 mm to 2 cm diameter) fragments are 60%–100% clay minerals that disintegrate when handled. Two fragments, one slightly less altered to clay (interval 329-U1366F-4H-5, 114–116 cm) and one nearly totally altered, were described. A thin section of the totally altered Sample 329-U1366F-4H-5, 110–111 cm, was made.

Based on remnant primary igneous features, Sample 329-U1366F-4H-5, 114–116 cm, was cryptocrystalline and aphyric with clinopyroxene and plagioclase making the bulk of the groundmass. Crystal size fines toward the edges, implying that the sample was a chilled margin. However, intensive alteration near

the margin replaced the primary mineralogy, so only alteration rinds remain. The presence of chilled margins and intense alteration suggests that the rock represented a flow top. Alteration rinds on the edges of the basalt fragments are very similar to the lithic sand that hosts the fragment, suggesting that the sand may be basaltic in origin.

Thin section observations of Sample 329-U1366F-4H-5, 110–111 cm, indicate that the basaltic fragments are nearly completely altered to clay minerals, with only a few remnant plagioclase and tiny (<0.05 mm) clinopyroxene crystals visible. Only skeletal primary textural features remain, implying that the rock was subophitic. No phenocrysts or pseudomorphs of phenocrysts were observed. Alteration is characterized by near-complete pale to dark brown replacement of the groundmass (Fig. F13). Alteration includes saponite (55%), iddingsite (35%), iron oxyhydroxides (3%), and minor secondary Fe-Ti oxides, possibly titanomagnetite (1%). No vesicles or veins are present.

Physical properties

At Site U1366, physical property measurements were made to provide basic information for characterizing lithologic units. After sediment cores reached thermal equilibrium with ambient temperature at ~20°C, gamma ray attenuation (GRA) density, magnetic susceptibility, and *P*-wave velocity were measured using the Whole-Round Multisensor Logger (WRMSL) on whole-round core sections. After WRMSL scanning, the whole-round sections were logged for natural gamma radiation (NGR). Thermal conductivity was measured using the full-space method on sediment cores. Discrete *P*-wave measurements were made on split sediment cores using the Section Half Measurement Gantry. Moisture and density (MAD) were measured on discrete subsamples collected from the working halves of the split sediment cores. Discrete measurements of electrical resistivity were made on the split sediment sections to calculate formation factor. The Section Half Image Logger and SHMSL were used to collect images and color reflectance of the split surfaces of the archive-half cores. Six holes were cored, but only Holes U1366B–U1366D and U1366F were relatively complete. Hole U1366B was the most complete for physical property logging. These holes have not been correlated and offsets exist.

Density and porosity

Bulk density values at Site U1366 were determined from both GRA measurements on whole cores and mass/volume measurements on discrete samples

from the working halves of split cores (see “[Physical properties](#)” in the “Methods” chapter [Expedition 329 Scientists, 2011a]). A total of 17 discrete samples were analyzed for MAD, 6 samples from Hole U1366B, 8 samples from Hole U1366B, 4 samples from Hole U1366C, 2 samples from Hole U1366D, 1 sample from Hole U1366E, and 2 samples from Hole U1366F.

In general, wet bulk density values determined from whole-round GRA density measurements and measurements from discrete samples agree well (Fig. F14A). Wet bulk density discrete samples have an average value and standard deviation of 1.26 and 0.10 g/cm³, respectively. GRA measurements of bulk density have an average and standard deviation of 1.02 and 0.56 g/cm³, respectively.

Measurements of grain density were determined from mass/volume measurements on discrete samples (Fig. F14B). The mean and standard deviation of grain density is 2.46 and 0.62 g/cm³, respectively. No depth-dependent variation is observed.

Measurements of porosity (see “[Physical properties](#)” in the “Methods” chapter [Expedition 329 Scientists, 2011a]) were determined from mass/volume measurements on discrete samples (Fig. F14C). The mean and standard deviation porosity is 83% and 4%, respectively. Below ~20 mbsf (lithologic Unit II in Hole U1366F) porosity is >85%.

Magnetic susceptibility

Volumetric magnetic susceptibilities were measured using the WRMSL, and point measurements were made on the SHMSL for all recovered cores at Site U1366. Uncorrected values of magnetic susceptibility are presented for Holes U1366B–U1366D and U1366F (Fig. F15). The spatial resolution of the WRMSL magnetic susceptibility loop is ~5 cm, and the observed “ringing” of values in Holes U1366D and U1366F is due to edge effects. Measured whole rounds from those holes were generally 10 cm long as a result of whole-round sampling prior to WRMSL measurements.

Natural gamma radiation

NGR results are reported in counts per second (cps) (Fig. F16). NGR counting intervals were ~1 h per whole-core interval, and NGR counts should be reliable. The tops of Holes U1366C and U1366F show high NGR counts at 0 mbsf (Figs. F16B, F16D), consistent with sampling an enriched concentration of radioactive elements at the sediment/water interface. The absence of an NGR peak in Hole U1366B (Fig. F16A) suggests that the mudline was not sampled. This peak is absent from the record of Hole U1366D

(Fig. F16C) because a whole-round sample spanning 0 to 10 cm below seafloor of Core 329-U1366D-1H was removed and refrigerated to provide an intact seafloor manganese nodule for microbiological and mineralogical study.

NGR counts are a maximum at the sediment/water interface and decrease with depth (Fig. F16). Distinct peaks that are particularly conspicuous in Hole U1366B are associated with manganese nodules. To quantify the concentrations of uranium, thorium, and potassium in these nodules, the nodules were removed from the cores and their NGR counts were measured. Concentrations of uranium, thorium, and potassium were estimated using a Monte Carlo inversion. Potassium concentration is 0.2–0.3 wt% and the Th/U ratios are >5 for all nodules measured (Table T2). These concentrations are compared with uranium and thorium concentrations in the uppermost section of Hole U1366E. Figure F17 shows that although the sediment/water interface is enriched in thorium, the NGR peak at the seafloor is primarily caused by uranium. Further, the uranium content of the nodule does not contribute significantly to the seafloor peak. In contrast to uranium, the nodule is enriched in thorium relative to the surrounding sediment. Deeper in the section, away from the nodule, sediment is enriched in thorium relative to uranium.

In Hole U1366C, NGR counts in lithologic Unit II are featureless, consistent with core disturbance (Fig. F16). The spatial resolution of NGR is ~ 12 cm, and the observed ringing of values in Holes U1366D and U1366E is due to by edge effects caused by whole-round sampling prior to WRMSL and NGR measurements. Measured whole rounds from these holes are generally only 10 cm in length.

P-wave velocity

Measurements of *P*-wave velocity at Site U1366 were determined from measurements on sediment whole cores and mass/volume measurements on discrete samples from the working halves of sediment split cores (see “Physical properties” in the “Methods” chapter [Expedition 329 Scientists, 2011a]). In general, discrete measurements are somewhat higher than whole-core measurements; this difference is attributed to incomplete saturation of the sediment (Fig. F18). The mean value is 1520 m/s (close to the compressional velocity of water) (Fig. F18B). In Hole U1366C, there is a slight shift to higher values in lithologic Unit II relative to Unit I, but this is likely due to core disturbance that was observed below ~ 15 mbsf. In Holes U1366D and U1366F, the greater apparent scatter is an artifact caused by edge effects, as

these measurements were made after whole-round sampling for biogeochemistry and microbiology.

Formation factor

Measurements of electrical conductivity were measured on working halves of the split sediment cores in Holes U1366C and U1366F. Measurements in Hole U1366C were made at a nominal interval of 10 cm. Because of clear evidence of core disturbance below ~ 15 mbsf in Hole U1366C, measurements were not made below this depth in this hole. Below this depth, measurements were made on working halves of split cores from Hole U1366F but with wider measurement spacing because of prior whole-round sampling. For each measurement, the temperature of the section was also noted. Surface seawater was used as a standard and measured at least twice per section (Table T3), normally prior to making measurements for that section and then around the 75 cm offset of each section. These measurements were used to compute drift (Fig. F19). The temperature dependence of electrical conductivity was corrected; all reported measurements correspond to a temperature of 20°C. Electrical conductivity measurements were transformed to a dimensionless formation factor by dividing the measurements for drift (Table T4). At depths less than ~ 15 mbsf, the formation factor in Hole U1366C increases with depth (Fig. F20). In Hole U1366F, the formation factor decreases from ~ 15 to 23 mbsf. This pattern inversely mimics the change in observed porosity (Fig. F14).

Thermal conductivity

Thermal conductivity measurements were conducted on sediment whole-round cores using the needle-probe method. Many of the needle-probe measurements on sediment are considered unreliable because temperature-time series of these measurements indicate that the measurements caused fluid to convect within the samples. Convection leads to unreasonably low estimates of thermal conductivity by causing the thermal response to heating to depart from the theoretical prediction. However, a subset of values >0.65 W/(m·K) are considered reliable. These values show similar magnitude and scatter to values determined from a piston core collected during the KNOX-02RR site survey (Fig. F21) (R. Harris, unpubl. data). The mean and standard deviation of these values are 0.7 and 0.1 W/(m·K), respectively.

Color spectrometry

Results from measurement of color reflectance are presented in Figures F22, F23, and F24. L^* values are

~40, with some clusters of higher values at ~240. The majority of a^* and b^* values are ~0 and 15, respectively. Both variables decrease slightly with depth. Color spectrometry values are relatively consistent across unit boundaries.

Paleomagnetism

At Site U1366, we measured natural remanent magnetization (NRM) of all archive-half sections from Holes U1366B–U1366F using the three-axis cryogenic magnetometer at 2.5 cm intervals before and after alternating-field demagnetization. The archive-half sections were demagnetized by alternating fields of 10 and 20 mT. The present-day normal field in this region, as expected from the geocentric axial dipole model at Site U1366, has a negative inclination (approximately -44.4°), so positive remanence inclinations indicate reversed polarity. Data from Holes U1366D and U1366F provide only a partial record because whole-round samples were taken for geochemical and microbiological analyses. From Hole U1366C, 18 discrete sediment samples (7 cm³ cubes) were additionally taken at an interval of one per section from the working halves, and compatibility of magnetization between archive half and working half was analyzed. Of these discrete samples, 12 were measured for NRM after demagnetization at peak fields of 10 mT and 20 mT using the pass-through magnetometer. The primary objective of the shipboard measurements for Site U1366 was to provide chronostratigraphic constraint by determining magnetic polarity stratigraphy. During coring operations at Site U1366, neither nonmagnetic core barrels nor the Flexit core orientation tool were used because of the shallow drilling depth of the sediment column (see “[Operations](#)”).

Results

Paleomagnetic data for Holes U1366B–U1366F are presented in Figures [F25](#), [F26](#), [F27](#), [F28](#), and [F29](#), together with the whole-core susceptibility data measured on the WRMSL. Magnetization directions are not interpretable throughout most of the Site U1366 cores, possibly because of a magnetic overprint acquired during coring (high negative inclination), viscous remanent magnetization, or diagenetic changes in the sediment. In addition, manganese nodules often hamper recognition of paleomagnetic events in the uppermost several meters of sediment (see “[Lithostratigraphy](#)”).

In Hole U1366B, the records of magnetic inclination and declination show polarity changes from 1.5 to

7.5 mbsf (Fig. [F25](#)). However, it is difficult to assign this record to any portion of the polarity timescale because

- Similar reversal records are not clearly identified in the other holes of Site U1366,
- This record does not clearly correspond to any specific portion of the polarity timescale,
- No independent shipboard evidence of age can be used to constrain polarity assignments, and
- The NRM record from 12 discrete samples from Hole U1366C significantly deviates from the half-core record at multiple horizons (Fig. [F26](#)).

Given the difficulty in determining sediment age by shipboard paleomagnetic studies, chronostratigraphy for Site U1366 must be determined by postexpedition studies, perhaps using other chronostratigraphic tools.

Biogeochemistry

The biogeochemistry program at Site U1366 continued to focus on samples for chemical analysis of

- Interstitial water,
- Solid carbon- and nitrogen-containing phases, and
- Gas phases of biogeochemical relevance to the cruise objectives.

Sixty-six interstitial water samples were collected by whole-round squeezing and 66 were collected by Rhizon samplers (for NO₃ analyses). Dissolved oxygen was measured using electrode and optode techniques (296 total measurements). Twenty-three samples were collected for methane quantification, 66 samples for hydrogen analyses, and 35 for solid organic phase analyses. Six interstitial water samples were also collected by whole-round squeezing for shore-based ¹⁴C analysis.

Because of the very thin sediment cover (25–30 m; see “[Lithostratigraphy](#)”) and because of the difficulty in drilling unconsolidated sediment containing several chert layers, we analyzed sediment from Hole U1366C (for dissolved O₂) and Holes U1366D and U1366F (all other measurements) to ensure adequate coverage of all sediment depths. Accordingly, some of the following discussion addresses interhole correlation and interpretations of hole quality (e.g., potential for flow-in to have occurred through certain depths). We also compare interstitial water data from cores that were stored for lengthy periods of time (in some cases >12 h) prior to extracting the interstitial water to data from cores that were stored for only few hours prior to squeezing or taking Rhizon samples.

Dissolved oxygen

Measurements of dissolved oxygen (O_2) using optode and electrode methods were made separately or in combination on Holes U1366B, U1366C, U1366D, and U1366F. Optode measurements of dissolved oxygen were made (after sampling in the core refrigerator on the Hold Deck) on intact 1.5 m core sections from Cores 329-U1366C-1H through 3H and 329-U1366F-4H and on 20–70 cm long whole-round sections from Cores 329-U1366F-1H through 3H. With the exception of Sections 329-U1366F-4H-4 and 4H-5, in which higher resolution optode measurements were made (see below), optode determinations of oxygen concentration were obtained at 25–50 cm intervals. Electrode measurements, using two individually calibrated electrode/picoammeter setups, were performed on 1.5 m sections in 20 cm intervals from Cores 329-U1366C-1H through 3H and similarly on 1.5 m sections from Core 329-U1366B-2H. The first core of Hole U1366B was damaged, and no electrode measurements were attempted. For Cores 329-U1366D-1H and 2H and Cores 329-U1366F-1H through 3H, electrode measurements were performed on whole-round sections remaining after biogeochemical and microbiological sampling.

The optode and electrode measurements show that dissolved oxygen penetrates through the entire sediment column to the basalt (Fig. F30; Tables T5, T6). In Holes U1366C and U1366F, optode measurements were highly reproducible between holes and show that oxygen declines from ~180 μM in the near-surface sediment to ~165 μM at 4 mbsf. At greater depths, the concentration declines linearly toward the basement, indicating a net flux for dissolved oxygen in the underlying basalt (Fig. F30A). Oxygen concentrations remain >110 μM throughout the sediment column, except at two depths at the base of the sediment column in Hole U1366F (29.75–29.77 and 29.86 mbsf). At these depths, the lowest oxygen concentrations were, respectively, 57 and 84 μM . These low values are bracketed by higher concentrations (110–111 μM). The cause of the low concentrations is not understood; however, their reproducibility and their position near the basalt/sediment interface are consistent with them having resulted from optode insertion into partially oxidized basalt clasts in the altered red groundmass.

Electrode measurements in Hole U1366C show a similar decrease from near-surface concentrations of ~180 to nearly 100 μM at 25.3 mbsf. Oxygen profiles from the upper 0–10 m exhibit a steep decrease (see profile from Hole U1366C in Fig. F30C) of 40 to 50 μM and are indicative of aerobic microbial respiration in the lithologic Unit I sediments. Measured

concentrations of dissolved oxygen (optode and electrode) were also similar to dissolved oxygen profiles obtained in the uppermost 8 mbsf during the site survey cruise (D'Hondt et al., 2009; Fischer et al., 2009). Moreover, the dissolved oxygen profile in Hole U1366C nearly matches the profiles in Holes U1365A and U1365B (see Fig. F56 in the “Site U1365” chapter [Expedition 329 Scientists, 2011b]). Below 10 mbsf, dissolved oxygen concentrations decrease toward the basement, which suggests a net flux of dissolved oxygen to the basement.

Overall, the dissolved oxygen profiles measured using electrodes are similar throughout all the investigated holes, but some hole-to-hole and method-to-method variability is evident. In particular, O_2 concentrations measured by electrode appear to be generally lower for Hole U1366D and generally higher for Hole U1366F than concentrations measured in Hole U1366C by electrode or optode or concentrations measured in Hole U1366F by optode. Although the cause(s) of these differences are not clear, their ultimate cause may be related to core handling; dissolved oxygen analyses of Holes U1366D and U1366F were limited to the short core pieces that remained after intensive sampling for biogeochemistry and microbiology whole-round samples. Oxygen analyses of the short core pieces were only performed in centers of pieces to minimize edge effects. Adverse effects of whole-round sampling are not observed in the optode measurements on the short core pieces from Section 329-U1366F-1H-3. Based on the good correspondence between electrode and optode measurements of Hole U1366C and optode measurements of Hole U1366F, we infer that the discrepancies between optode and electrode measurements for Hole U1366F may be due to the several-hour delay in taking the electrode measurements. The only exception is the lowermost 6 m of Core 329-U1366F-4H, which was analyzed by optode, but not electrode, prior to whole-round sampling.

Dissolved hydrogen and methane

Dissolved hydrogen gas (H_2) concentration was quantified in 66 samples (0.50–29.5 mbsf) collected in the ship's core refrigerator from Holes U1366D and U1366F. Based on the average of 13 blanks, the detection limit at this site was calculated to be 5.2 nM. The concentration of H_2 is below the detection limit in the uppermost 7 m of the sediment column (Fig. F31; Table T7). Below 14 mbsf, H_2 concentration increases with depth to several tens of nanomolar in the lowermost sediment.

Methane concentration is below the detection limit (<1.3 μM) in all samples from Holes U1366B (IODP

standard safety protocol), U1366D, and U1366F (refined protocol). The detection limit is defined here as three times the standard deviation of the blank (ambient air).

Interstitial water samples

Interstitial water was extracted from 66 whole-round samples from Holes U1366D and U1366F. High-resolution sampling of three samples per section (approximately one sample every 50 cm) was obtained (Table T8). Rhizon samples for dissolved nitrate analyses were obtained from all of the whole-round samples before squeezing.

Profiles of dissolved nitrate concentration in Holes U1366D and U1366F show good correlation between the holes (Fig. F32A). Nitrate concentration near the sediment surface (Sample 329-U1366D-1H-1, 30–40 cm) is 34.87 μM but gradually increases with depth to 40.03 μM at 28.75 mbsf (Sample 329-U1366F-4H-4, 70–80 cm). In conjunction with the consistent decrease in dissolved O_2 with increasing depth ($\sim 55 \mu\text{M}$ decrease from 3 to 30 mbsf; see Fig. F30), the increase in nitrate concentration with depth (by $\sim 5 \mu\text{M}$) implies oxidation of reduced nitrogen species (nitrification) derived from aerobic decomposition of organic matter. However, the increase of nitrate concentration from surface sediment to 15 mbsf ($\sim 5 \mu\text{M}$) is relatively small compared to the increase at gyre-margin Site U1365 ($\sim 10 \mu\text{M}$), suggesting that organic matter in the subseafloor sediment may diminish as marine primary productivity decreases toward the center of the gyre.

Dissolved phosphate concentrations decrease with increasing depth in Holes U1366D and U1366F (Fig. F32B). The peak concentration of 1.94 μM in near-surface sediment (1.35 mbsf; Sample 329-U1365D-1H-1, 130–140 cm) is $\sim 0.7 \mu\text{M}$ lower than overlying bottom water concentrations reported for this region of the Pacific Ocean (2.6 μM ; Talley, 2007). Phosphate concentration decreases to $<1 \mu\text{M}$ by 15 mbsf and then decreases less steeply to $\sim 0.5 \mu\text{M}$ at 29.36 mbsf near the basement (Sample 329-U1365F-4H-5, 40–50 cm). The pooled standard deviation is 0.070 μM (1σ) for all phosphate concentration data from both Holes U1366D and U1366F. The low concentration relative to bottom water may reflect removal by adsorption onto mineral or metal oxide surfaces. Overall, the phosphate profile indicates a flux of phosphate from the ocean to the sediment.

Concentrations of dissolved silicate are lower by 50–75 μM at Site U1366 than at the previous Site U1365 (Fig. F32C). They still, however, substantially exceed typical bottom water values (123 μM ; Talley, 2007)

for this region of the Pacific Ocean. Concentrations of dissolved Si range from 220 to 300 μM throughout the sediments and exhibit no clearly discernible trend with depth. A slight excursion in the dissolved Si concentration corresponds to the layers of porcellanite near 20 mbsf in lithologic Unit II (interval 329-U1365F-3H-5, 30–40 cm).

Alkalinity increases from 2.6 mM in the 0–0.1 mbsf interval to 2.8 mM at 15 mbsf in Holes U1366D and U1366F (Fig. F32D), perhaps caused by oxidation of organic matter. From 15 to 20 mbsf, alkalinity gradually decreases to 2.6 mM with depth. In the lower sediment column (20–30 mbsf), the data points scatter ~ 2.6 –2.8 mM. Standard deviation and error for our measurements of alkalinity in standard seawater (CRM94) are 0.015 and 0.003 mM ($N = 19$), respectively.

Dissolved inorganic carbon (DIC) increases from 2.5 mM at 0.35 mbsf to 2.8 mM at 13.25 mbsf before decreasing to ~ 2.6 mM at 20 mbsf (Fig. F32E). Below 20 mbsf, DIC values scatter between 2.5 and 2.8 mM. The range in DIC values is 0.3 mM. Average standard deviation of triplicate injection of the samples is 0.018 mM. The values from Holes U1366D and U1365F are generally consistent with one another.

Dissolved sulfate concentrations are 27–29 mM throughout the entire section (Fig. F32F). Between 0.35 and 8.85 mbsf, the sulfate anomaly ratio varies $<0.5\%$ (Fig. F32G). Between 10 and 28 mbsf, the sulfate anomaly exhibits a larger range, varying in an S-shaped pattern between -4% and -7% . Below 25 mbsf, sulfate increases smoothly and nearly monotonically from 27.8 to 28.1 mM, except for the deepest sample, which is offset to 29.4 mM. The variations in sulfate and sulfate anomaly are correlated with the lithologic units, suggesting that the small offsets from seawater concentrations may be due to adsorption and desorption during sample recovery and extraction.

Chloride concentrations in Holes U1366D and U1366F are continuous without offset (Fig. F32H). Concentrations at the top of the holes are indistinguishable from present-day bottom waters in this region (554 mM). Concentrations increase monotonically and reach a maximum of ~ 571 mM in the lowermost 5 m of Hole U1366F (a 3% increase). This increase may be due to relict glacial seawater and perhaps hydration of the underlying basement.

At Site U1366, the precision of the measurements of cations by inductively coupled plasma–atomic emission spectroscopy (ICP-AES) are as follows, as quantified by multiple triplicate analyses of International Association for the Physical Sciences of the Oceans)

IAPSO standard seawater and internal matrix matched standards:

- Ca = 1.3% of the measured value,
- Mg = 1.5% of the measured value,
- Na = 1% of the measured value,
- Sr = 0.4% of the measured value, and
- B = 0.7% of the measured value.

Accuracy of the ICP-AES results, as quantified by comparison to analysis of IAPSO standard not included in the calibration, is within precision of the measurement. Because of difficulties with the instrument, K was not analyzed. Concentrations of Fe and Mn hover near or below their respective detection limits (both 3 μM) and are plotted for illustrative purposes only. For the ion chromatography analyses, precision was as follows, as quantified by multiple triplicate analysis of IAPSO standard seawater:

- Ca = 0.77%,
- Mg = 0.25%,
- Na = 0.12%, and
- K = 0.40%.

Profiles of dissolved Ca, Mg, and Sr are closely related in their distribution (Figs. F32I, F32J, F32K).

Each of these constituents exhibits a slight and essentially constant increase with depth through the nearly 30 m of recovered material. There are two important aspects of these profiles. First, although basalt was recovered at the base of Hole U1366F, active Ca and Mg flux across this sediment/basalt interface is not evident. This circumstance is unlike Site U1365 (and many other sequences drilled by DSDP/Ocean Drilling Program/IODP) with active Mg/Ca exchange in the basaltic basement. Second, the three “whole-round stored shorter” (WSS) samples (see “Biogeochemistry” in the “Methods” chapter [Expedition 329 Scientists, 2011a]) yielded concentrations of Ca, Mg, and Sr that are either higher (for Ca and Mg) or lower (for Sr) in concentration than in interstitial waters that were collected by squeezing the whole rounds stored in the core refrigerator prior to extracting the interstitial water. The Ca and Mg contrast between the WSS samples and the other samples may reflect carbonate precipitation during storage. However, the Sr contrast between the WSS samples and the samples taken in the core refrigerator is difficult to explain solely by changes in the carbonate system.

Concentrations of dissolved Na (Fig. F32L) slightly increase with depth, similar to concentrations of dissolved Ca, Mg, and Sr. The WSS samples analyzed by ICP-AES bound the higher concentration range of Na and suggest some form of Na uptake during brief sample storage, possibly by reaction with authigenic clay.

Trends in Ca and Mg profiles and the absolute values measured by the Dionex ion chromatograph agree with the ICP-AES profiles. An offset of up to 2% between ion chromatography and ICP-AES values is observed in the uppermost 13 m of the Na profile, yet the agreement in trend remains excellent. Unlike the increase observed in Na, Mg, and Ca concentrations in WSS samples measured by ICP-AES, the ion chromatography Na data and Mg and Ca data from the WSS sample pool show no deviation from the main trend.

We had analytical difficulties measuring dissolved K by ICP-AES at this site, so we only report K data from the ion chromatograph (Fig. F32M). Potassium slightly decreases with depth (~0.5 mM). The profile is linear with some scatter and no defined structure. The profile of dissolved B (Fig. F32N) is characterized by a relative maximum between 10 and 16 mbsf, superimposed on an overall increase with depth.

Concentrations of dissolved Fe are at the detection limit but are shown in Figure F32O for illustrative purposes, given the importance of Fe to biogeochemical redox processes. Concentrations of Mn are also near the detection limit, except for the interval from 10 to 16 mbsf, which shows dissolved Mn at concentrations nominally within our detection range (3 μM ; Fig. F32P). This is the same depth interval that presents elevated concentrations of total carbon (Fig. F33B) and elevated B concentrations (Fig. F32N). Shore-based analyses of Fe and Mn will focus on improving our analytical determinations through this depth interval.

Concentrations of dissolved Ba and Li are below the analytical detection limit and are not discussed further here.

Solid-phase carbon and nitrogen

Contents of total nitrogen, total organic carbon (TOC), total carbon, and total inorganic carbon (TIC) were determined for 35 samples from Hole U1366D and U1366F (Fig. F33; Table T9).

Total nitrogen decreases almost linearly from 0.044 wt% at 0.01 mbsf to 0.006 wt% at 15.25 mbsf (Fig. F33A). Below 15.35 mbsf, the total nitrogen content is below the detection limit. TOC rapidly decreases from 0.20 wt% at 0.01 mbsf to 0.05 wt% at 2.35 mbsf and then gradually decreases to 0.03 wt% at 10.75 mbsf (Fig. F33B). TOC then remains at or below 0.03 wt% until basement.

Total carbon decreases from 0.20 wt% at 0.01 mbsf to 0.06 wt% at 7.35 mbsf. At greater depth, two maximums of total carbon occur, centered at 14 and 25 mbsf, reaching 0.18 wt% and 0.09 wt%, respectively.

Most samples show a very small difference between total carbon and TOC content (≤ 0.05 wt%, with only 10 samples ≤ 0.16 wt%), indicating that the contribution of TIC is small. TIC was determined independently using the coulometer system. The TIC profile exhibits the same two maximums centered at 14 and 25 mbsf as observed in the total carbon profile. The first peak reaches TIC values of 0.14 wt%, whereas the second peak only reaches 0.07 wt%. TIC values in the uppermost 5 mbsf are consistently lower (≤ 0.03 wt%) than in the rest of the sediment column. Calcium carbonate content computed from the TIC values indicate an average content of ~ 0.15 wt% in the uppermost 5 m, whereas values reach 1.14 and 0.68 wt% at the first and second maximum, respectively (Fig. F33C).

Microbiology

Sediment samples for microbiological studies were obtained using the APC system, primarily from Hole U1366F. During APC coring, sample contamination was monitored by PFT injection into the drilling fluid. Samples for cell abundance were taken from the cut cores facing interstitial water whole-round cores. After core recovery on the catwalk, core sections were immediately transferred to the core refrigerator on the Hold Deck, where we subsampled microbiological whole-round cores. The temperature of the core refrigerator during subsampling was $\sim 7^{\circ}$ – 10° C. Microbiological whole-round cores were generally taken at a high depth resolution from the first core (329-U1366F-1H), as well as from the core just above the sediment/basalt interface (Core 4H). Because of disturbance in the lowermost cores in Holes U1366D and U1366E, oxygen measurements were taken from these cores prior to microbiological sampling, requiring the core sections to be equilibrated to the temperature of the Microbiology Laboratory cold room (8.5° C) prior to sampling.

Cell abundance

Microbial cells were enumerated using epifluorescence microscopy (see “Microbiology” in the “Methods” chapter [Expedition 329 Scientists, 2011a]). Sediment subcore samples (2 cm^3) were taken from Hole U1366F cores using tip-cut syringes for shipboard analysis. For shore-based analysis, 10 cm whole-round cores were taken from Hole U1366F and frozen at -80° C. Seventy 2 cm^3 syringe samples (Table T10) and nine whole-round cores (Sections 329-U1366F-1H-1, 1H-4, 2H-1, 2H-3, 2H-5, 3H-2, 3H-6, 4H-2, and 4H-4) were taken at Site U1366 for cell enumeration.

Four blanks were prepared and counted during processing of the samples from Site U1366, resulting in a mean blank of 6.6×10^2 cells/cm³ with a standard deviation of 2.4×10^2 cells/cm³. The minimum detection limit (MDL; blank plus three times standard deviation) was calculated to be 1.4×10^3 cells/cm³. As the blanks showed little variation between sites, they were pooled from all sites and the MDL for all sites calculated based on extended database at the end of the expedition. The overall MDL is 1.4×10^3 cells/cm³.

Cell counts did not show any clear trend with depth (Fig. F34). Between 3 and 25 mbsf, the data scatter from below the detection limit to maximum values close to 10^4 cells/cm³. In sediment deeper than 25 mbsf, all values are below the detection limit. From comparison with the cell count data from the site survey cruise (D’Hondt et al., 2009), the uppermost 40–50 cm of the sediment column might have been lost during drilling. Several samples from the upper part of the core were counted without cell extraction. All were below the mean blank for nonextracted counts (3.2×10^4 cells/cm³).

The sediment/basalt interface sample was collected in a core liner from Section 329-U1366F-4H-5, which included a large piece of basalt. Cell numbers in the basaltic rock sample were directly counted without cell separation. Before counting, the basalt sample was processed by washing and flaming and then ground into powder (see “Microbiology” in the “Methods” chapter [Expedition 329 Scientists, 2011a]). The cell count for the interface basalt in Hole U1366F is 2.3×10^4 cells/cm³. However, because our MDL is 4.9×10^4 cells/cm³ (equivalent to 5 cells per 300 fields of microscopic view), this count is below our MDL.

Virus abundance

Sediment samples from Sections 329-U1366F-1H-1, 1H-2, 2H-3, 3H-4, and 4H-3 were used for viral extraction (see “Microbiology” in the “Methods” chapter [Expedition 329 Scientists, 2011a]). The extracted virus-like particles (VLPs) were stained with SYBR Gold and counted using epifluorescence microscopy. Additional samples were taken and preserved at -80° C for shore-based analysis of viral abundance.

Abundance of VLPs in Hole U1366F is $\sim 8 \times 10^5$ VLP/cm³ for the uppermost sample (0.4 mbsf; Fig. F34). The abundance of VLPs decreases with depth to $\sim 2 \times 10^4$ VLP/cm³ at 9.5 mbsf.

During the estimation of VLP abundance from Sections 329-U1366F-2H-3, 3H-4, and 4H-3, the num-

bers of VLPs appeared to be very low (Table T11) and showed weaker fluorescence than samples from shallower depths. Additionally, ship movement during transit prohibited confident detection of VLPs. Thus, data on VLP counts in deeper sediment samples are considered to be preliminary. All samples will be re-analyzed postcruise.

Cultivation

Multiple cultivations were initiated onboard using a variety of media for heterotrophic (aerobic and anaerobic) and autotrophic microorganisms. The whole-round cores were subsampled aseptically with tip-cut syringes to make slurries for inoculation in liquid or on solid media (Table T12). Additional samples were stored either in N₂-flushed serum bottles or in syringes packed in sterile foil packs stored at 4°C for future cultivation experiments (referred to as SLURRY in Table T12). For future cultivation efforts, 0.2 µm filtered bottom water was transferred to sterile 50 mL serum bottles, sparged with N₂ for 5 min, and capped with rubber stoppers and aluminum crimp caps. The bottles were stored at 4°C for preparing liquid media on shore.

Molecular analyses

Sediment samples

Whole-round cores for shore-based molecular analyses were taken throughout the entire sediment column of Hole U1366F and transferred to -80°C freezers for storage. These samples will be used to determine microbial diversity, community composition, and the presence or absence of selected functional genes. Eight 10 cm whole-round core samples (MBO) were taken as routine microbiology samples (RMS) for storage at -80°C at the Gulf Coast Core Repository (Texas A&M, College Station, Texas) for future sample requests (Sections 329-U1366F-1H-2, 2H-3, 3H-1, 4H-1, 4H-2, and 4H-5).

Deep seawater control sample

As a control sample for shore-based molecular analysis, 300 mL of bottom seawater was collected from the mudline Core 329-U1366B-1H in a sterile plastic bag and immediately stored at 4°C in the Microbiology Laboratory. The bottom seawater sample was then filtered through 0.2 µm pore sized polycarbonate membrane filters under aseptic conditions, and the filters were stored at -80°C for shore-based microbiological analyses.

Basalt samples

Samples from the sediment/basalt interface and alteration material from Section 329-U1366F-4H-5 were stored at -80°C. Before being frozen, the basalt piece was separated from surrounding soft materials, washed three times with 3% NaCl solution, briefly flamed, and crushed into powder. Some portions of these interface samples were incubated at 4°C in RNAlater solution (Qiagen) overnight and then frozen at -80°C.

Fluorescence in situ hybridization analysis

Duplicate 10 cm³ subcores of sediment from Sections 329-U1366F-1H-1 through 1H-3, 2H-3, 3H-4, 4H-2, and 4H-5 were fixed as described in “Microbiology” in the “Methods” chapter (Expedition 329 Scientists, 2011a) for shore-based fluorescence in situ hybridization analyses.

Radioactive and stable isotope tracer incubation experiments

Stable isotope (¹³C and ¹⁵N) experiments to measure carbon and nitrogen uptake activities were initiated on board in the Isotope Isolation Van. Sediment subcores (15 cm³) were taken from the inner part of 20 cm whole-round cores, placed in a sterile glass vial, flushed with N₂, sealed with a rubber stopper, and stored until processing in the core refrigerator on the Hold Deck (see “Microbiology” in the “Methods” chapter [Expedition 329 Scientists, 2011a]). From Site U1366, five whole-round cores (Sections 329-U1366D-1H-2 and 2H-3 and 329-U1366F-2H-3, 3H-5, and 4H-5) were processed for incubation experiments, as described in “Microbiology” in the “Site U1365” chapter (Expedition 329 Scientists, 2011b).

The following whole-round intervals from Site U1366 were used for sediment slurry experiments on potential metabolic activities (i.e., assimilation and dissimilative respiration) using radio and stable isotopes: Samples 329-U1366D-1H-2, 120–130 cm; 3H-2, 110–120 cm; and 4H-3, 120–130 cm (see “Microbiology” in the “Methods” chapter [Expedition 329 Scientists, 2011a]). These incubation slurry samples from Site U1366 were processed 19–21 November 2010, at the same time as other samples from Sites U1365, U1367, and U1368, in the Isotope Isolation Van.

Samples of sediment, basalt, and alteration material from the sediment/basalt interface (Section 329-U1366F-4H-5) were stored at 4°C. Incubations of the

sediment/basalt interface samples with ^{15}N -labeled NO_3^- and ^{13}C -labeled HCO_3^- or acetate were initiated onboard.

Contamination assessment

We used perfluoromethylcyclohexane as PFT to monitor the level of drilling fluid contamination in sediment cores. The PFT was constantly injected into drilling fluids during APC coring in Holes U1366D and U1366DF. Three cubic centimeters subcores of sediments were taken from whole-round cores in the cold room and stored in glass vials with 2 mL of water for shore-based analyses (see “Microbiology” in Expedition 329 Scientists, 2011a, 2011b).

References

- D'Hondt, S., Abrams, L.J., Anderson, R., Dorrance, J., Durbin, A., Ellett, L., Ferdelman, T., Fischer, J., Forschner, S., Fuldauer, R., Goldstein, H., Graham, D., Griffith, W., Halm, H., Harris, R., Harrison, B., Hasiuk, F., Horn, G., Kallmeyer, J., Lever, M., Meyer, J., Morse, L., Moser, C., Murphy, B., Nordhausen, A., Parry, L., Pockalny, R., Puschell, A., Rogers, J., Schrum, H., Smith, D.C., Soffientino, B., Spivack, A.J., Stancin, A., Steinman, M., and Walczak, P., 2011. KNOX-02RR: drilling site survey—life in subseafloor sediments of the South Pacific Gyre. *In* D'Hondt, S., Inagaki, F., Alvarez Zarikian, C.A., and the Expedition 329 Scientists, *Proc. IODP, 329*: Tokyo (Integrated Ocean Drilling Program Management International, Inc.). doi:10.2204/iodp.proc.329.112.2011
- D'Hondt, S., Inagaki, F., and Alvarez Zarikian, C., 2010. South Pacific Gyre Microbiology. *IODP Sci. Prosp.*, 329. doi:10.2204/iodp.sp.329.2010
- D'Hondt, S., Spivack, A.J., Pockalny, R., Ferdelman, T.G., Fischer, J.P., Kallmeyer, J., Abrams, L.J., Smith, D.C., Graham, D., Hasiuk, F., Schrum, H., and Stancine, A.M., 2009. Subseafloor sedimentary life in the South Pacific Gyre. *Proc. Natl. Acad. Sci. U. S. A.*, 106(28):11651–11656. doi:10.1073/pnas.0811793106
- Expedition 329 Scientists, 2011a. Methods. *In* D'Hondt, S., Inagaki, F., Alvarez Zarikian, C.A., and the Expedition 329 Scientists, *Proc. IODP, 329*: Tokyo (Integrated Ocean Drilling Program Management International, Inc.). doi:10.2204/iodp.proc.329.102.2011
- Expedition 329 Scientists, 2011b. Site U1365. *In* D'Hondt, S., Inagaki, F., Alvarez Zarikian, C.A., and the Expedition 329 Scientists, *Proc. IODP, 329*: Tokyo (Integrated Ocean Drilling Program Management International, Inc.). doi:10.2204/iodp.proc.329.103.2011
- Fischer, J.P., Ferdelman, T.G., D'Hondt, S., Røy, H., and Wenzhöfer, F., 2009. Oxygen penetration deep into the sediment of the South Pacific gyre. *Biogeosciences*, 6:1467–1478. http://www.biogeosciences.net/6/1467/2009/bg-6-1467-2009.pdf
- Gradstein, F.M., Ogg, J.G., and Smith, A. (Eds.), 2004. *A Geologic Time Scale 2004*: Cambridge (Cambridge Univ. Press). http://cambridge.org/uk/catalogue/catalogue.asp?isbn=9780521781428
- Graham, I.J., Glasby, G.P., and Churchman, G.J., 1997. Provenance of the detrital component of deep-sea sediments from the SW Pacific Ocean based on mineralogy, geochemistry and Sr isotopic composition. *Mar. Geol.*, 140(1–2):75–96. doi:10.1016/S0025-3227(97)00006-6
- Hein, J.R., Ross, C.R., Alexander, E., and Yeh, H.W., 1979. Mineralogy and diagenesis of surface sediments from DOMES Area A, B, and C. *In* Bishoff, J.L., and Piper, D.Z. (Eds.), *Marine Geology and Oceanography of the Pacific Manganese Nodule Province*. NATO Conf. Ser. IV, 365–396.
- Kastner, M., 1986. Mineralogy and diagenesis of sediments at Site 597: preliminary results. *In* Leinen, M., Rea, D.K., et al., *Init. Repts. DSDP, 92*: Washington, DC (U.S. Govt. Printing Office), 345–349. doi:10.2973/dsdp.proc.92.116.1986
- Kastner, M., Keene, J.B., and Gieskes, J.M., 1977. Diagenesis of siliceous oozes, I. Chemical controls on the rate of opal-A to opal-CT transformation—an experimental study. *Geochim. Cosmochim. Acta*, 41(8):1041–1051. doi:10.1016/0016-7037(77)90099-0
- Keene, J.B., 1975. Cherts and porcellanites from the North Pacific DSDP, Leg 32. *In* Larson, R.L., Moberly, R., et al. *Init. Repts. DSDP, 32*: Washington, DC (U.S. Govt. Printing Office), 429–507. doi:10.2973/dsdp.proc.32.114.1975
- Larson, R.L., Pockalny, R.A., Viso, R.F., Erba, E., Abrams, L.J., Luyendyk, B.P., Stock, J.M., and Clayton, R.W., 2002. Mid-Cretaceous tectonic evolution of the Tongareva triple junction in the southwestern Pacific Basin. *Geology*, 30(1):67–70. doi:10.1130/0091-7613(2002)030<0067:MCTEOT>2.0.CO;2
- Smith, W.H.F., and Sandwell, D.T., 1997. Global sea floor topography from satellite altimetry and ship depth soundings. *Science*, 277(5334):1956–1962. doi:10.1126/science.277.5334.1956
- Talley, L.D., 2007. *Hydrographic Atlas of the World Ocean Circulation Experiment (WOCE) (Vol. 2): Pacific Ocean*. Sparrow, M., Chapman, P., and Gould, J. (Eds.): Southampton, U.K. (International WOCE Project Office). http://www-pord.ucsd.edu/whp_atlas/pacific_index.html

Publication: 13 December 2011
MS 329-104

Figure F1. Multibeam bathymetry of the Site U1366 survey area with the KNOX-02RR survey track overlain. sol = start of seismic line, eol = end of seismic line, z = time (Greenwich Mean Time), sp = shotpoint.

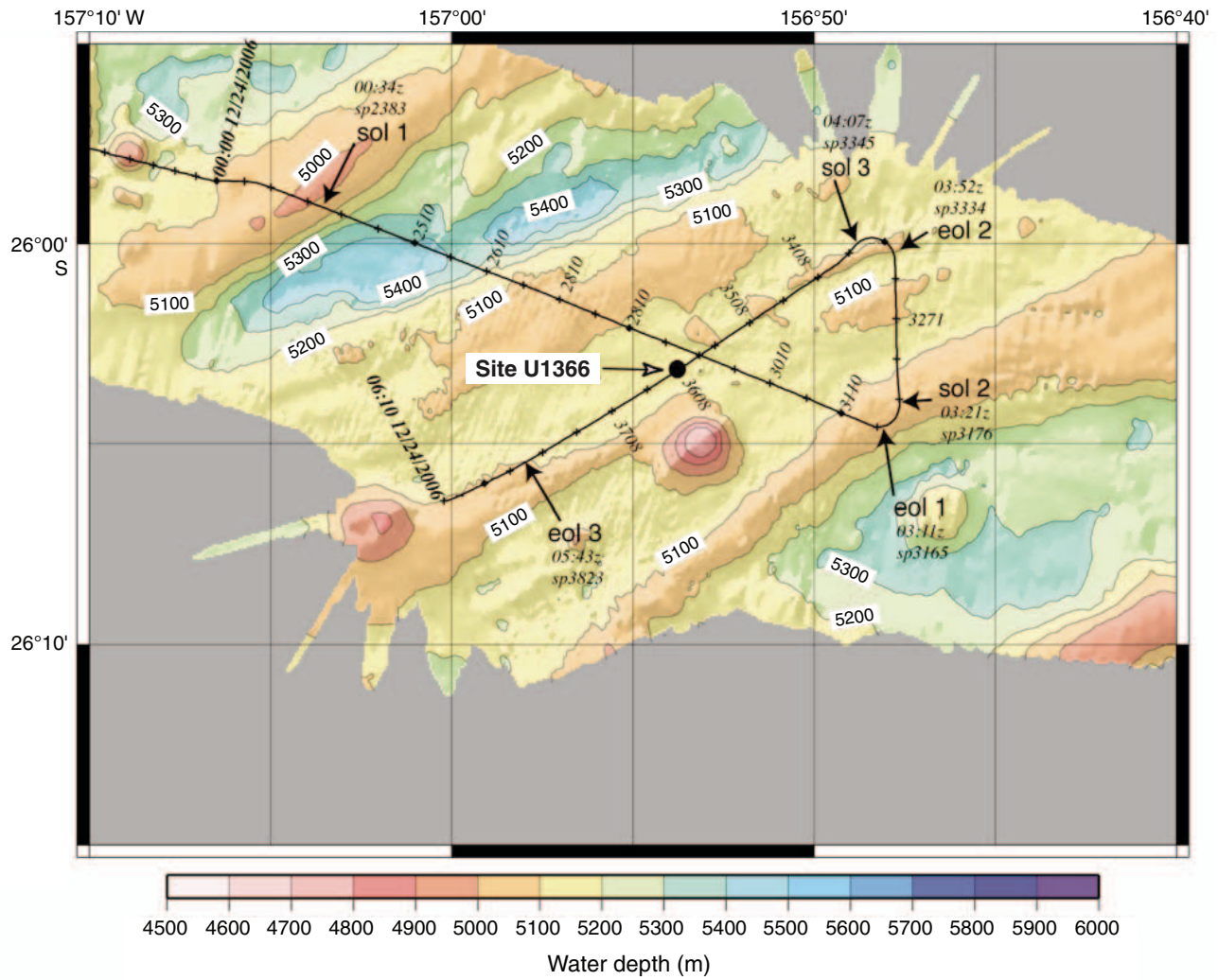


Figure F2. KNOX-02RR seismic survey track, Site U1366. sol = start of seismic line, eol = end of seismic line, z = time (Greenwich Mean Time), sp = shotpoint.

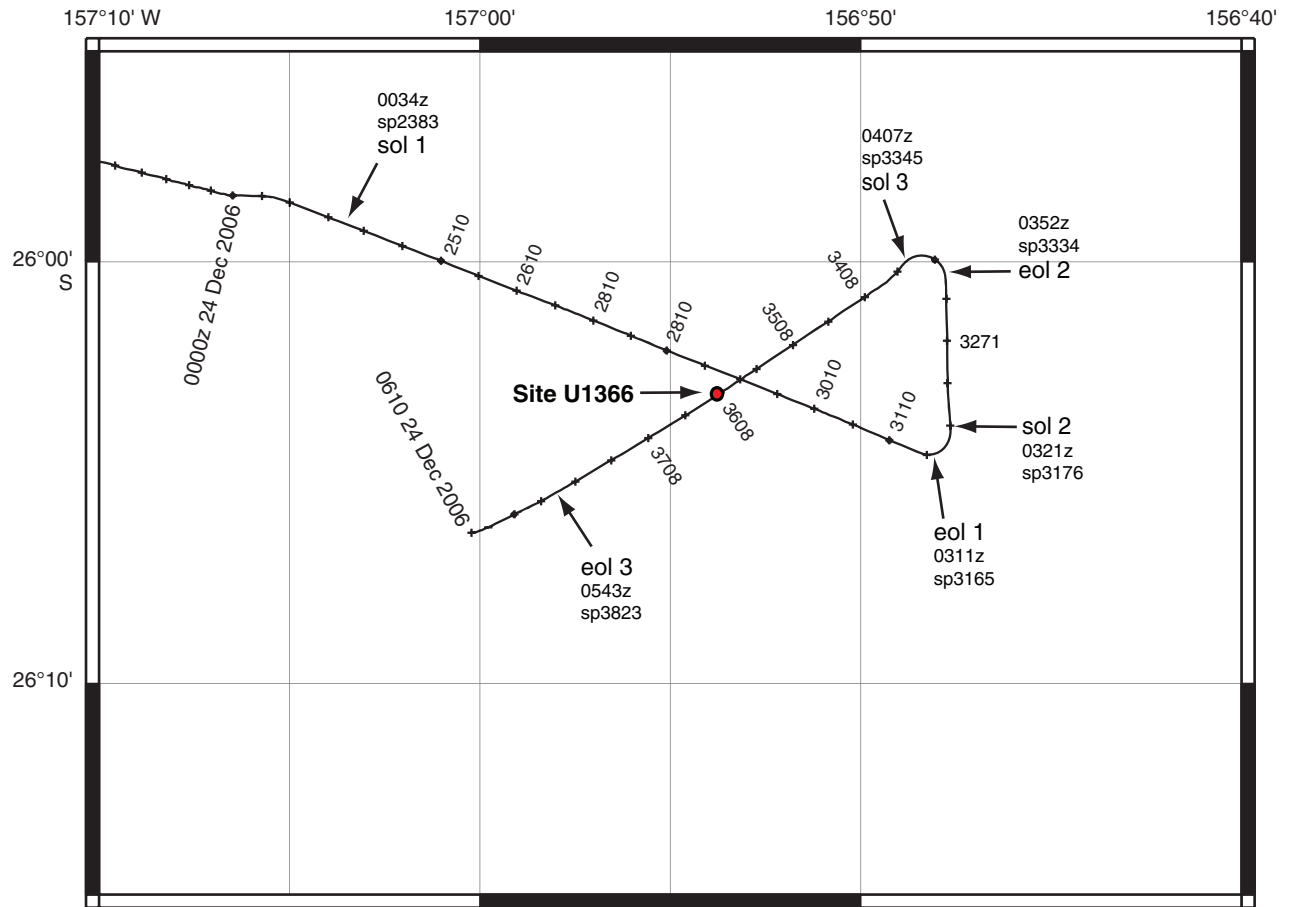




Figure F3. Portion of KNOX-02RR Channel 48 of MCS Line 3 across Site U1366. z = time (Greenwich Mean Time), SP = shotpoint, MORB = mid-ocean-ridge basalt, WD = water depth, SCS = single-channel seismic, BP = band-pass, AGC = automatic gain control, VE = vertical exaggeration.

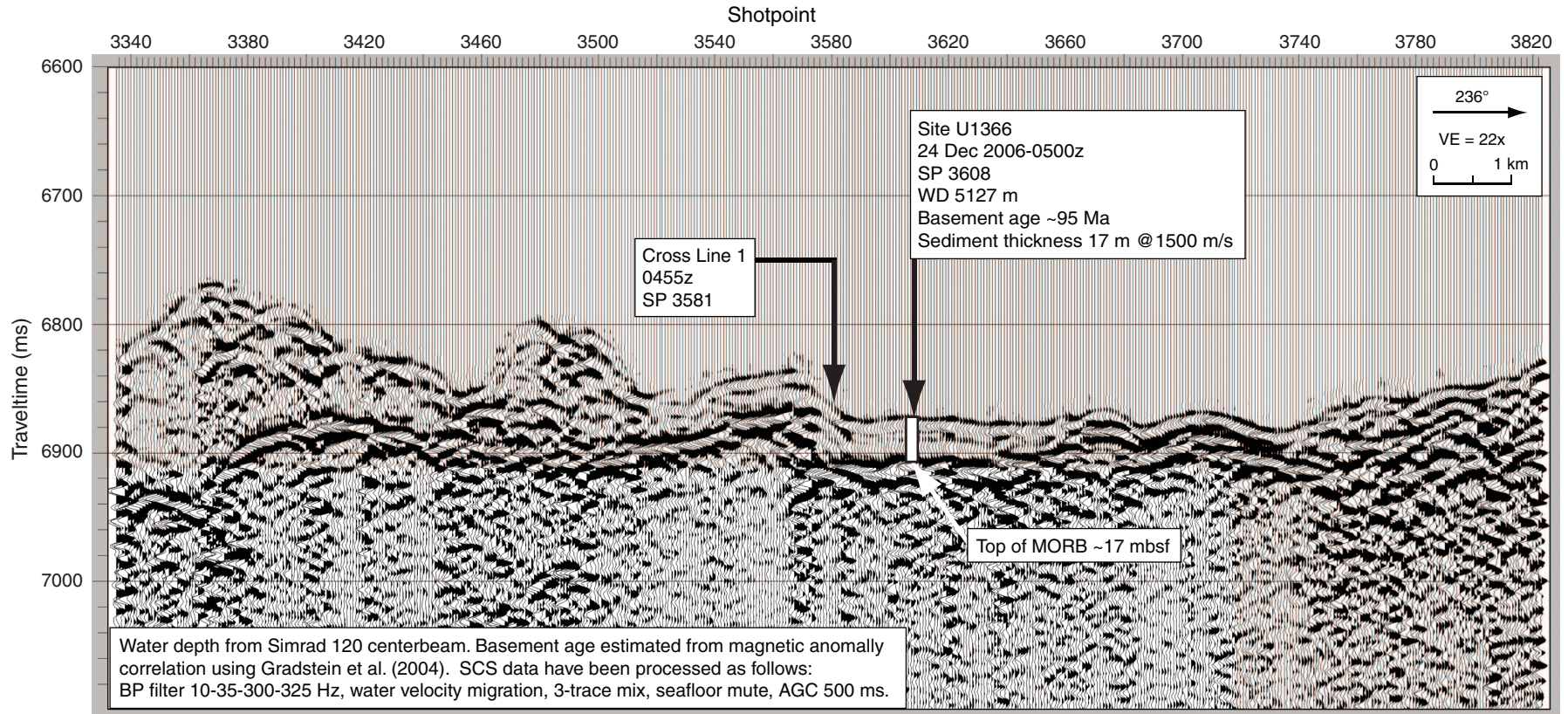




Figure F4. Portion of KNOX-02RR Channel 48 of MCS Line 1 crossing MCS Line 3, northeast of Site U1366. z = time (Greenwich Mean Time), SP = shotpoint, MORB = mid-ocean-ridge basalt, WD = water depth, SCS = single-channel seismic, BP = band-pass, AGC = automatic gain control, VE = vertical exaggeration.

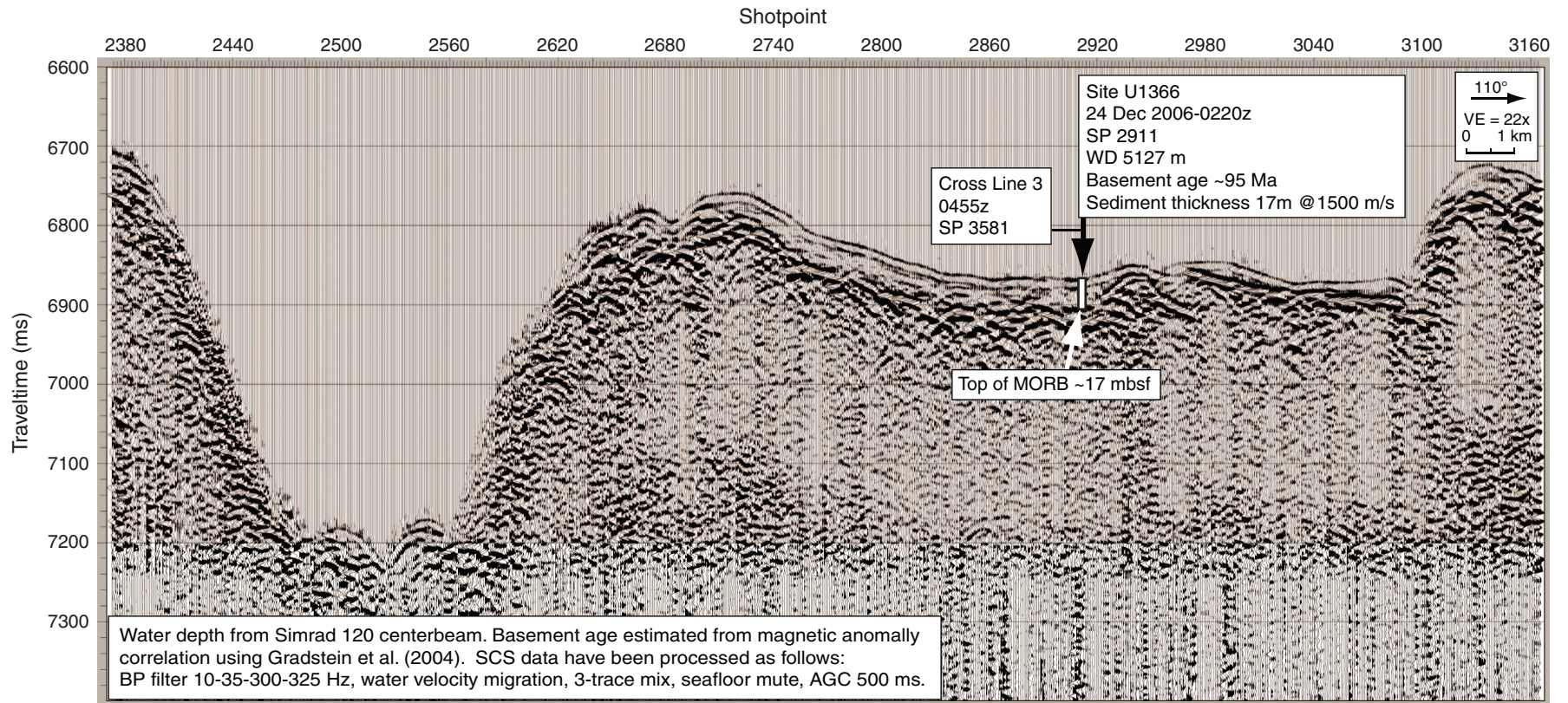




Figure F5. Portion of KNOX-02RR 3.5 kHz seismic Line 3 across Site U1366. MORB = mid-ocean-ridge basalt.

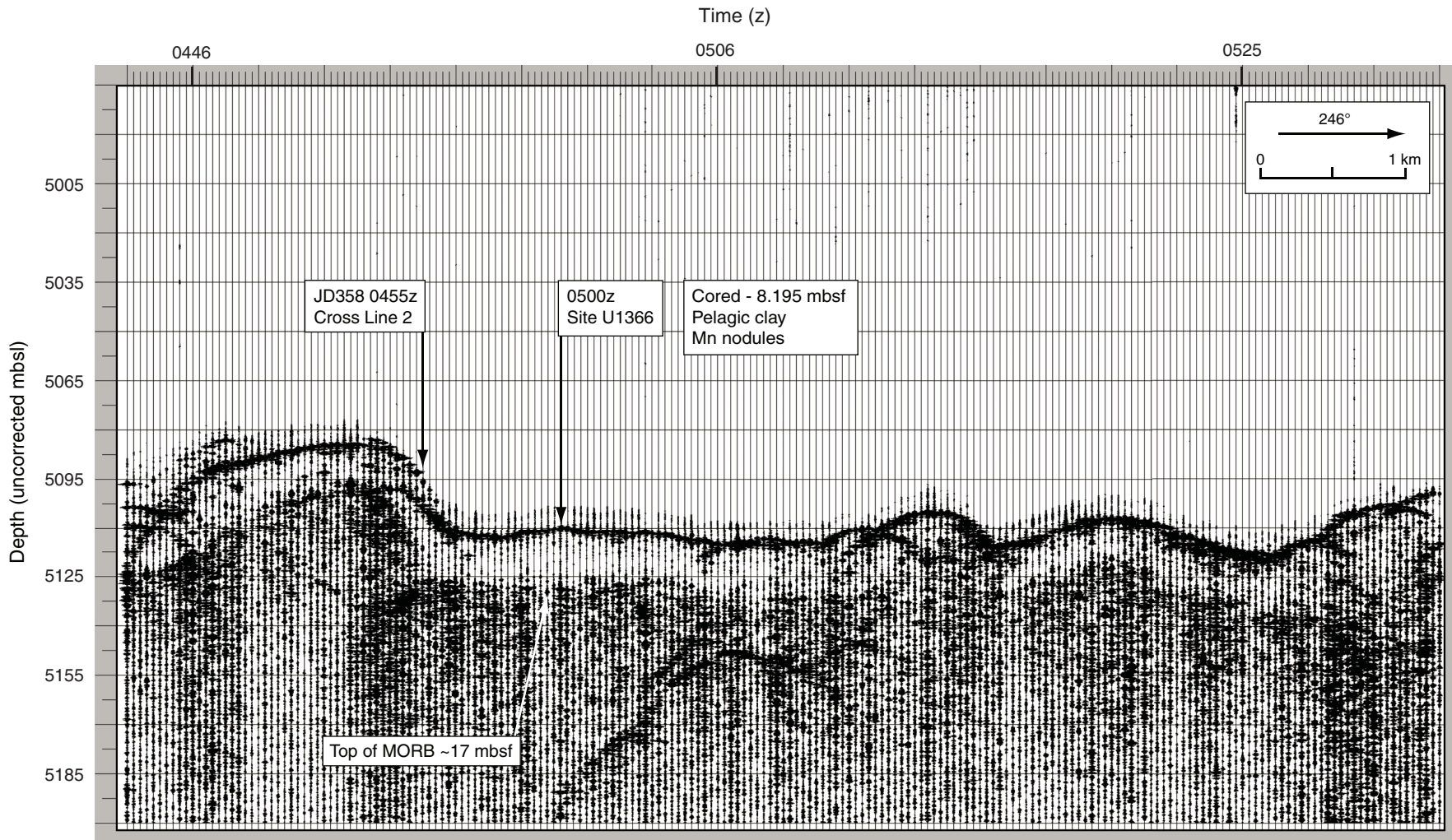




Figure F6. Portion of KNOX-02RR 3.5 kHz seismic Line 1 crossing 3.5 kHz seismic Line 3, northeast of Site U1366. CPA = closest point of approach, MORB = mid-ocean-ridge basalt.

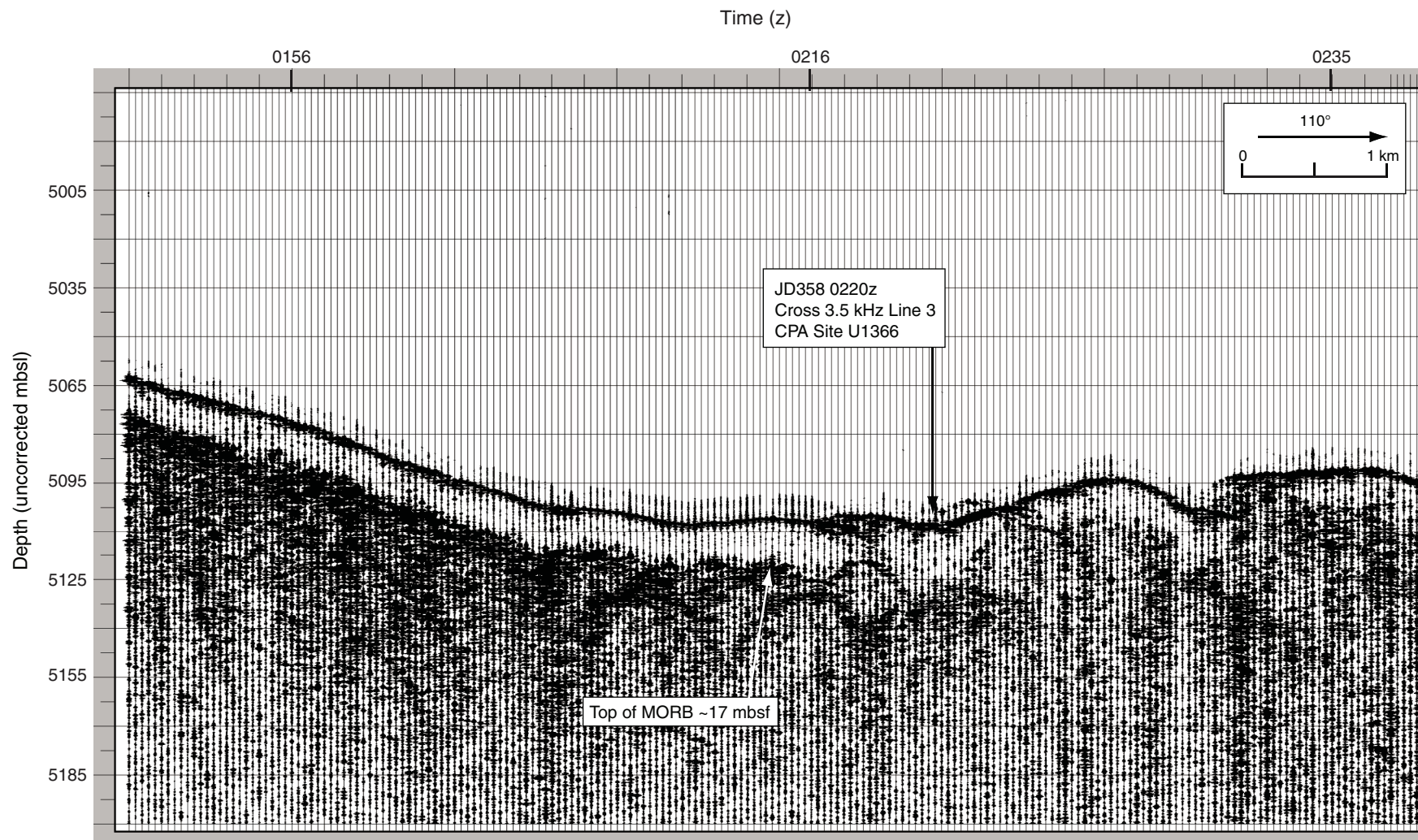


Figure F7. Lithology summary and physical property data. MS = magnetic susceptibility, GRA = gamma ray attenuation, NGR = natural gamma radiation, RSO = red-brown to yellow-brown semiopaque oxide. **A.** Hole U1366C. Summary based on the complete coring recovery of Unit I. (Continued on next page.)

A

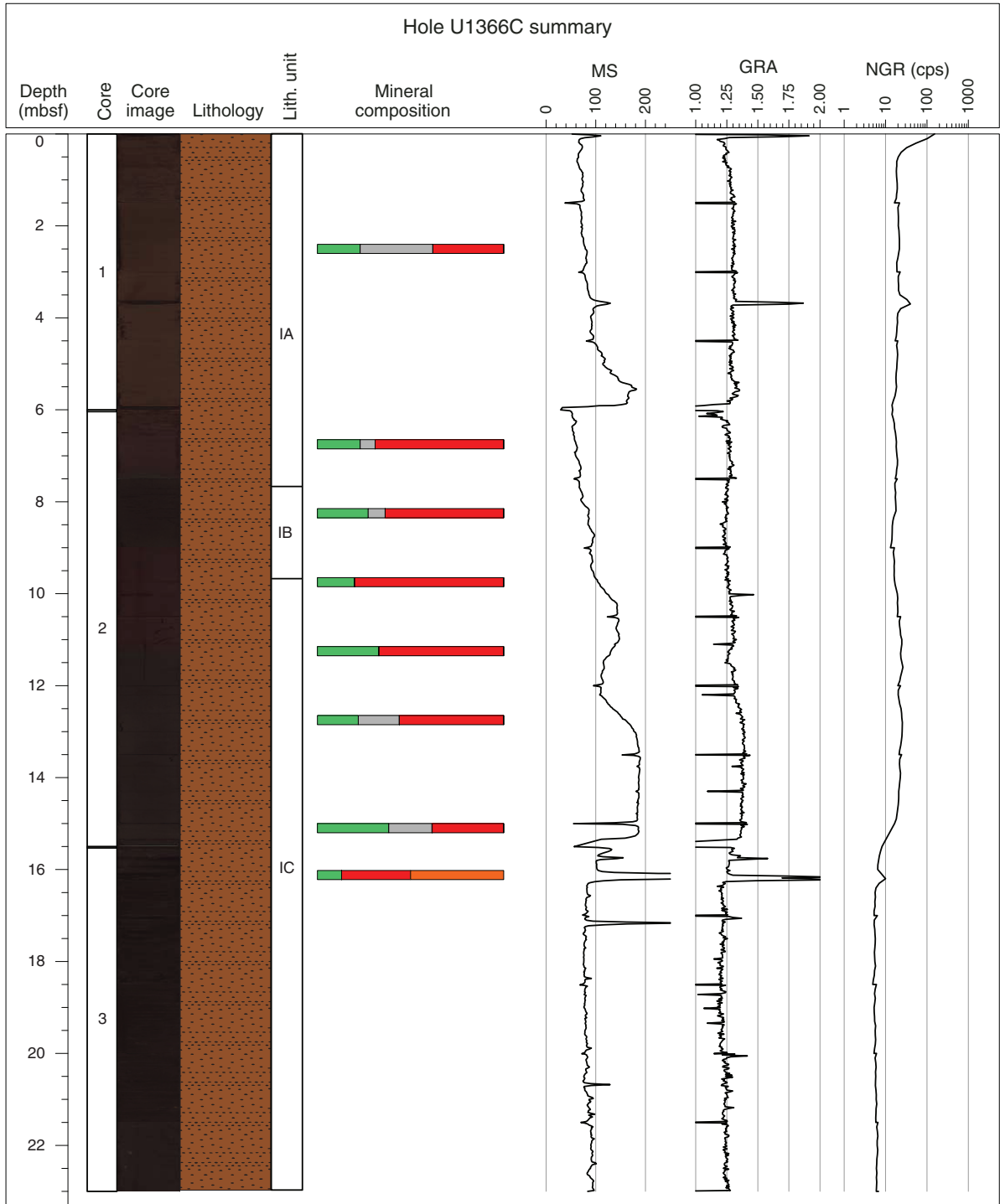


Figure F7 (continued). B. Hole U1366F. Summary based on partial lithologies of Units I and II.

B

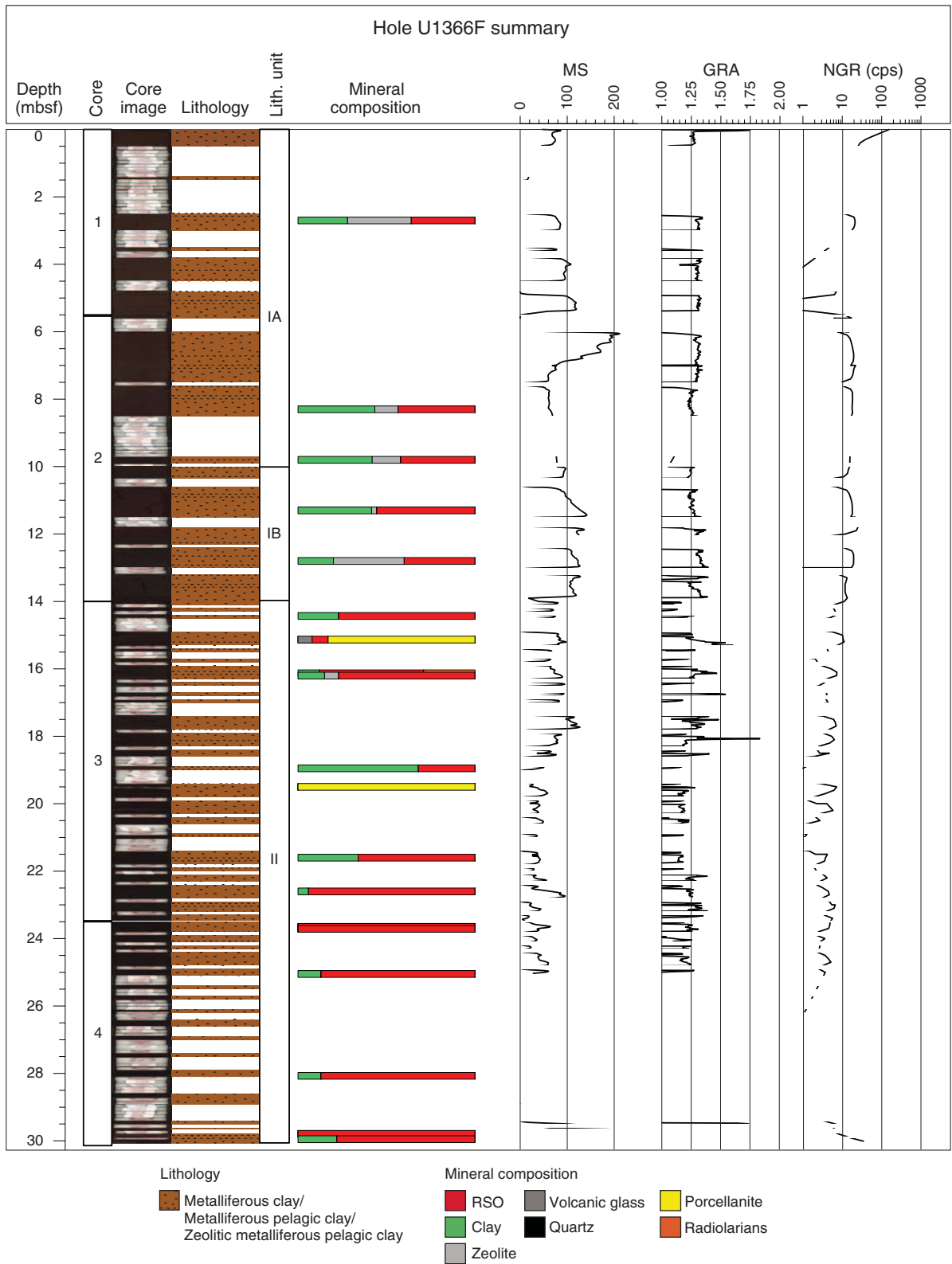




Figure F8. Diagram of lithostratigraphic correlation among holes at Site U1366.

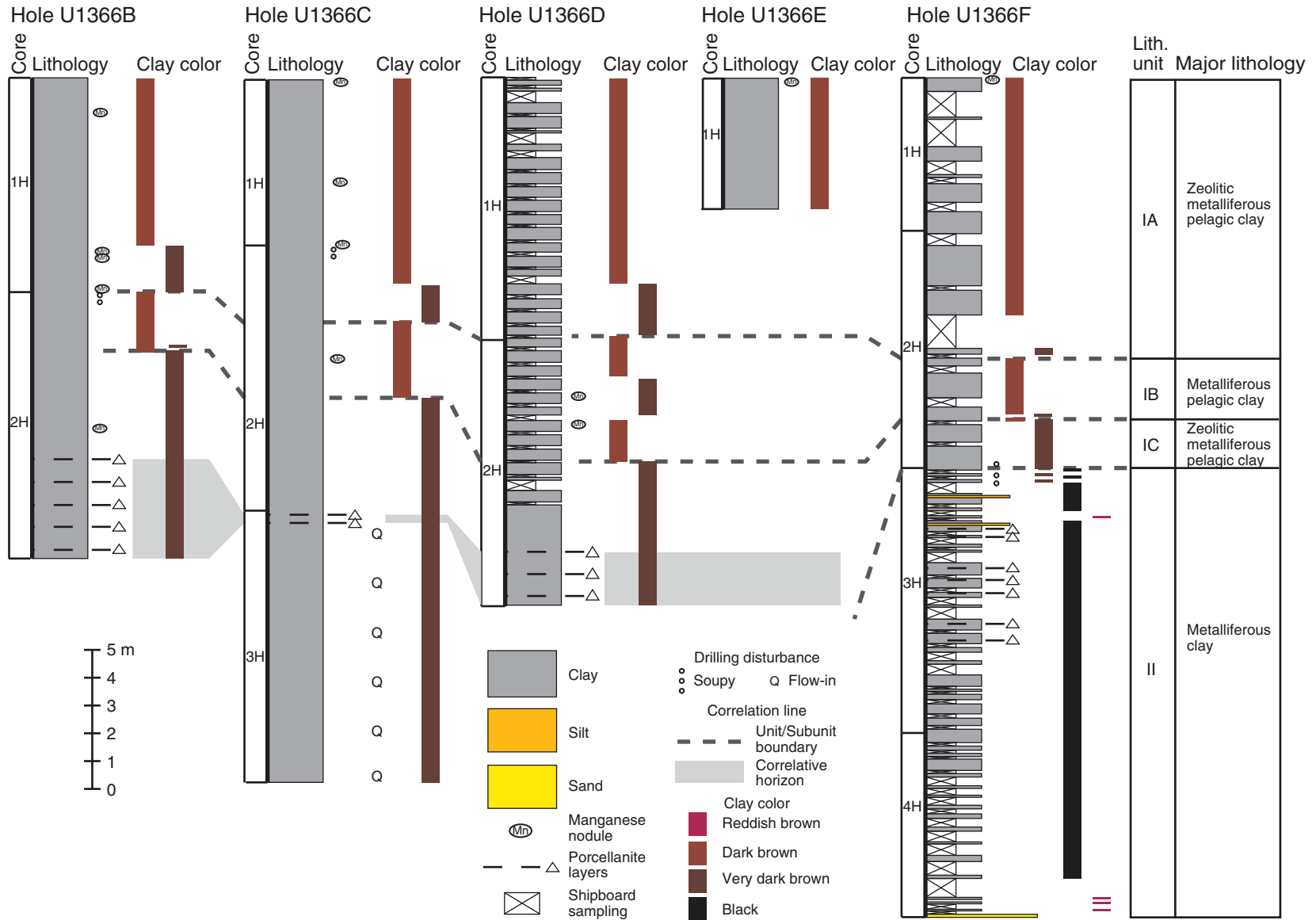




Figure F9. Core photographs, Site U1366. **A.** Dark brown zeolitic metalliferous pelagic clay in Subunit IA (interval 329-U1366F-1H-1, 0–30 cm). A manganese nodule is at the top of the core. **B.** Dark brown metalliferous pelagic clay in Subunit IB (interval 329-U1366F-2H-4, 120–150 cm). **C.** Very dark brown zeolitic metalliferous pelagic clay in Subunit IC (interval 329-U1366B-2H-6, 120–150 cm). Porcellanite intercalations are in the lower part of this subunit (interval 329-U1366A-2H-6, 120–150 cm). **D.** Very dark brown metalliferous clay in Unit II (interval 329-U1366F-3H-4, 90–120 cm). Note white porcellaneous ash/altered ash layer. **E.** Metalliferous clay (dark reddish brown to very dark brown) overlaying lithic sand (dark reddish gray) in Unit II (interval 329-U1366F-4H-5, 87–117 cm).

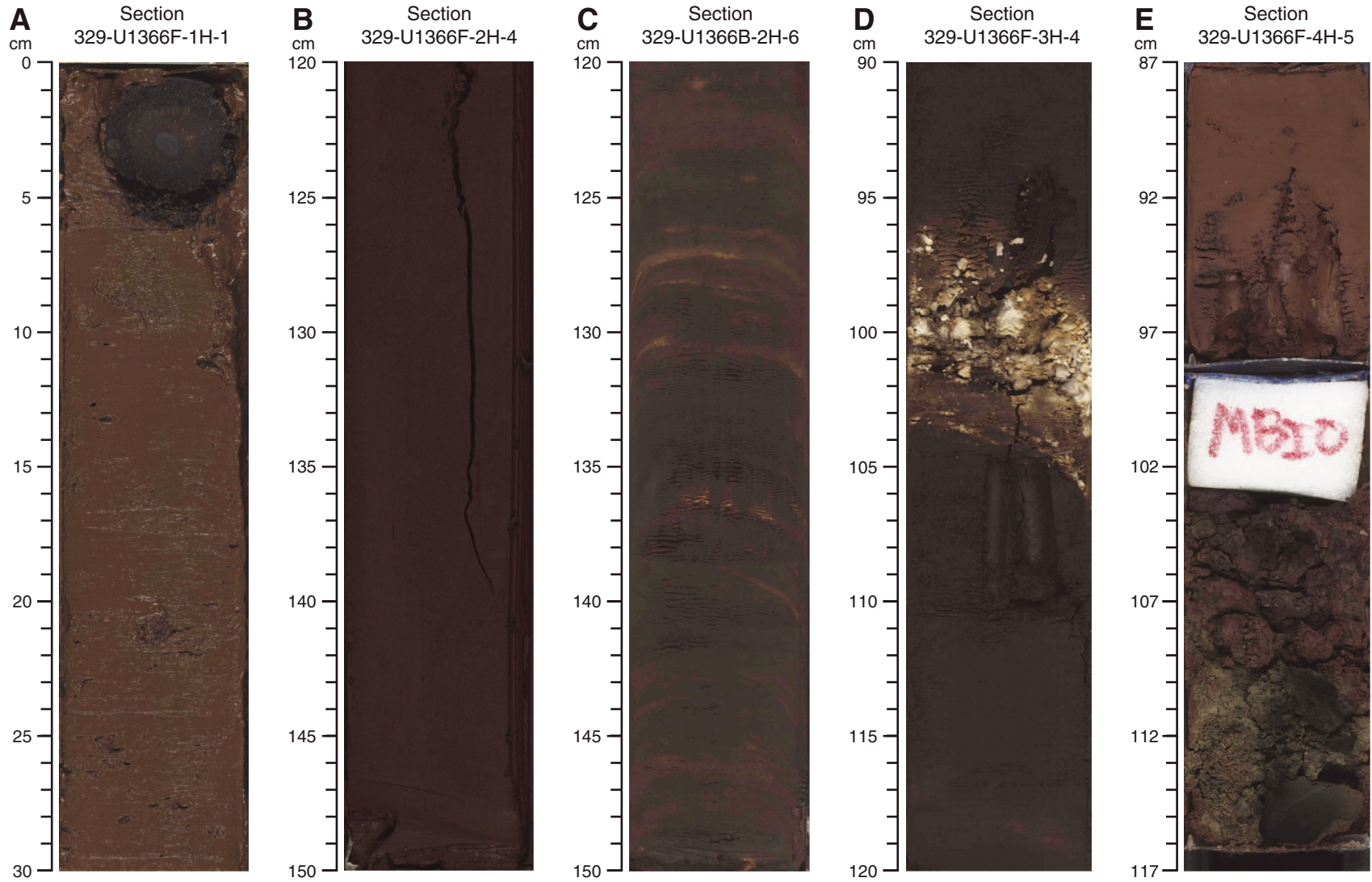




Figure F10. Selected smear slide photomicrographs of clay sediment, Site U1366. **A.** Zeolitic metalliferous pelagic clay in Subunit IA (Sample 329-U1366F-1H-2, 120 cm). **B.** Metalliferous pelagic clay in Subunit IB (Sample 329-U1366F-2H-4, 130 cm). **C.** Metalliferous clay in Unit II (Sample 329-U1366F-3H-1, 43 cm). **D.** Radiolarian silt layer intercalated with metalliferous clay in Unit II (Sample 329-U1366F-3H-2, 63 cm).

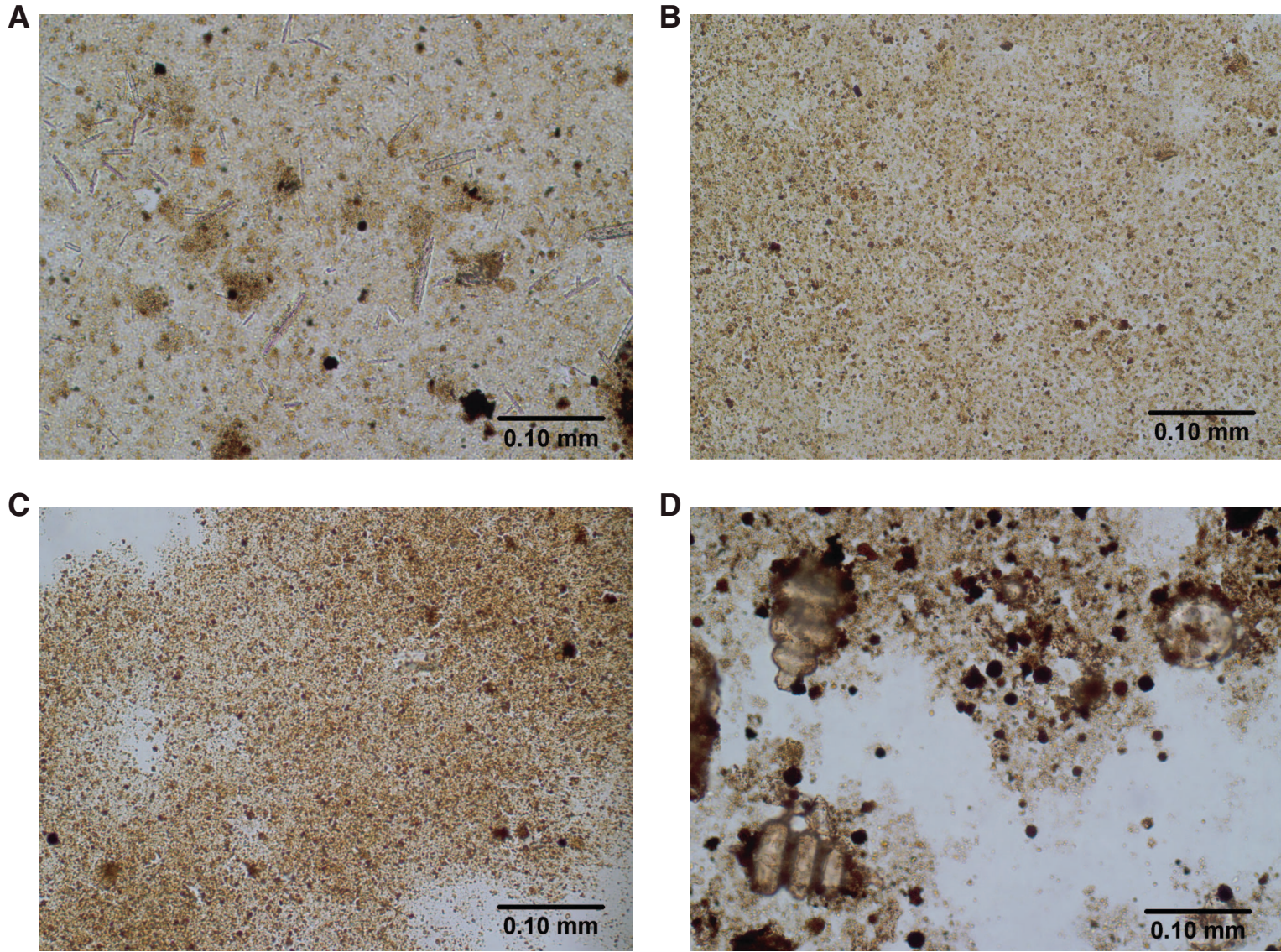


Figure F11. Photograph of ichthyolith recovered in Sample 329-U1366-2H-CC.



Figure F12. Annotated X-ray diffractogram of hematitic clay from the lowest sediment interval in Hole U1366F (Sample 329-U1366F-4H-5, 88–90 cm).

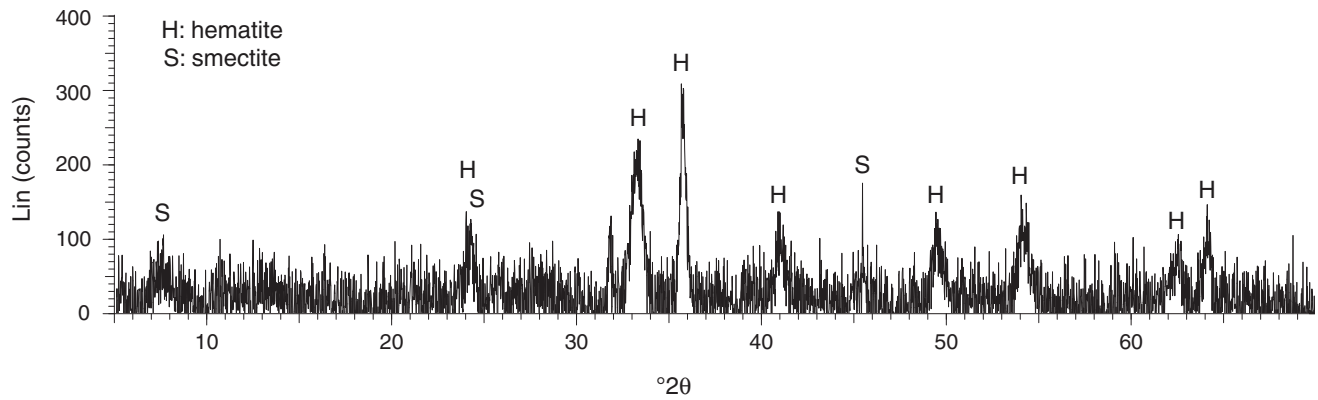


Figure F13. Core image (interval 329-U1366F-4H-5, 104–116 cm) and photomicrograph (Sample 329-U1366F-4H-5, 110–111 cm) of the basaltic contact in Hole U1366F. Cross-polarized light at 5× magnification.

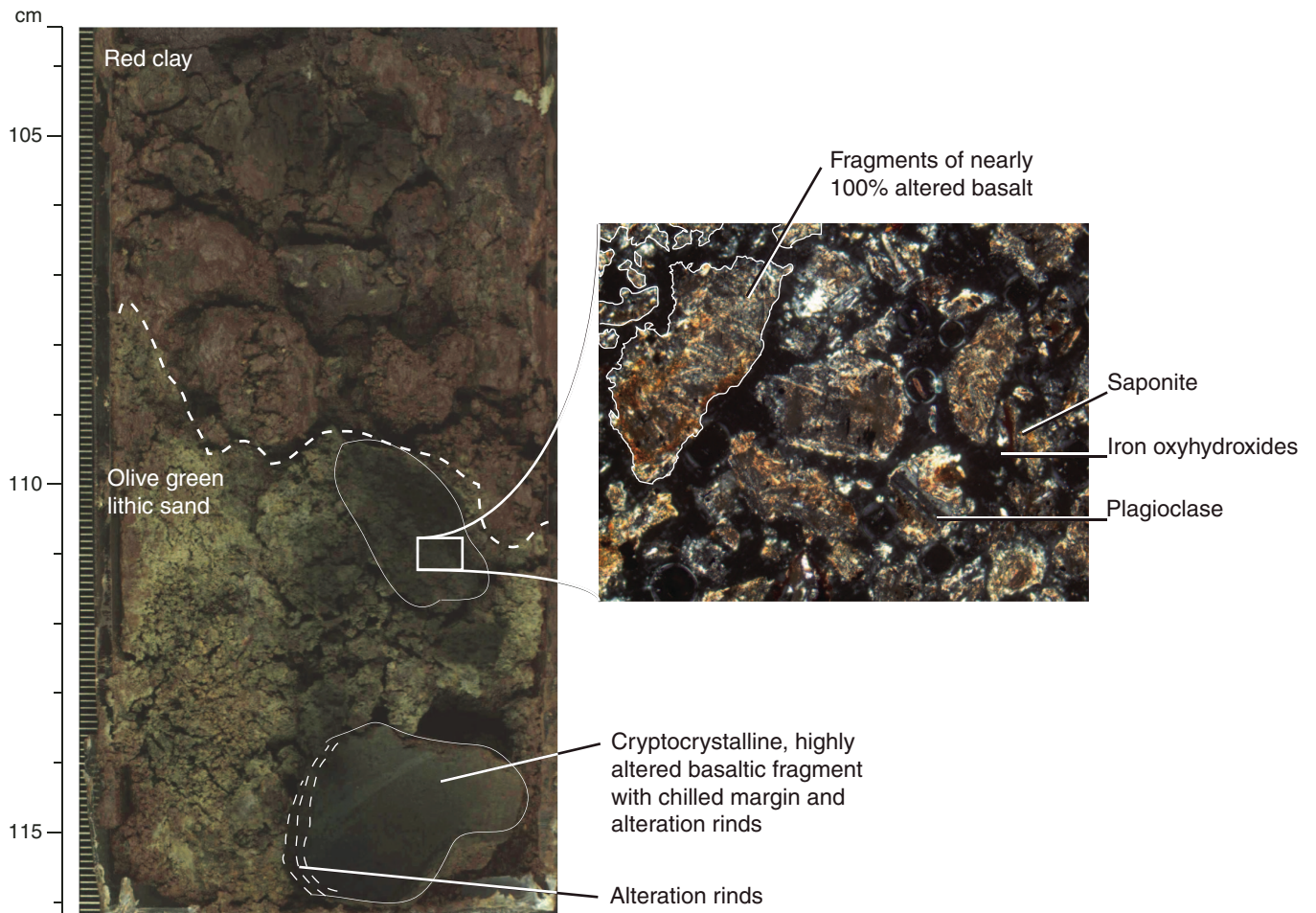


Figure F14. Plots of combined results of density and porosity measurements, Site U1366. **A.** Gamma ray attenuation (GRA) density measured with the Whole-Round Multisensor Logger on whole-round core sections (small circles) and wet bulk density measured on discrete samples using the mass/volume method (large circles). **B.** Grain density measured on discrete samples using moisture and density (MAD) mass/volume methods. **C.** Porosity determined using MAD Method C.

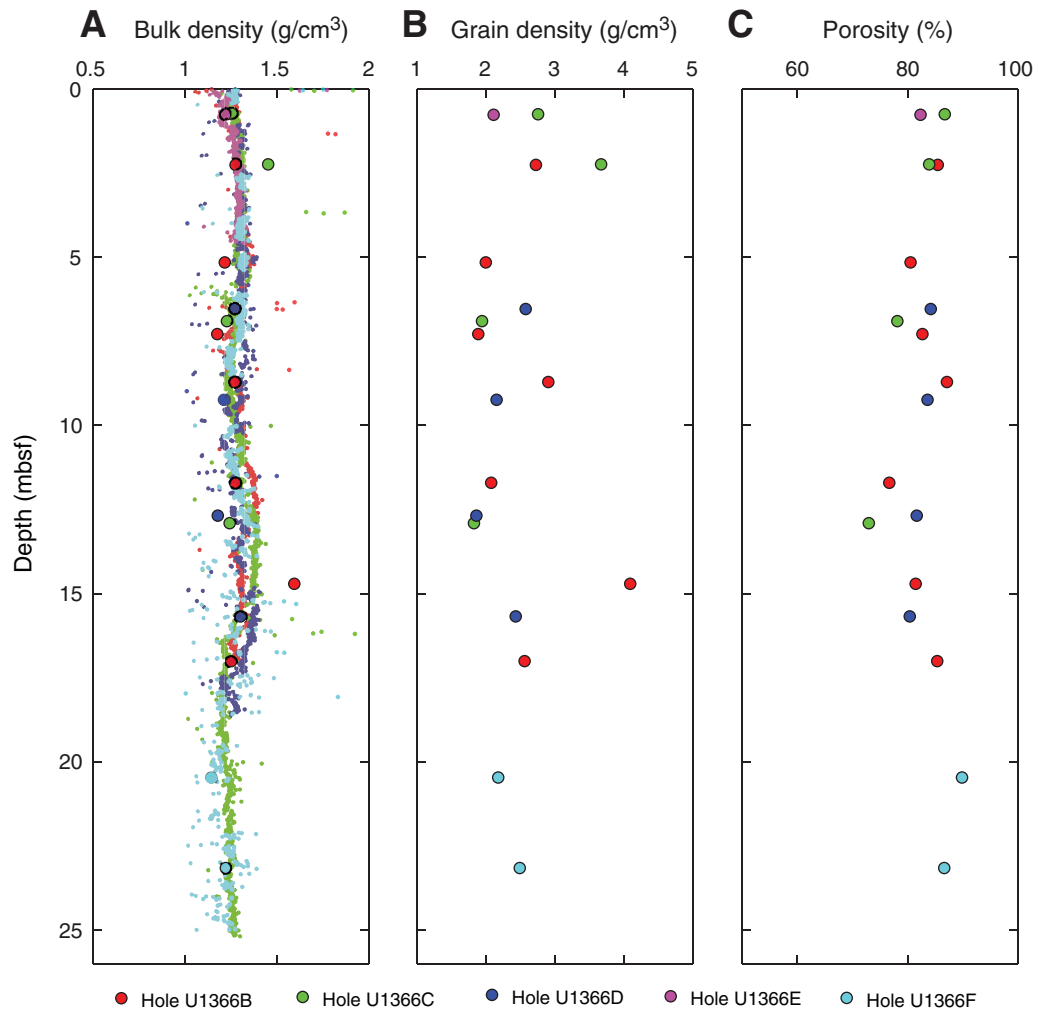


Figure F15. Plots of (A–D) magnetic susceptibility measurements made on the Whole-Round Multisensor Logger and (E–H) point magnetic susceptibility measurements made on the Section Half Multisensor Logger.

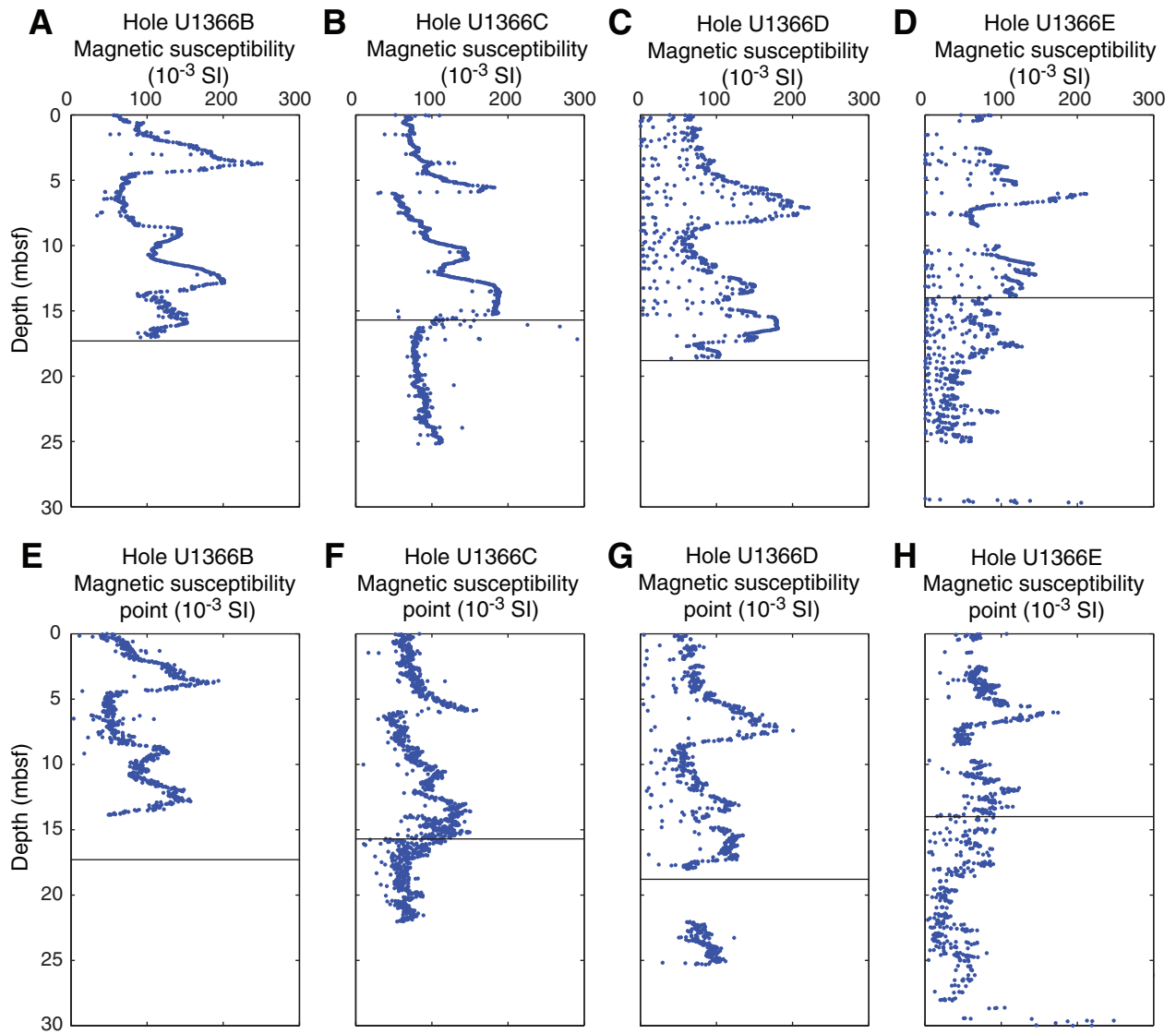


Figure F16. Plots of natural gamma radiation (NGR) as a function of depth for Holes (A) U1366B, (B) U1366C, (C) U1366D, and (D) U1366E.

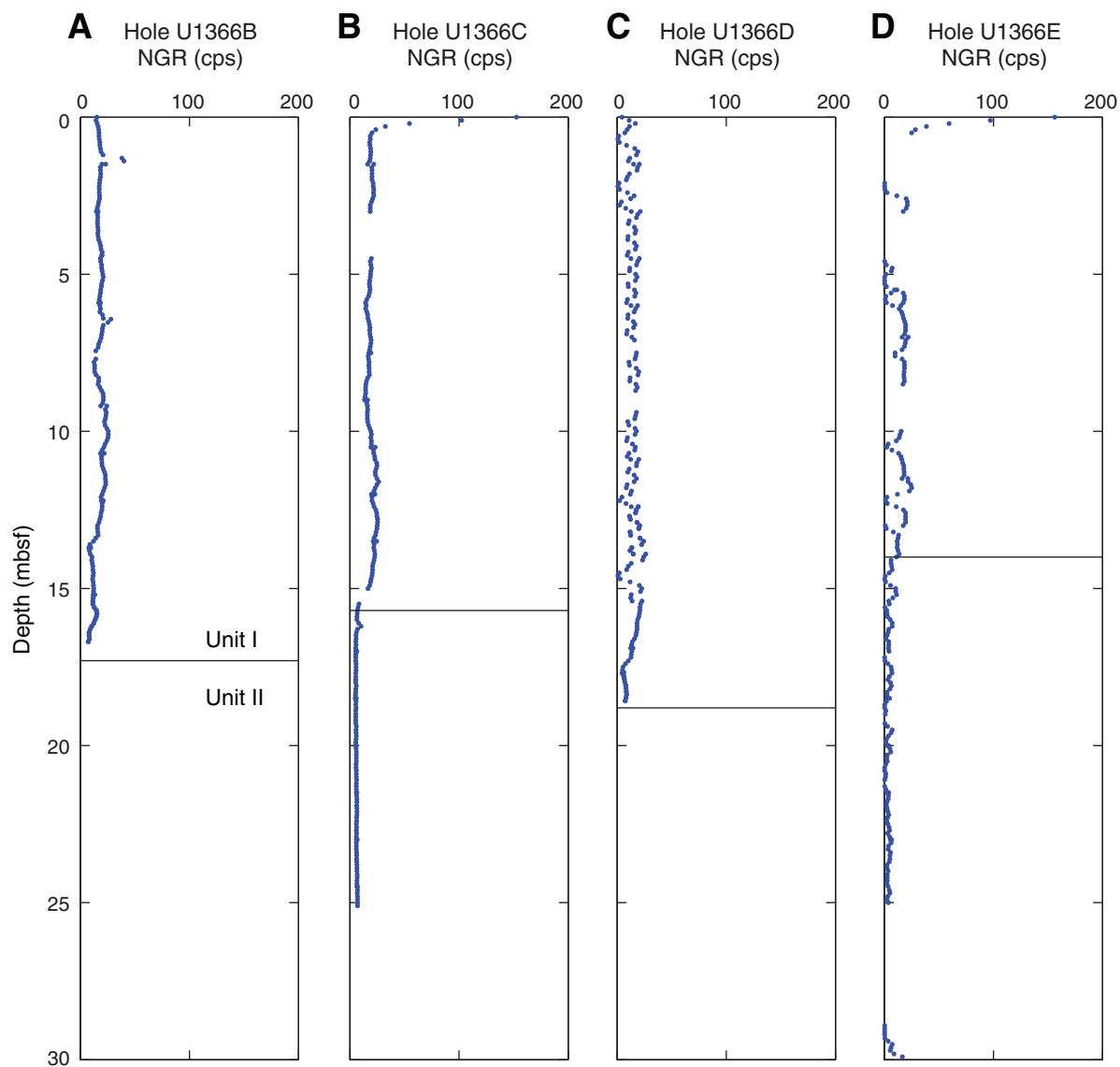


Figure F17. Plots of natural gamma radiation (NGR) analyses of the uppermost section of Hole U1366E. Circles show measurements on section as a function of depth, dashed lines show nodule concentrations of uranium, thorium, and their ratio in their respective panels.

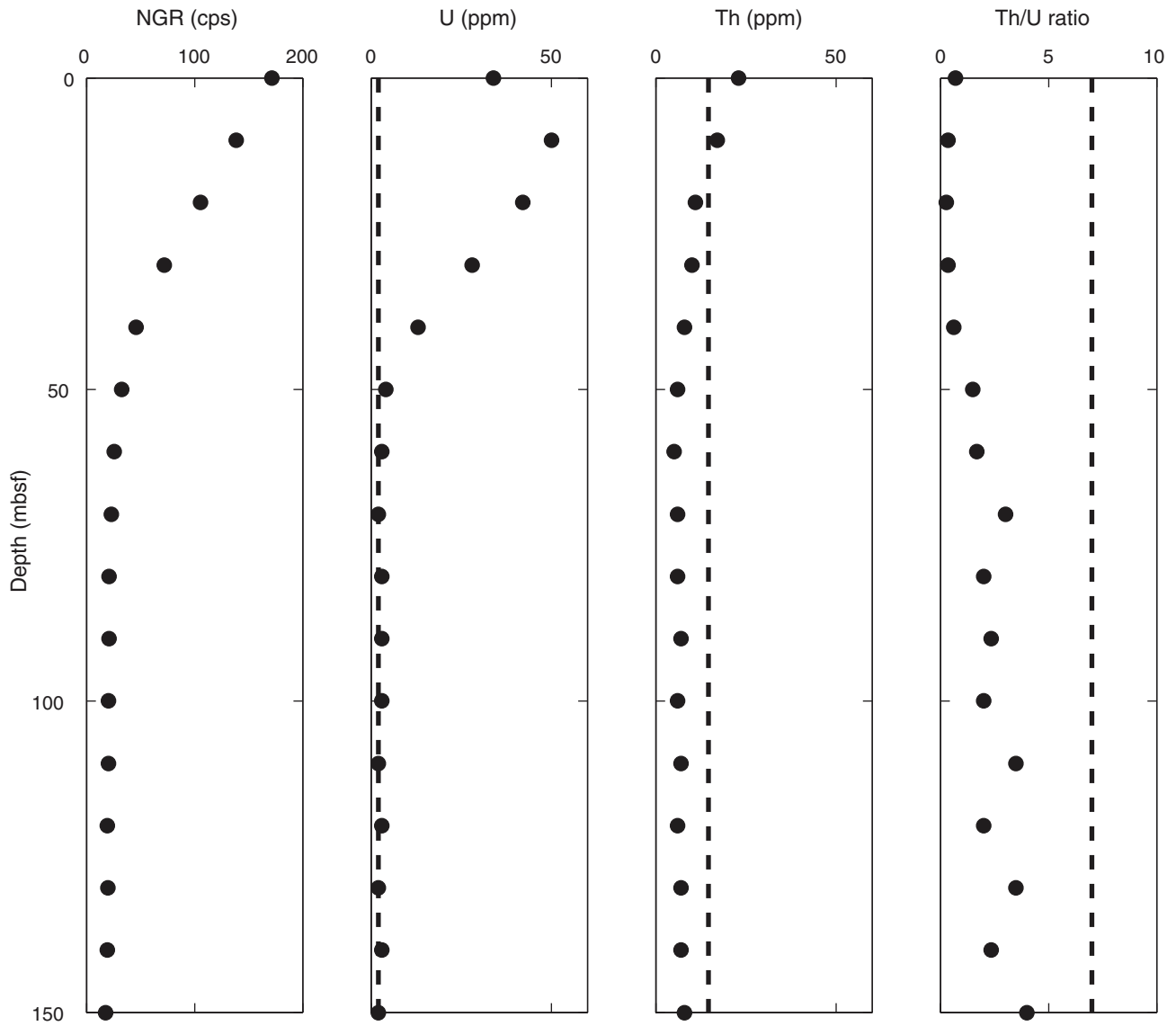


Figure F18. A. Plots of compressional wave velocity measured on the WRMSL for Holes U1366B–U1366D and U1366F. Red = discrete measurements along *x*-axis. B. Histogram of *P*-wave velocity from all holes.

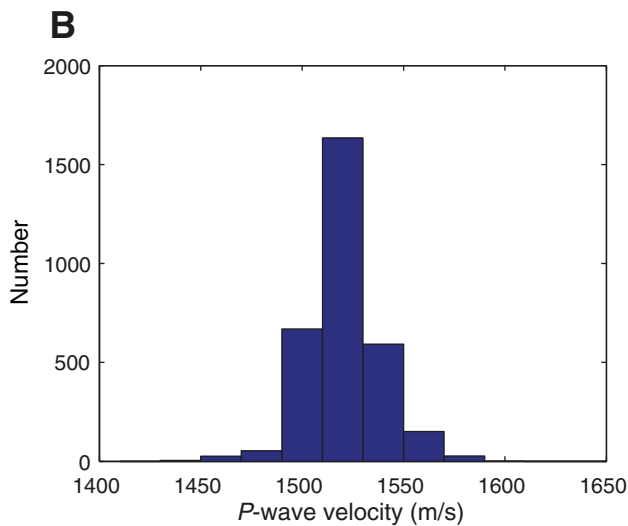
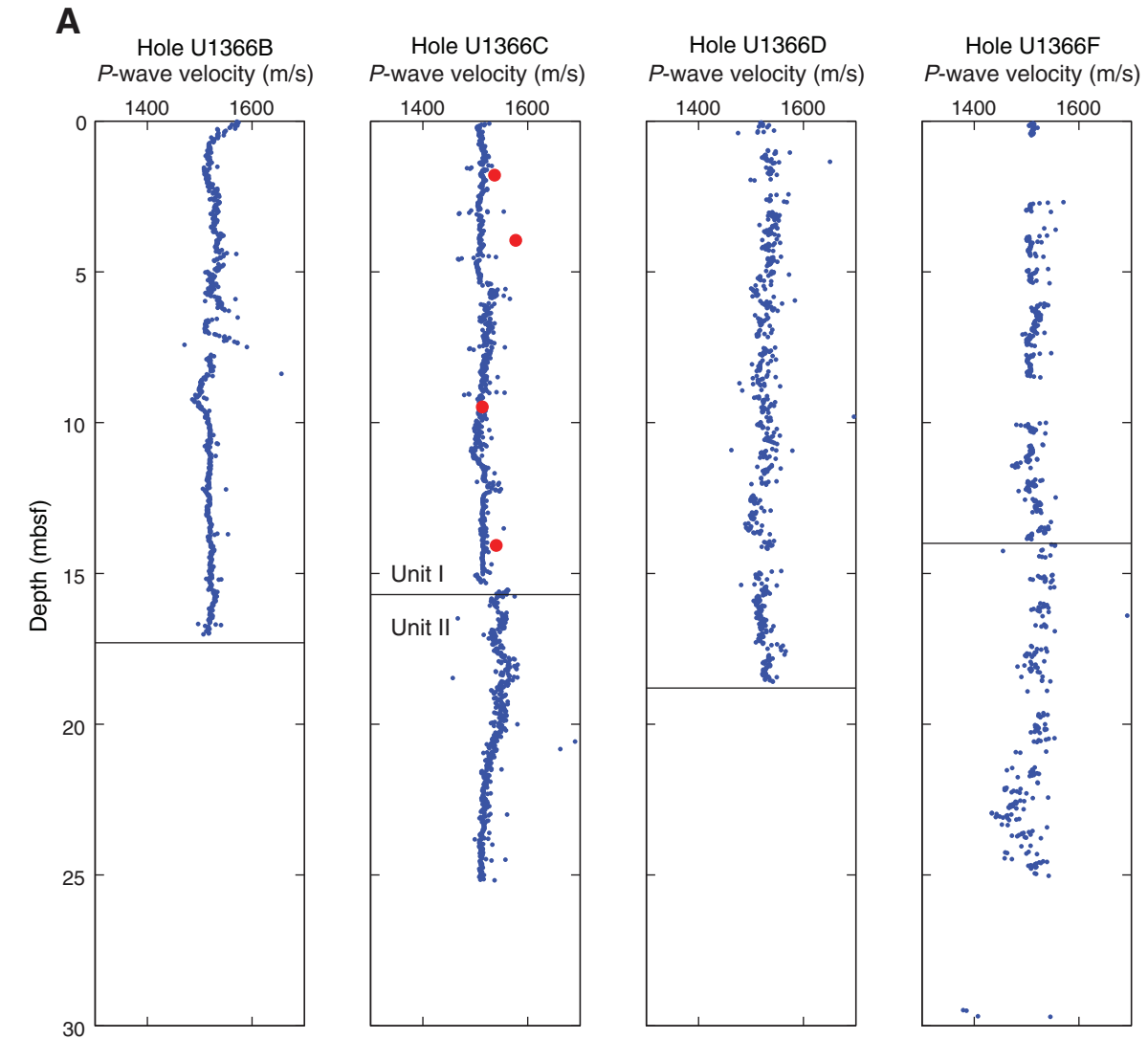


Figure F19. Plot of electrical conductivity measured on IAPSO standard and on surface seawater. Line shows best linear fit to data. Best fitting slope and y -intercept are -0.0071 mS/m/measurement number and 50.6345 mS/m, respectively.

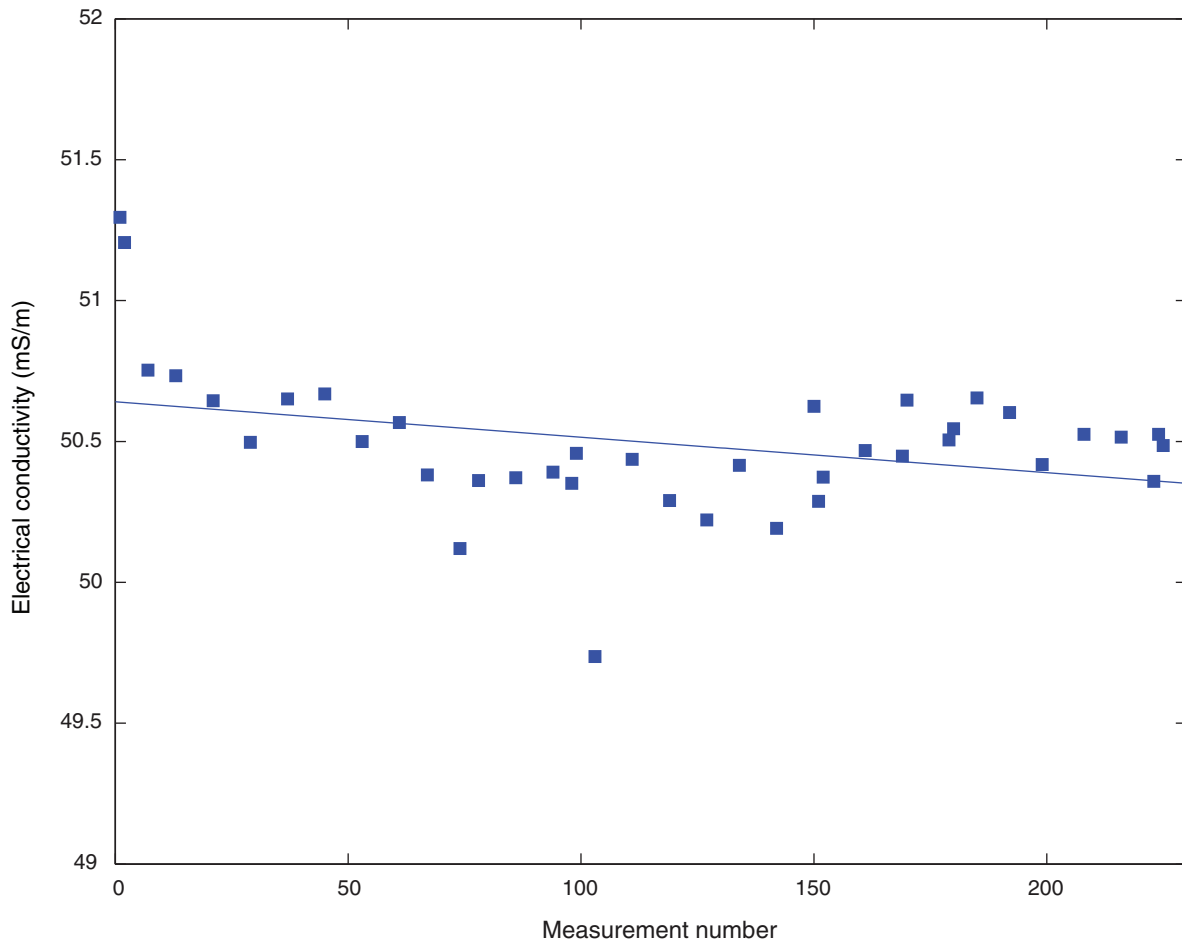


Figure F20. Plot of formation factor as a function of depth, Holes U1366C (blue) and U1366F (red).

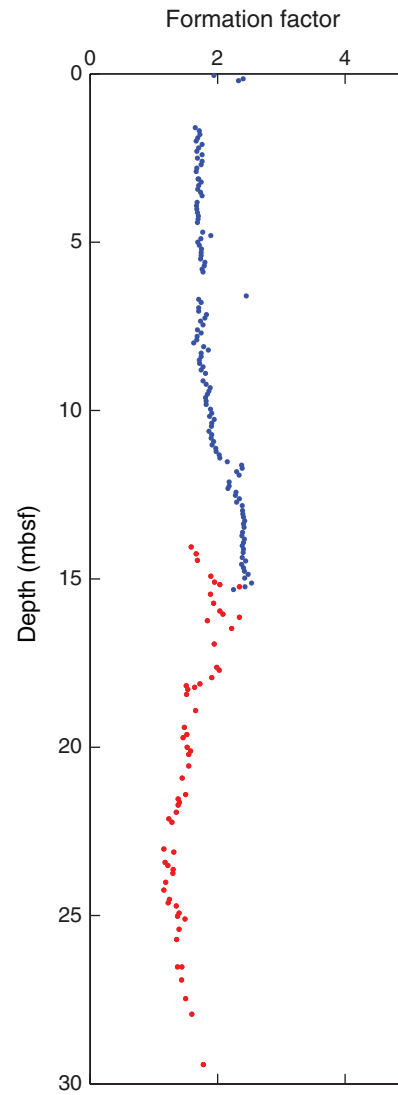


Figure F21. Plot of full-space thermal conductivity measurements, Site U1366. Open circles are unreliable likely because of fluid convection within the sample. Solid blue circles denote values from Site U1366 and red circles denote values from the site survey cruise at this location. The mean of the reliable measurements in lithologic Units I and III is $0.8 \text{ W}/(\text{m}\cdot\text{K})$.

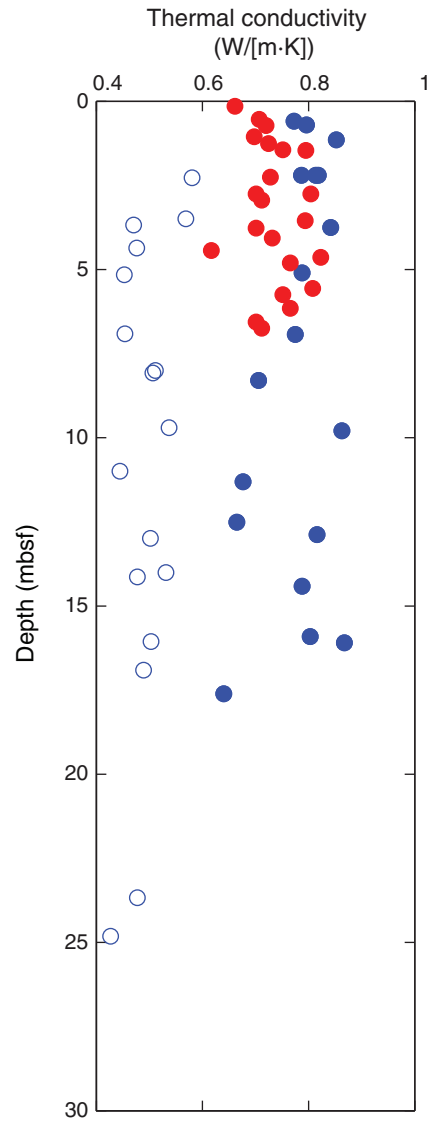


Figure F22. Plots of color spectrometry L* values, Holes U1366B–U1366E.

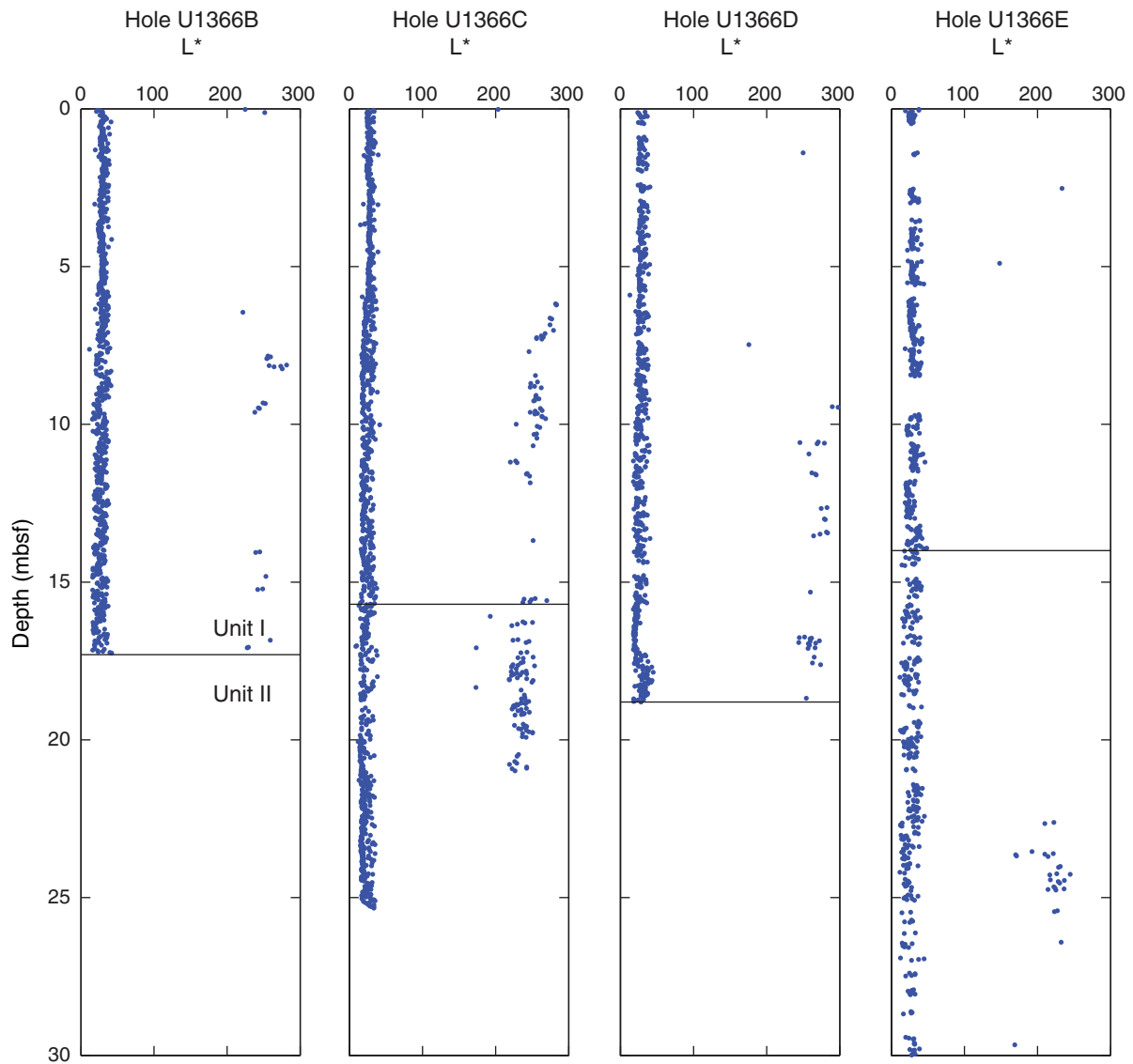


Figure F23. Plots of color spectrometry a* values, Holes U1366B–U1366E.

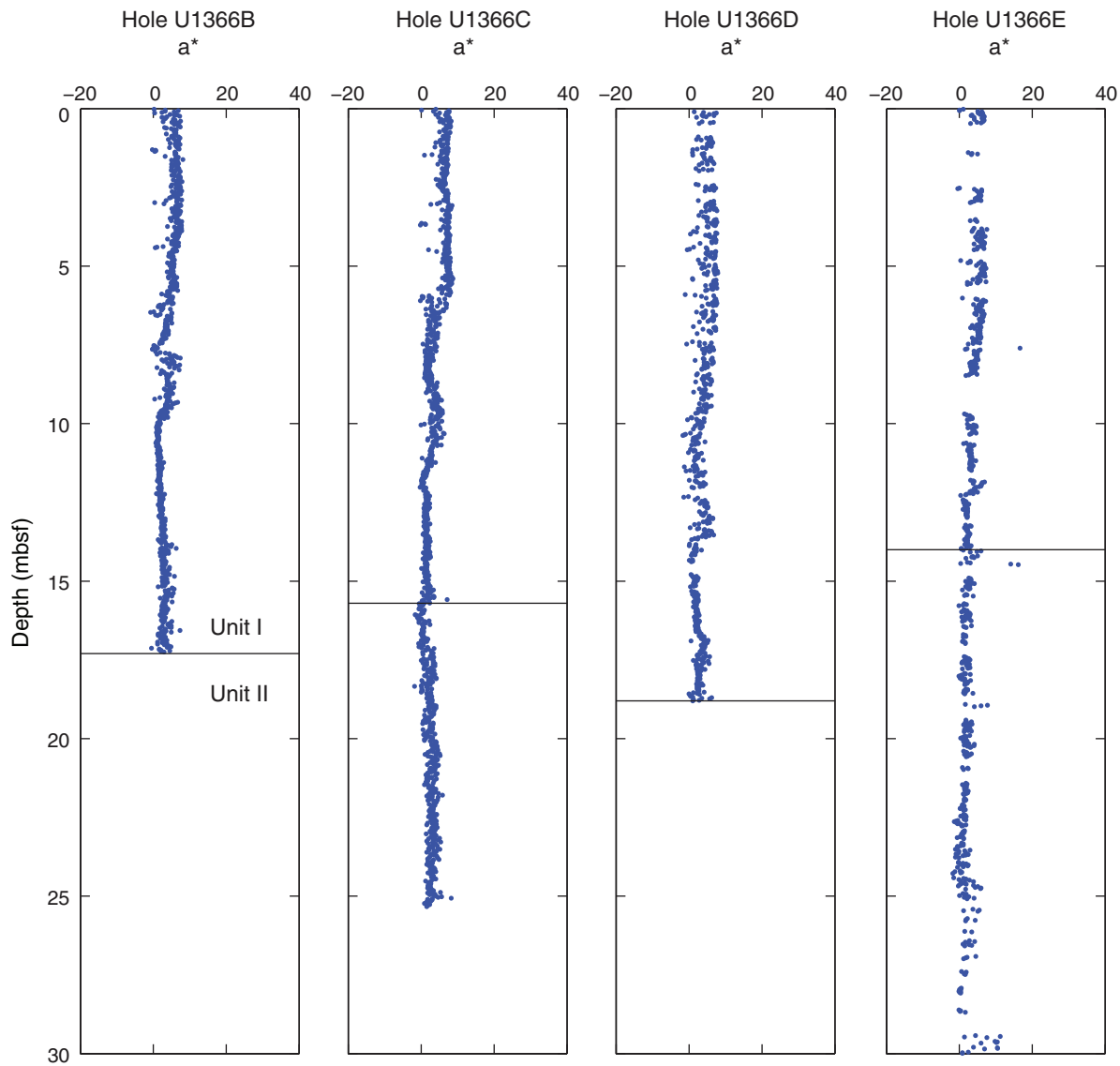


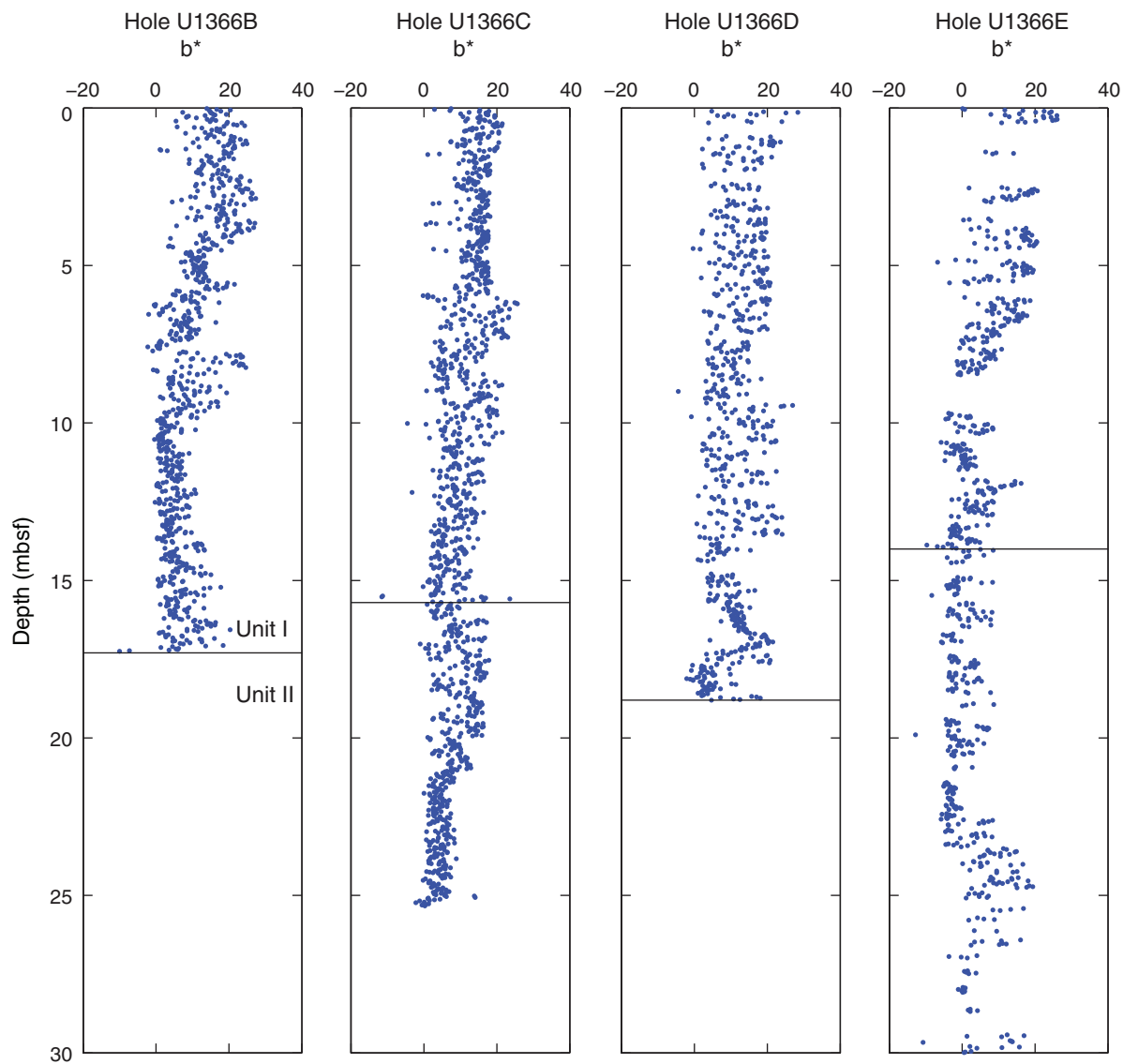
Figure F24. Plots of color spectrometry b^* values, Holes U1366B–U1366E.

Figure F25. Summary of magnetic susceptibility and paleomagnetic intensity, Hole U1366B. Gray = measurement before demagnetization, red = measurement after 20 mT AF demagnetization step (inclination and intensity), blue = declination measurements, green = magnetic susceptibility data.

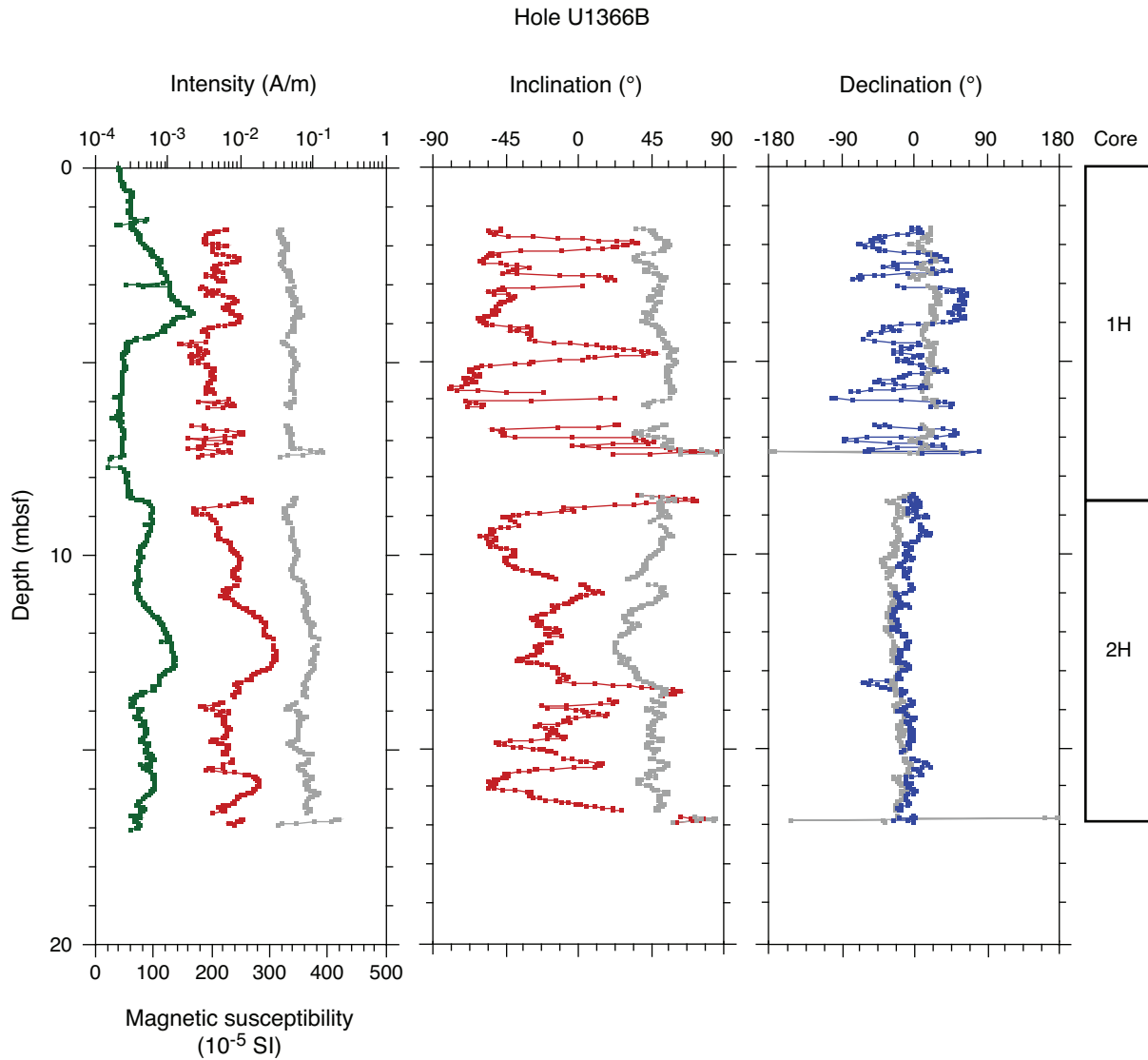


Figure F26. Summary of magnetic susceptibility and paleomagnetic results, Hole U1366C. Gray = measurement before demagnetization, red = measurement after 20 mT AF demagnetization step (inclination and intensity), blue = declination measurements, green = magnetic susceptibility data. Black squares = magnetic directions of discrete cube samples from the working-half cores.

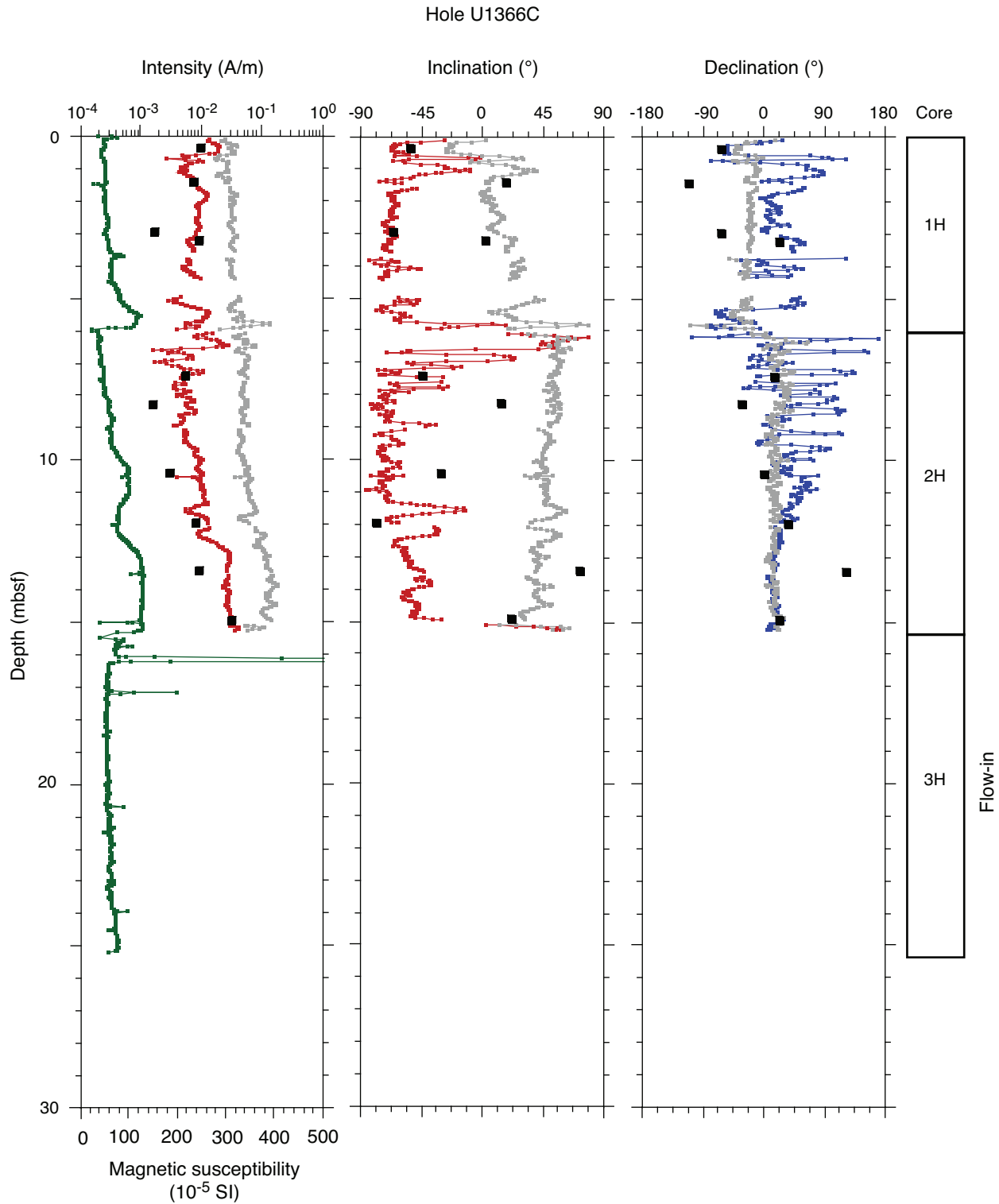


Figure F27. Summary of magnetic susceptibility and paleomagnetic results, Hole U1366D. Gray = measurement before demagnetization, red = measurement after 20 mT AF demagnetization step (inclination and intensity), blue = declination measurements, green = magnetic susceptibility data.

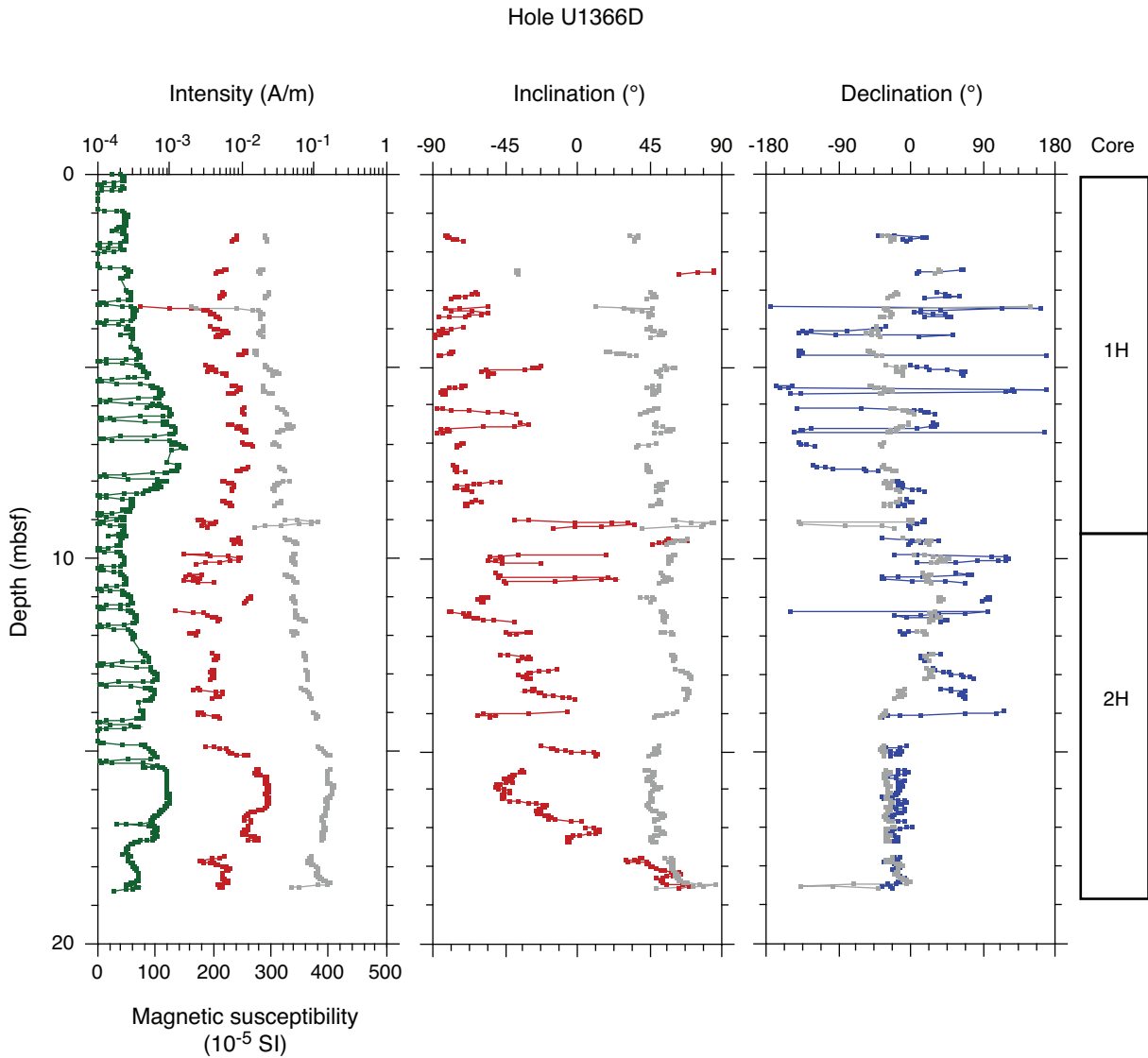


Figure F28. Summary of magnetic susceptibility and paleomagnetic results, Hole U1366E. Gray = measurement before demagnetization, red = measurement after 20 mT AF demagnetization step (inclination and intensity), blue = declination measurements, green = magnetic susceptibility data.

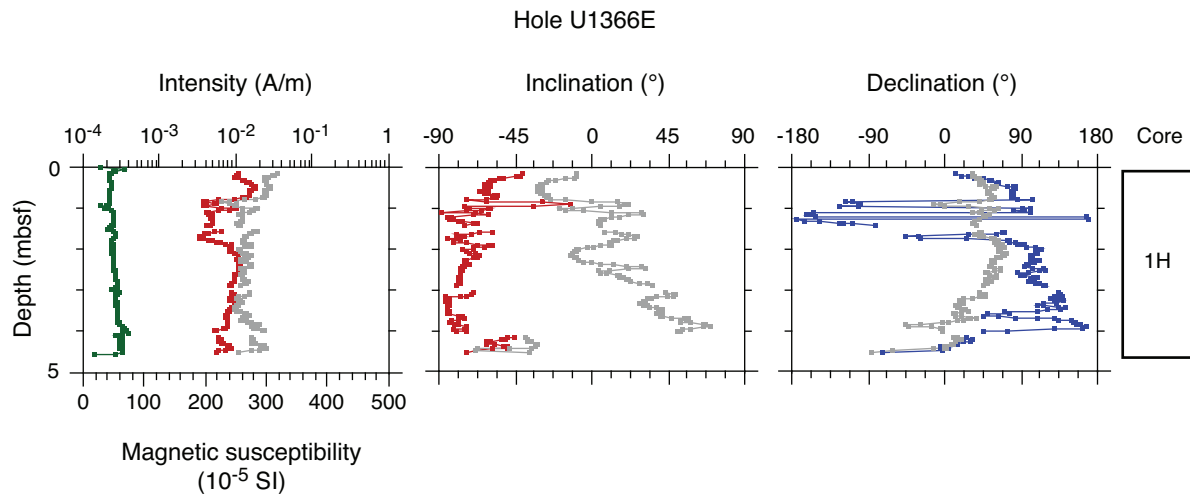


Figure F29. Summary of magnetic susceptibility and paleomagnetic results, Hole U1366F. Gray = measurement before demagnetization, red = measurement after 20 mT AF demagnetization step (inclination and intensity), blue = declination measurements, green = magnetic susceptibility data.

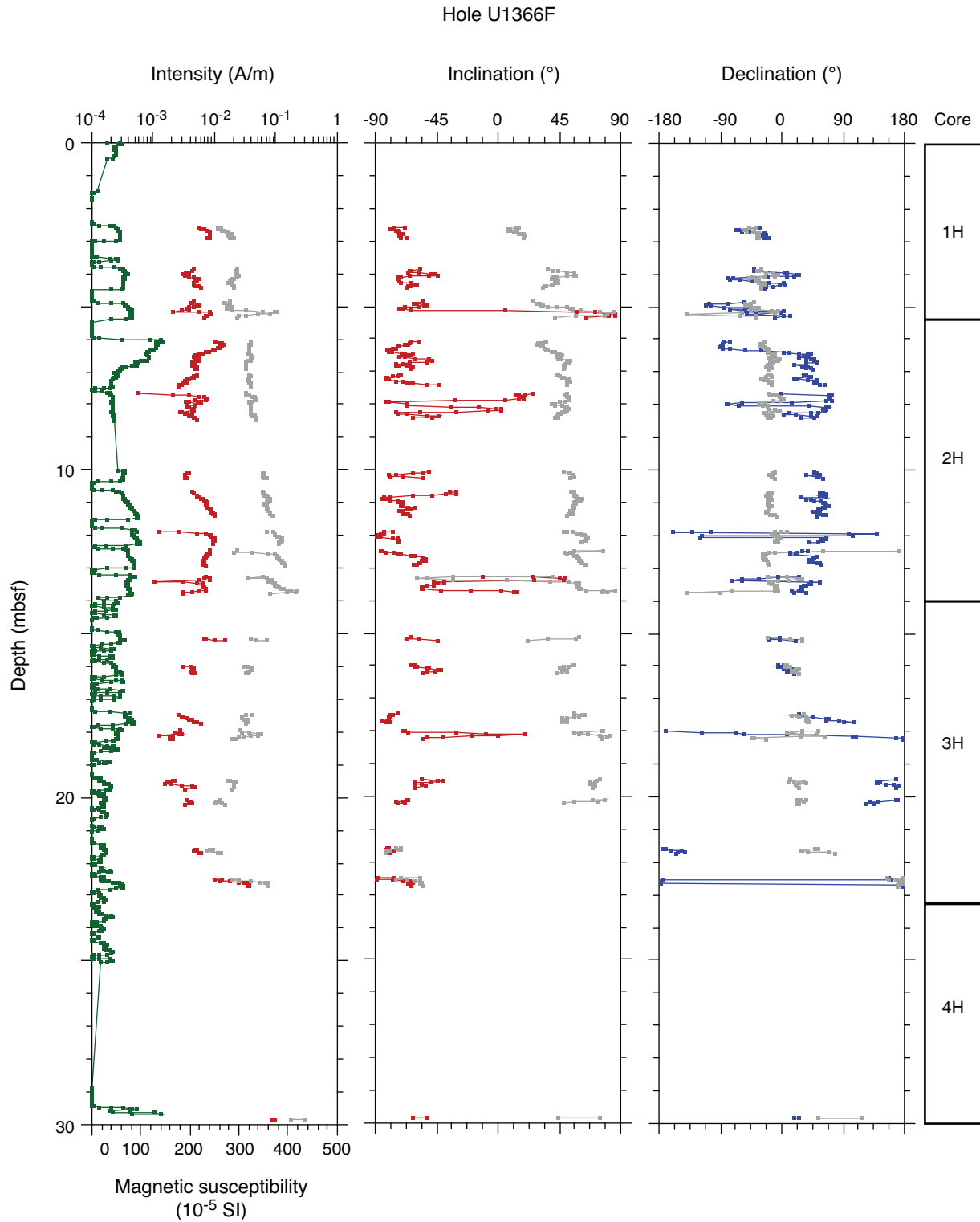




Figure F30. Plots of combined dissolved oxygen optode and electrode data, Site U1366. **A.** Combined optode measurements in Holes U1366C and U1366F. **B.** Electrode data for Holes U1366B–U1366D and U1366F. **C.** Comparison of electrode and optode data in the uppermost 10 m in Hole U1366C.

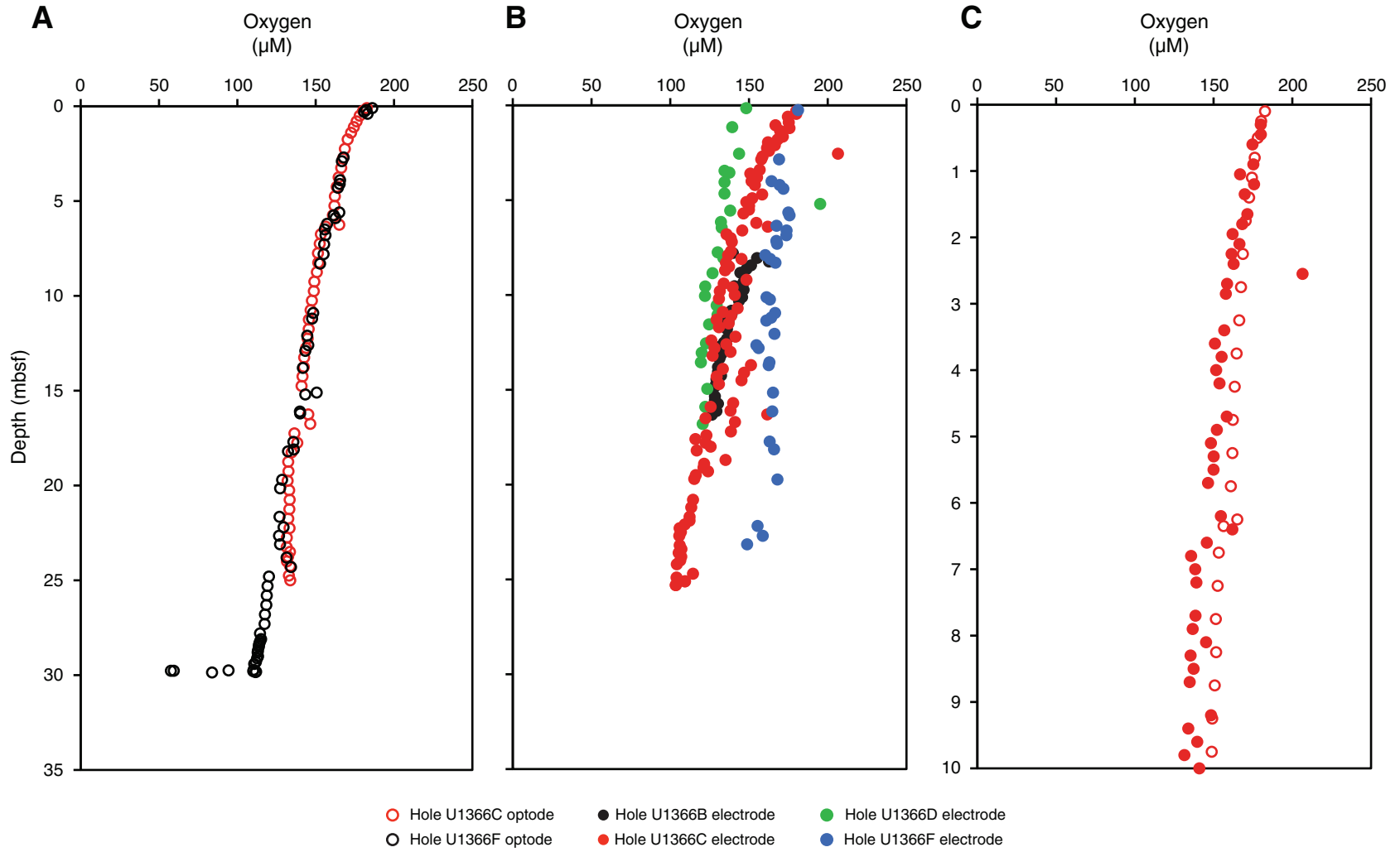




Figure F32. Plots of dissolved interstitial water constituents, Site U1366. Black and red circles represent samples taken either as whole rounds for squeezing or using Rhizon samplers. Blue triangles represent samples taken as whole rounds directly from the Hold Deck refrigerator for “whole round stored shorter” (WSS) analyses. IC = ion chromatography, ICP = inductively coupled plasma–atomic emission spectroscopy. **A.** Nitrate. **B.** Phosphate. **C.** Silicate. **D.** Alkalinity. **E.** Dissolved inorganic carbon (DIC). (Continued on next three pages.)

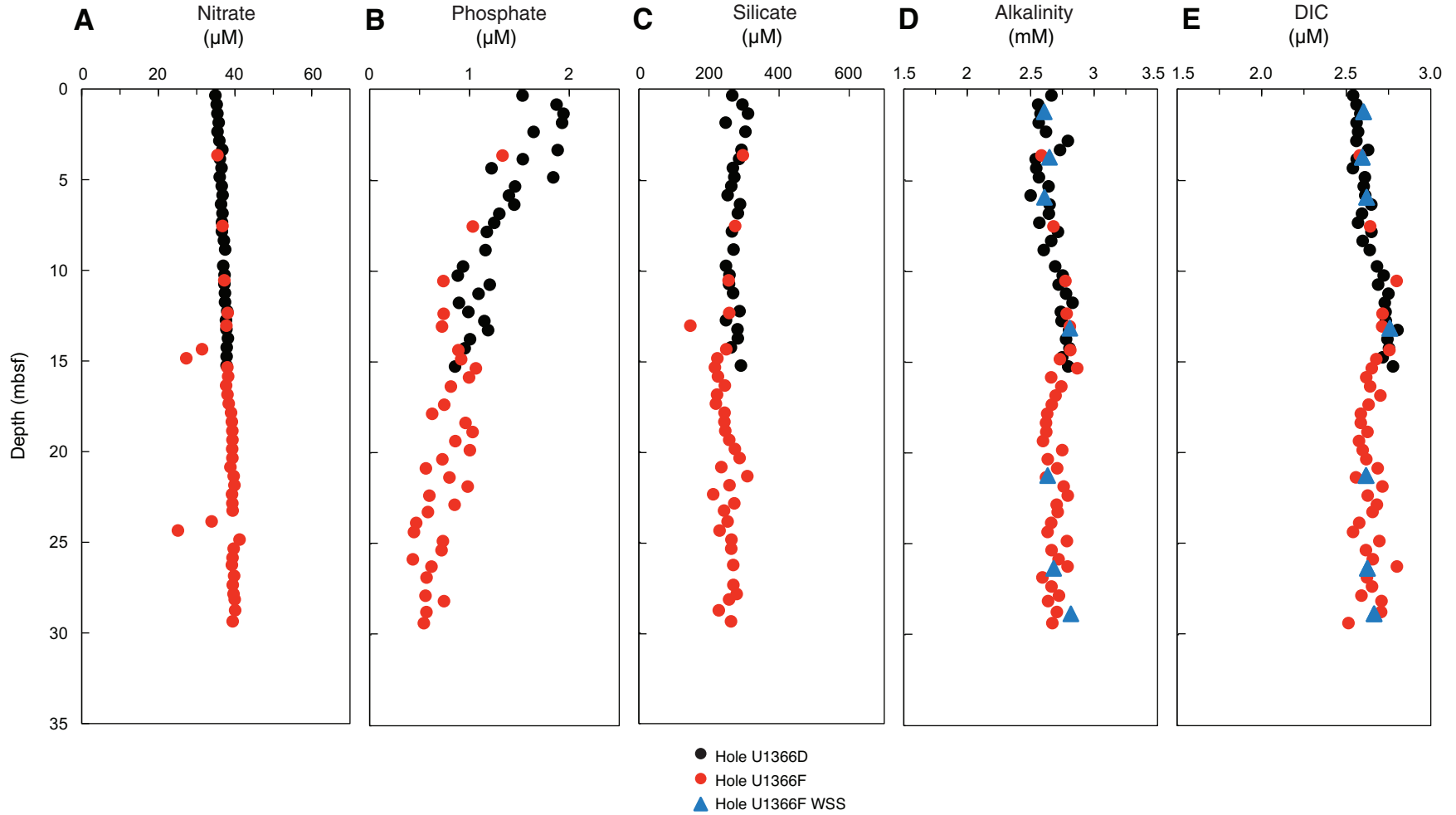




Figure F32 (continued). F. Sulfate. G. Sulfate anomaly H. Chloride. I. Calcium. J. Magnesium. (Continued on next page.)

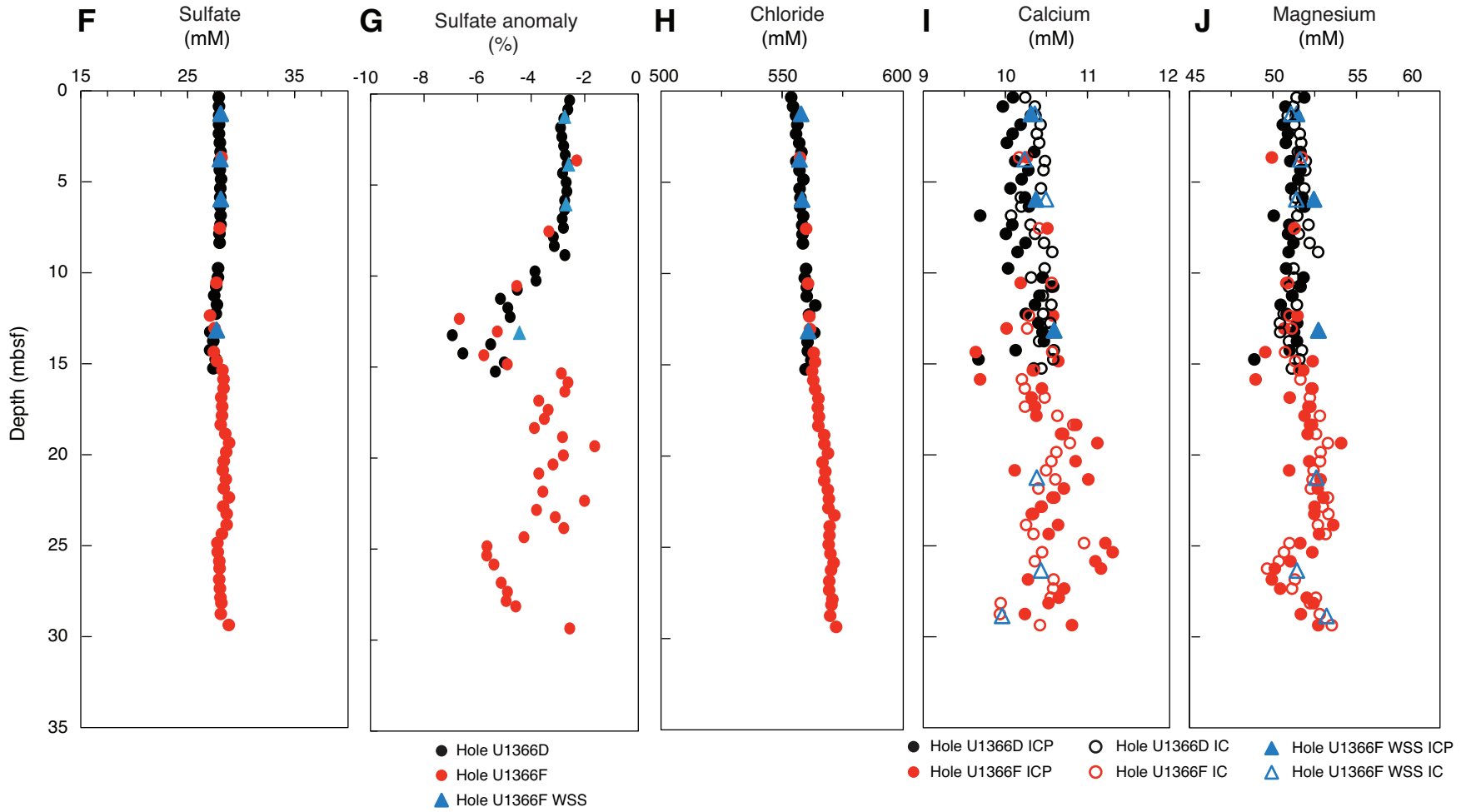




Figure F32 (continued). K. Strontium. L. Sodium. M. Potassium. N. Boron. O. Iron. (Continued on next page.)

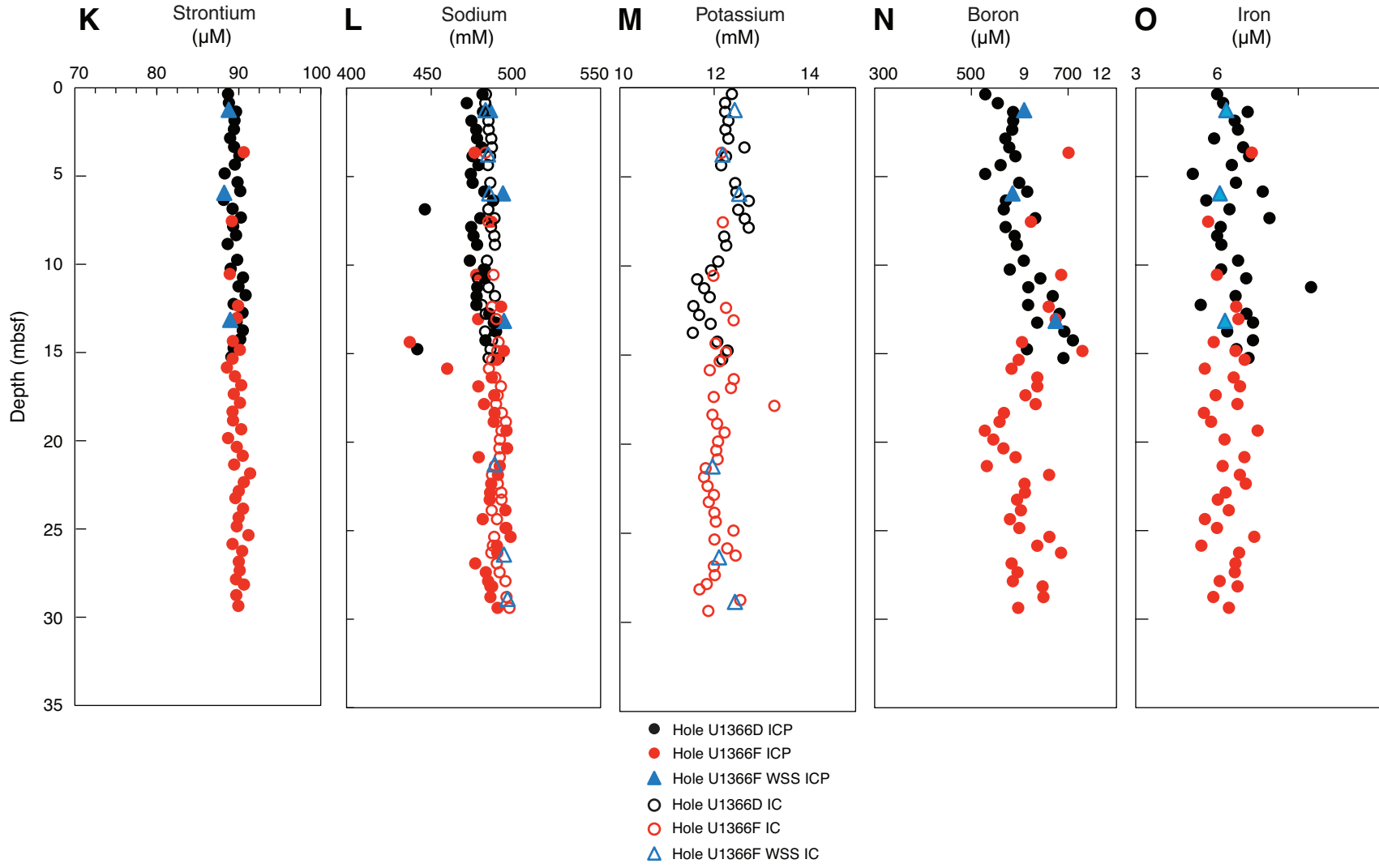




Figure F32 (continued). P. Manganese.

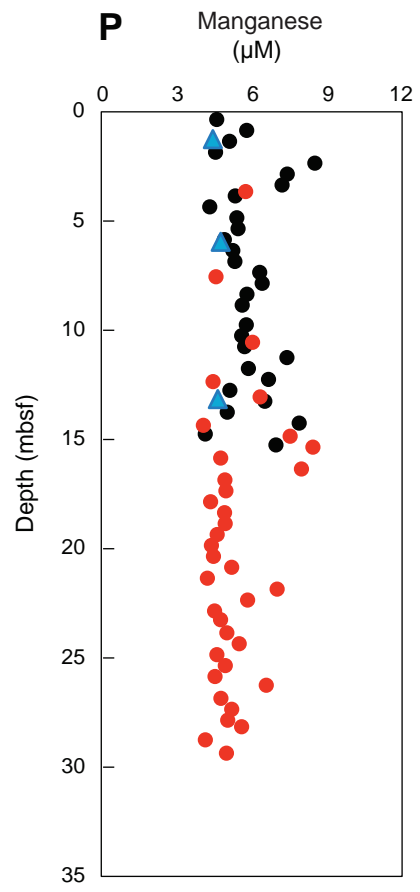


Figure F33. Plots of solid-phase nitrogen and carbon content, Holes U1366D and U1366F. WSS = whole round stored shorter. **A.** Total nitrogen (TN). **B.** Total organic carbon (TOC). **C.** Calcium carbonate (CaCO₃).

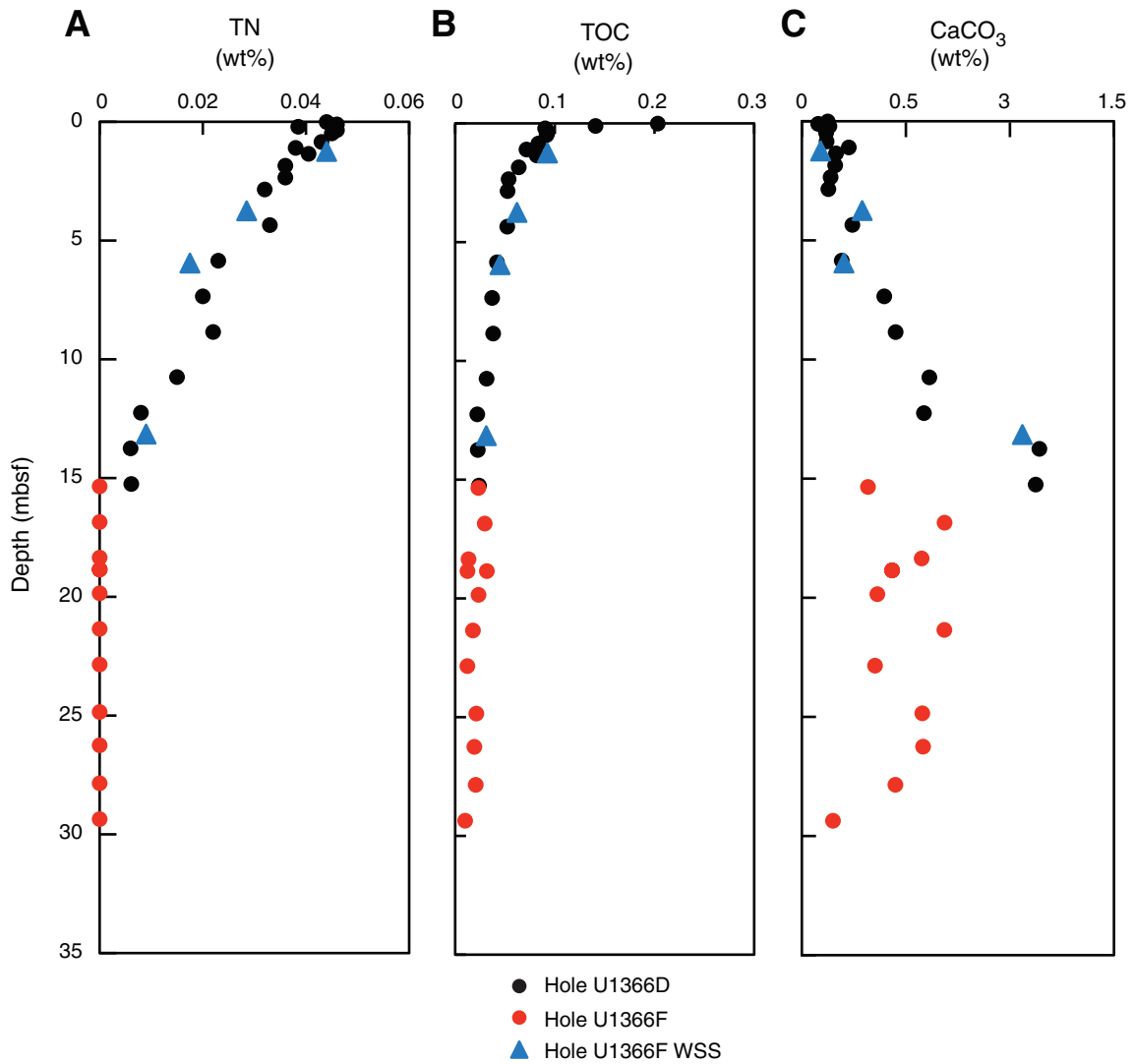


Figure F34. Plot of abundances of microbial cells and virus-like particles in Site U1366 sediment quantified by epifluorescence microscopy. Counts below the blank are shown as 10^2 cells/cm³ in order to present them in the graph. See “**Microbiology**” in the “Methods” chapter (Expedition 329 Scientists, 2011a) for a detailed description of the blank and minimum detection limit (MDL) calculation. Red line = MDL for cell counts from extracts, blue line = MDL for nonextracted samples, solid red circles = extracted cell counts above the MDL, open red circles = extracted counts below the MDL, solid black squares = VLP counts, open blue diamonds = nonextracted counts below the MDL.

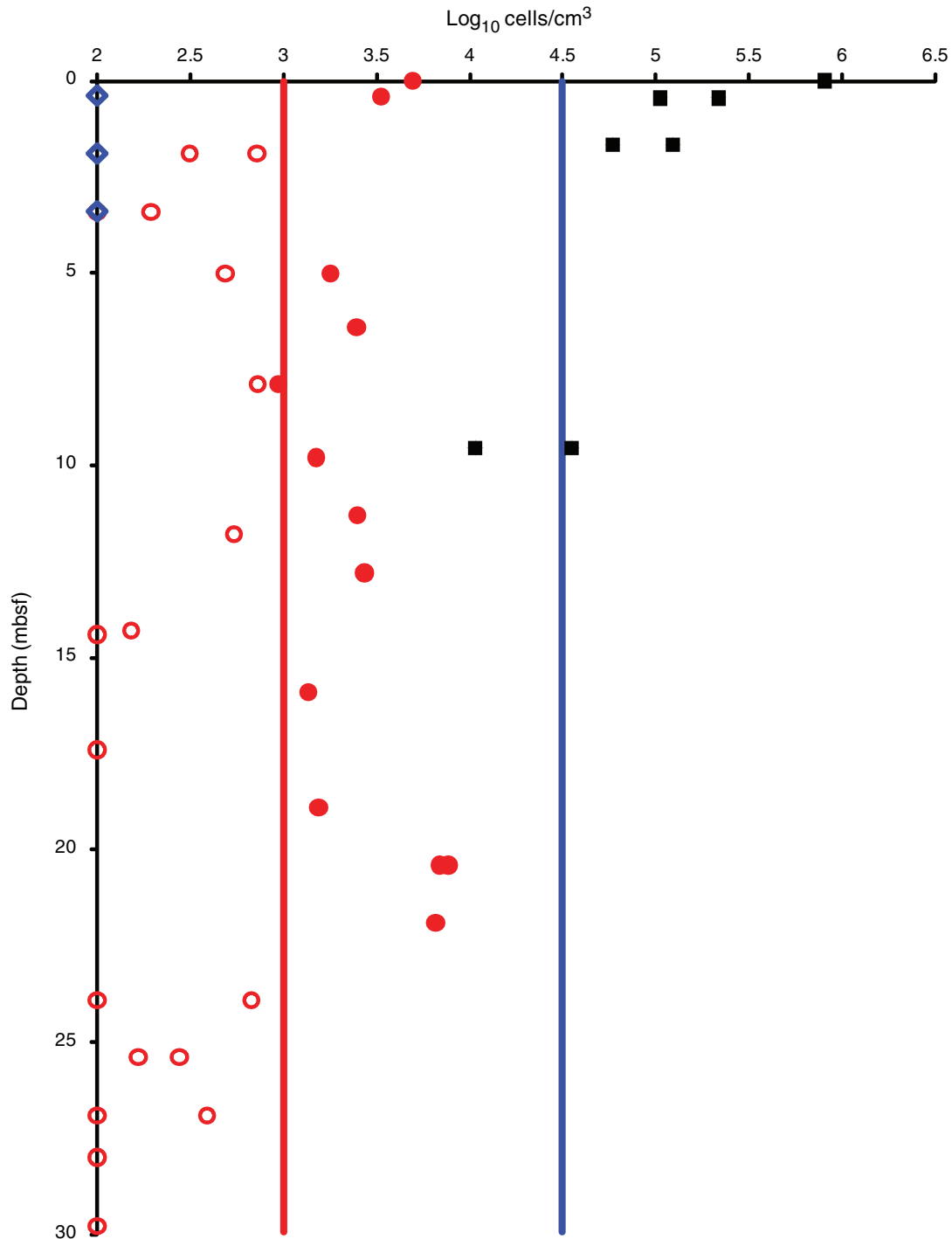


Table T1. Operations summary, Site U1366. (Continued on next page.)**Hole U1366A**

Latitude: 26°3.0945'S
 Longitude: 156°53.6591'W
 Time on hole (h): 10.5
 Seafloor (drill pipe measurement below rig floor, m DRF): 5146.0
 Distance between rig floor and sea level (m): 11.2
 Water depth (drill pipe measurement from sea level, mbsl): 5135
 Total penetration (drilling depth below seafloor, m DSF): 17.8
 Total length of cored section (m): washdown to basement
 Total core recovered (m): NA
 Core recovery (%): NA
 Total number of cores: NA

Hole U1366B

Latitude: 26°3.0950'S
 Longitude: 156°53.6714'W (20 m west of Hole U1366A)
 Time on hole (h): 4.25
 Seafloor (drill pipe measurement below rig floor, m DRF): 5141.8
 Distance between rig floor and sea level (m): 11.2
 Water depth (drill pipe measurement from sea level, mbsl): 5130.8
 Total penetration (drilling depth below seafloor, m DSF): 17.2
 Total length of cored section (m): 17.2
 Total core recovered (m): 17.31
 Core recovery (%): 100.6
 Total number of cores: 2

Hole U1366C

Latitude: 26°3.0845'S
 Longitude: 156°53.6700'W (20 m north of Hole U1366B)
 Time on hole (h): 4.25
 Seafloor (drill pipe measurement below rig floor, m DRF): 5140.5
 Distance between rig floor and sea level (m): 11.2
 Water depth (drill pipe measurement from sea level, mbsl): 5129.5
 Total penetration (drilling depth below seafloor, m DSF): 25
 Total length of cored section (m): 25
 Total core recovered (m): 25.42
 Core recovery (%): 101.7
 Total number of cores: 3

Hole U1366D

Latitude: 26°3.0850'S
 Longitude: 156°53.6652'W (20 m east of Hole U1366C)
 Time on hole (h): 6.25
 Seafloor (drill pipe measurement below rig floor, m DRF): 5137.1
 Distance between rig floor and sea level (m): 11.2
 Water depth (drill pipe measurement from sea level, mbsl): 5126.1
 Total penetration (drilling depth below seafloor, m DSF): 20.9
 Total length of cored section (m): 18.9
 Total core recovered (m): 18.86
 Core recovery (%): 99.8
 Total number of cores: 3

Hole U1366E

Latitude: 26°3.0843'S
 Longitude: 156°53.6825'W (40 m west of Hole U1366D)
 Time on hole (h): 0.75
 Seafloor (drill pipe measurement below rig floor, m DRF): 5138.8
 Distance between rig floor and sea level (m): 11.2
 Water depth (drill pipe measurement from sea level, mbsl): 5127.8
 Total penetration (drilling depth below seafloor, m DSF): 4.7
 Total length of cored section (m): 4.7
 Total core recovered (m): 4.71
 Core recovery (%): 100.2
 Total number of cores: 1

Table T1 (continued).

Hole U1366F

Latitude: 26°3.0836'S
 Longitude: 156°53.6937'W (20 m west of Hole U1366E)
 Time on hole (h): 18
 Seafloor (drill pipe measurement below rig floor, m DRF): 5138.0
 Distance between rig floor and sea level (m): 11.2
 Water depth (drill pipe measurement from sea level, mbsl): 5127.0
 Total penetration (drilling depth below seafloor, m DSF): 30.1
 Total length of cored section (m): 30.1
 Total core recovered (m): 30.15
 Core recovery (%): 100.2
 Total number of cores: 4

Core	Date (2010)	Time (h)	Depth DSF (m)		Interval advanced (m)	Depth CSF (m)		Length of core recovered (m)	Recovery (%)	Sections (N)	Coring shoe type	Remarks
			Top of cored interval	Bottom of cored interval		Top of cored interval	Bottom of cored interval					
320-U1366A-1H	30 Oct	2000	0.0	17.8	17.8	0.0	0.00	0.00	0	0		
320-U1366B-1H	30 Oct	2115	0.0	7.7	7.7	0.0	7.73	7.73	100	7	STD	
320-U1366B-2H	30 Oct	2250	7.7	17.2	9.5	7.7	17.28	9.58	101	8	STD	
320-U1366C-1H	31 Oct	0015	0.0	6.0	6.0	0.0	6.04	6.04	101	5	STD	
320-U1366C-2H	31 Oct	0135	6.0	15.5	9.5	6.0	15.53	9.53	100	8	STD	
320-U1366C-3H	31 Oct	0300	15.5	25.0	9.5	15.5	25.35	9.85	104	8	STD	
320-U1366D-1H	31 Oct	0430	0.0	9.4	9.4	0.0	9.44	9.44	100	8	STD	
320-U1366D-2H	31 Oct	0600	9.4	18.9	9.5	9.4	18.82	9.42	99	8	STD	
320-U1366D-3H	31 Oct	0725	18.9	18.9	0.0	18.9	18.90	0.00	0	0	STD	
320-U1366D-4X	31 Oct	0910	18.9	20.9	2.0	18.9	18.90	0.00	0	0		Changed to XCB
320-U1366E-1H	31 Oct	1040	0.0	4.7	4.7	0.0	4.71	4.71	100	5	STD	
320-U1366F-1H	31 Oct	1215	0.0	5.5	5.5	0.0	5.54	5.54	101	5	STD	
320-U1366F-2H	31 Oct	1340	5.5	14.0	8.5	5.5	14.00	8.50	100	7	STD	
320-U1366F-3H	31 Oct	1515	14.0	23.5	9.5	14.0	23.47	9.47	100	8	STD	
320-U1366F-4H	31 Oct	1700	23.5	30.1	6.6	23.5	30.14	6.64	101	6	STD	
Advanced total:					115.7			96.45	99	83		
Total interval cored:					95.9							

NA = not applicable. DSF = drilling depth below seafloor, CSF = core depth below seafloor. H = APC core, X = extended core barrel (XCB) core. STD = standard. Time is UTC.

Table T2. Formation factor measurements, Site U1366. (Continued on next two pages.)

Core, section, interval (cm)	Depth (mbsf)	Measurement number	Temperature-corrected seawater conductivity (mS/cm)	Sediment temperature (°C)	Sediment electrical conductivity (mS/cm)	Correction factor at 20°C (mS/cm)	Sediment electrical conductivity at 20°C (mS/cm)	Drift-corrected sediment electrical conductivity at 20°C (mS/cm)	Formation factor
329-U1366C-									
1H-1, 5	0.05	100	50.64	20.00	25.94	47.89	25.94	26.00	1.94
1H-1, 15	0.15	101	50.64	20.10	21.01	48.00	20.97	21.02	2.40
1H-1, 20	0.20	102	50.63	20.00	21.66	47.89	21.66	21.71	2.33
1H-2, 10	1.60	104	50.63	20.60	30.95	48.51	30.56	30.64	1.65
1H-2, 20	1.70	105	50.63	20.50	29.72	48.40	29.41	29.48	1.71
1H-2, 30	1.80	106	50.63	20.50	29.61	48.40	29.30	29.38	1.72
1H-2, 40	1.90	107	50.63	20.50	30.10	48.40	29.78	29.86	1.69
1H-2, 50	2.00	108	50.63	20.50	30.55	48.40	30.23	30.31	1.67
1H-2, 60	2.10	109	50.63	20.50	28.96	48.40	28.65	28.73	1.76
1H-2, 70	2.20	110	50.62	20.50	29.80	48.40	29.49	29.57	1.71
1H-2, 80	2.30	112	50.62	20.30	30.29	48.20	30.10	30.18	1.67
1H-2, 90	2.40	113	50.62	20.30	28.85	48.20	28.67	28.75	1.76
1H-2, 100	2.50	114	50.62	20.30	30.12	48.20	29.93	30.01	1.68
1H-2, 110	2.60	115	50.62	20.30	28.83	48.20	28.65	28.73	1.76
1H-2, 120	2.70	116	50.62	20.30	29.03	48.20	28.85	28.93	1.75
1H-2, 130	2.80	117	50.62	20.30	30.27	48.20	30.08	30.17	1.67
1H-2, 140	2.90	118	50.61	20.30	30.41	48.20	30.22	30.31	1.67
1H-3, 10	3.12	120	50.61	20.40	29.97	48.30	29.72	29.81	1.69
1H-3, 20	3.22	121	50.61	20.40	29.14	48.30	28.89	28.98	1.74
1H-3, 30	3.32	122	50.61	20.40	29.80	48.30	29.55	29.64	1.70
1H-3, 40	3.42	123	50.61	20.40	30.01	48.30	29.76	29.85	1.69
1H-3, 50	3.52	124	50.61	20.40	29.27	48.30	29.02	29.11	1.73
1H-3, 60	3.62	125	50.61	20.40	28.88	48.30	28.64	28.73	1.76
1H-3, 80	3.82	126	50.60	20.40	30.20	48.30	29.94	30.04	1.68
1H-3, 90	3.92	128	50.60	20.10	30.23	48.00	30.17	30.26	1.67
1H-3, 100	4.02	129	50.60	20.10	30.12	48.00	30.06	30.15	1.67
1H-3, 110	4.12	130	50.60	20.10	29.88	48.00	29.82	29.91	1.69
1H-3, 120	4.22	131	50.60	20.10	29.64	48.00	29.58	29.67	1.70
1H-3, 130	4.32	132	50.60	20.10	29.69	48.00	29.63	29.72	1.70
1H-3, 140	4.42	133	50.60	20.10	29.94	48.00	29.88	29.98	1.68
1H-3, 10	3.12	135	50.59	20.40	29.81	48.30	29.56	29.66	1.70
1H-4, 20	4.70	136	50.59	20.40	28.68	48.30	28.44	28.53	1.77
1H-4, 30	4.80	137	50.59	20.40	26.81	48.30	26.58	26.67	1.89
1H-4, 40	4.90	138	50.59	20.40	29.20	48.30	28.95	29.05	1.74
1H-4, 50	5.00	139	50.59	20.40	30.03	48.30	29.78	29.88	1.69
1H-4, 60	5.10	140	50.59	20.40	29.58	48.30	29.33	29.43	1.71
1H-4, 70	5.20	141	50.59	20.40	29.05	48.30	28.80	28.91	1.75
1H-4, 80	5.30	143	50.58	20.10	28.97	48.00	28.91	29.01	1.74
1H-4, 90	5.40	144	50.58	20.10	28.97	48.00	28.91	29.01	1.74
1H-4, 100	5.50	145	50.58	20.10	29.12	48.00	29.06	29.16	1.73
1H-4, 110	5.60	146	50.58	20.10	28.03	48.00	27.97	28.07	1.80
1H-4, 120	5.70	147	50.58	20.10	28.08	48.00	28.02	28.12	1.79
1H-4, 130	5.80	148	50.58	20.10	28.67	48.00	28.61	28.71	1.76
1H-4, 138	5.88	149	50.58	20.10	28.39	48.00	28.33	28.43	1.77
2H-1, 60	6.60	3	50.57	19.60	20.50	47.49	20.68	20.68	2.45
2H-1, 70	6.70	4	50.57	19.60	29.39	47.49	29.64	29.64	1.71
2H-1, 80	6.80	5	50.57	19.60	28.76	47.49	29.01	29.01	1.75
2H-1, 95	6.95	6	50.57	19.60	29.41	47.49	29.66	29.67	1.71
2H-1, 105	7.05	8	50.57	19.60	29.42	47.49	29.67	29.68	1.71
2H-1, 115	7.15	9	50.57	19.60	27.51	47.49	27.75	27.75	1.82
2H-1, 125	7.25	10	50.57	19.60	27.83	47.49	28.07	28.08	1.80
2H-1, 135	7.35	11	50.56	19.60	28.95	47.49	29.20	29.21	1.73
2H-1, 145	7.45	12	50.56	19.60	28.30	47.49	28.54	28.55	1.77
2H-2, 10	7.60	14	50.56	19.60	29.84	47.49	30.10	30.11	1.68
2H-2, 20	7.70	15	50.56	19.60	28.85	47.49	29.10	29.11	1.74
2H-2, 30	7.80	16	50.56	19.60	29.85	47.49	30.11	30.12	1.68
2H-2, 40	7.90	17	50.56	19.60	29.98	47.49	30.24	30.25	1.67
2H-2, 50	8.00	18	50.55	19.60	30.79	47.49	31.05	31.07	1.63
2H-2, 60	8.10	19	50.55	19.60	28.10	47.49	28.34	28.35	1.79
2H-2, 70	8.20	20	50.55	19.60	27.03	47.49	27.26	27.28	1.86
2H-2, 80	8.30	22	50.55	19.60	28.77	47.49	29.02	29.03	1.74
2H-2, 90	8.40	23	50.55	19.60	28.74	47.49	28.99	29.00	1.75
2H-2, 100	8.50	24	50.55	19.50	29.21	47.39	29.52	29.54	1.71
2H-2, 110	8.60	25	50.55	19.50	29.12	47.39	29.43	29.45	1.72
2H-2, 120	8.70	26	50.54	19.50	28.25	47.39	28.55	28.57	1.77

Table T2 (continued). (Continued on next page.)

Core, section, interval (cm)	Depth (mbsf)	Measurement number	Temperature-corrected seawater conductivity (mS/cm)	Sediment temperature (°C)	Sediment electrical conductivity (mS/cm)	Correction factor at 20°C (mS/cm)	Sediment electrical conductivity at 20°C (mS/cm)	Drift-corrected sediment electrical conductivity at 20°C (mS/cm)	Formation factor
2H-2, 130	8.80	27	50.54	19.50	28.75	47.39	29.06	29.08	1.74
2H-2, 140	8.90	28	50.54	19.50	27.64	47.39	27.94	27.96	1.81
2H-3, 10	9.12	30	50.54	19.40	28.16	47.28	28.52	28.54	1.77
2H-3, 20	9.22	31	50.54	19.40	27.40	47.28	27.75	27.77	1.82
2H-3, 30	9.32	32	50.54	19.40	26.51	47.28	26.85	26.87	1.88
2H-3, 40	9.42	33	50.54	19.40	26.75	47.28	27.10	27.12	1.87
2H-3, 50	9.52	34	50.53	19.40	27.08	47.28	27.43	27.45	1.84
2H-3, 60	9.62	35	50.53	19.40	27.54	47.28	27.90	27.92	1.81
2H-3, 70	9.72	36	50.53	19.40	27.43	47.28	27.78	27.81	1.82
2H-3, 80	9.82	38	50.53	19.50	27.45	47.39	27.74	27.77	1.82
2H-3, 94	9.96	39	50.53	19.50	26.48	47.39	26.76	26.79	1.89
2H-3, 106	10.08	40	50.53	19.50	26.24	47.39	26.52	26.55	1.91
2H-3, 115	10.17	41	50.52	19.50	26.64	47.39	26.93	26.95	1.88
2H-3, 125	10.27	42	50.52	19.50	25.64	47.39	25.92	25.94	1.95
2H-3, 135	10.37	43	50.52	19.50	26.17	47.39	26.45	26.48	1.91
2H-3, 145	10.47	44	50.52	19.50	26.27	47.39	26.55	26.58	1.90
2H-4, 10	10.62	46	50.52	19.40	26.74	47.28	27.08	27.12	1.87
2H-4, 20	10.72	47	50.51	19.40	26.17	47.28	26.51	26.54	1.91
2H-4, 30	10.82	48	50.51	19.40	26.23	47.28	26.57	26.60	1.90
2H-4, 40	10.92	49	50.51	19.40	25.76	47.28	26.09	26.12	1.94
2H-4, 50	11.02	50	50.51	19.40	26.05	47.28	26.39	26.42	1.91
2H-4, 60	11.12	51	50.51	19.40	25.31	47.28	25.64	25.67	1.97
2H-4, 70	11.22	52	50.51	19.40	25.21	47.28	25.54	25.57	1.98
2H-4, 80	11.32	54	50.51	19.40	24.60	47.28	24.92	24.95	2.03
2H-4, 90	11.42	55	50.50	19.40	24.47	47.28	24.79	24.82	2.04
2H-4, 100	11.52	56	50.50	19.40	23.15	47.28	23.45	23.48	2.15
2H-4, 110	11.62	57	50.50	19.40	21.00	47.28	21.27	21.30	2.37
2H-4, 120	11.72	58	50.50	19.40	20.89	47.28	21.16	21.19	2.39
2H-4, 130	11.82	59	50.50	19.40	21.67	47.28	21.95	21.98	2.30
2H-4, 140	11.92	60	50.50	19.40	21.29	47.28	21.56	21.60	2.34
2H-5, 10	12.12	62	50.50	19.20	22.70	47.08	23.09	23.13	2.19
2H-5, 22	12.24	63	50.49	19.20	22.76	47.08	23.15	23.19	2.18
2H-5, 30	12.32	64	50.49	19.20	22.91	47.08	23.31	23.34	2.17
2H-5, 41	12.43	65	50.49	19.20	21.71	47.08	22.08	22.12	2.29
2H-5, 50	12.52	66	50.49	19.20	21.75	47.08	22.13	22.16	2.28
2H-5, 60	12.62	68	50.49	19.20	21.16	47.08	21.53	21.56	2.34
2H-5, 70	12.72	69	50.49	19.20	21.57	47.08	21.94	21.98	2.30
2H-5, 80	12.82	70	50.49	19.20	20.80	47.08	21.16	21.20	2.39
2H-5, 95	12.97	71	50.48	19.20	20.73	47.08	21.09	21.13	2.39
2H-5, 105	13.07	72	50.48	19.20	20.68	47.08	21.04	21.07	2.40
2H-5, 115	13.17	73	50.48	19.20	20.61	47.08	20.97	21.00	2.41
2H-5, 125	13.27	75	50.48	19.20	20.42	47.08	20.77	20.81	2.43
2H-5, 135	13.37	76	50.48	19.20	20.61	47.08	20.97	21.01	2.41
2H-5, 145	13.47	77	50.48	19.20	20.52	47.08	20.87	20.91	2.42
2H-6, 10	13.62	79	50.48	19.10	20.68	46.98	21.08	21.12	2.39
2H-6, 20	13.72	80	50.47	19.10	20.77	46.98	21.17	21.22	2.38
2H-6, 30	13.82	81	50.47	19.10	20.42	46.98	20.82	20.86	2.42
2H-6, 40	13.92	82	50.47	19.10	20.54	46.98	20.94	20.98	2.41
2H-6, 50	14.02	83	50.47	19.10	20.74	46.98	21.14	21.19	2.39
2H-6, 60	14.12	84	50.47	19.10	20.53	46.98	20.93	20.97	2.41
2H-6, 70	14.22	85	50.47	19.10	20.61	46.98	21.01	21.06	2.40
2H-6, 84	14.36	87	50.47	19.10	20.74	46.98	21.14	21.19	2.38
2H-6, 95	14.47	88	50.46	19.10	20.24	46.98	20.63	20.68	2.44
2H-6, 105	14.57	89	50.46	19.10	20.79	46.98	21.19	21.24	2.38
2H-6, 115	14.67	90	50.46	19.10	20.54	46.98	20.94	20.99	2.41
2H-6, 125	14.77	91	50.46	19.10	20.41	46.98	20.81	20.85	2.42
2H-6, 135	14.87	92	50.46	19.10	19.95	46.98	20.34	20.38	2.48
2H-6, 145	14.97	93	50.46	19.10	20.35	46.98	20.75	20.79	2.43
2H-7, 10	15.12	95	50.46	19.10	19.54	46.98	19.92	19.97	2.53
2H-7, 22	15.24	96	50.45	19.10	20.32	46.98	20.72	20.76	2.43
2H-7, 30	15.32	97	50.45	19.00	21.89	46.88	22.36	22.42	2.25
329-U1366F-									
3H-1, 5	14.05	153	50.45	19.30	31.15	47.18	31.62	31.74	1.59
3H-1, 25	14.25	154	50.45	18.90	29.47	46.78	30.17	30.29	1.67
3H-1, 45	14.45	155	50.45	19.00	29.21	46.88	29.84	29.96	1.68
3H-1, 92	14.92	156	50.44	19.10	26.03	46.98	26.54	26.64	1.89

Table T2 (continued).

Core, section, interval (cm)	Depth (mbsf)	Measurement number	Temperature-corrected seawater conductivity (mS/cm)	Sediment temperature (°C)	Sediment electrical conductivity (mS/cm)	Correction factor at 20°C (mS/cm)	Sediment electrical conductivity at 20°C (mS/cm)	Drift-corrected sediment electrical conductivity at 20°C (mS/cm)	Formation factor
3H-1, 110	15.10	157	50.44	19.20	25.26	47.08	25.70	25.80	1.96
3H-1, 117	15.17	158	50.44	19.10	24.19	46.98	24.66	24.76	2.04
3H-1, 124	15.24	159	50.44	19.20	21.08	47.08	21.44	21.53	2.34
3H-1, 145	15.45	160	50.44	19.50	26.35	47.39	26.63	26.74	1.89
3H-2, 22	15.73	162	50.44	19.70	25.74	47.59	25.91	26.01	1.94
3H-2, 45	15.96	163	50.44	19.30	24.32	47.18	24.69	24.79	2.03
3H-2, 53	16.04	164	50.43	19.30	23.76	47.18	24.12	24.22	2.08
3H-2, 63	16.14	165	50.43	19.30	21.10	47.18	21.42	21.51	2.35
3H-2, 73	16.24	166	50.43	19.30	26.85	47.18	27.25	27.37	1.84
3H-2, 97	16.48	167	50.43	19.80	22.54	47.69	22.64	22.73	2.22
3H-2, 143	16.94	168	50.43	19.90	25.70	47.79	25.75	25.86	1.95
3H-3, 62	17.63	171	50.43	19.90	25.24	47.79	25.29	25.40	1.99
3H-3, 70	17.71	172	50.42	19.90	24.75	47.79	24.80	24.91	2.02
3H-3, 92	17.93	173	50.42	19.90	26.23	47.79	26.29	26.40	1.91
3H-3, 111	18.12	174	50.42	19.90	29.13	47.79	29.19	29.32	1.72
3H-3, 116	18.17	175	50.42	19.90	33.26	47.79	33.33	33.48	1.51
3H-3, 121	18.22	176	50.42	19.90	30.57	47.79	30.64	30.77	1.64
3H-3, 127	18.28	177	50.42	19.90	32.65	47.79	32.72	32.86	1.53
3H-3, 142	18.43	178	50.42	20.10	33.25	48.00	33.18	33.33	1.51
3H-4, 42	18.92	181	50.41	20.30	30.54	48.20	30.35	30.48	1.65
3H-4, 91	19.41	182	50.41	20.00	33.94	47.89	33.94	34.09	1.48
3H-4, 112	19.62	183	50.41	20.00	33.10	47.89	33.10	33.25	1.52
3H-4, 122	19.72	184	50.41	20.00	34.30	47.89	34.30	34.46	1.46
3H-5, 1	20.01	186	50.41	20.20	33.04	48.10	32.90	33.05	1.53
3H-5, 11	20.11	187	50.41	20.20	31.96	48.10	31.82	31.97	1.58
3H-5, 21	20.21	188	50.40	20.20	32.47	48.10	32.33	32.48	1.55
3H-5, 56	20.56	189	50.40	20.20	32.52	48.10	32.38	32.53	1.55
3H-5, 92	20.92	190	50.40	20.20	34.83	48.10	34.68	34.85	1.45
3H-5, 141	21.41	191	50.40	20.20	33.59	48.10	33.45	33.61	1.50
3H-6, 3	21.54	193	50.40	20.00	36.31	47.89	36.31	36.48	1.38
3H-6, 13	21.64	194	50.40	20.10	35.92	48.00	35.84	36.02	1.40
3H-6, 22	21.73	195	50.40	20.20	36.36	48.10	36.21	36.38	1.39
3H-6, 42	21.93	196	50.39	20.20	37.15	48.10	36.99	37.17	1.36
3H-6, 62	22.13	197	50.39	20.10	40.74	48.00	40.65	40.85	1.23
3H-6, 72	22.23	198	50.39	20.20	39.26	48.10	39.09	39.29	1.28
3H-7, 2	23.02	200	50.39	20.10	43.48	48.00	43.39	43.60	1.16
3H-7, 12	23.12	201	50.39	20.40	38.62	48.30	38.29	38.49	1.31
3H-7, 42	23.42	202	50.39	20.10	42.78	48.00	42.69	42.90	1.17
4H-1, 2	23.52	203	50.39	20.50	41.47	48.40	41.03	41.24	1.22
4H-1, 13	23.63	204	50.38	20.50	38.73	48.40	38.32	38.52	1.31
4H-1, 24	23.74	205	50.38	20.50	38.97	48.40	38.56	38.76	1.30
4H-1, 52	24.02	206	50.38	20.30	42.47	48.20	42.20	42.42	1.19
4H-1, 74	24.24	207	50.38	20.40	43.62	48.30	43.25	43.47	1.16
4H-1, 102	24.52	209	50.38	20.20	40.41	48.10	40.24	40.45	1.25
4H-1, 112	24.62	210	50.38	20.20	41.05	48.10	40.88	41.09	1.23
4H-1, 121	24.71	211	50.38	20.30	37.32	48.20	37.08	37.28	1.35
4H-1, 143	24.93	212	50.37	20.50	36.32	48.40	35.94	36.13	1.39
4H-2, 2	25.02	213	50.37	20.70	37.11	48.61	36.56	36.76	1.37
4H-2, 41	25.41	214	50.37	20.70	36.48	48.61	35.94	36.13	1.39
4H-2, 71	25.71	215	50.37	20.70	37.50	48.61	36.95	37.15	1.36
4H-2, 11	25.11	217	50.37	20.50	34.07	48.40	33.71	33.89	1.49
4H-3, 2	26.52	218	50.37	20.50	36.94	48.40	36.55	36.75	1.37
4H-3, 2	26.52	219	50.37	20.70	35.28	48.61	34.76	34.95	1.44
4H-3, 41	26.91	220	50.36	20.70	35.43	48.61	34.91	35.10	1.43
4H-3, 96	27.46	221	50.36	20.80	33.96	48.71	33.39	33.57	1.50
4H-3, 143	27.93	222	50.36	20.90	31.95	48.81	31.35	31.52	1.60
4H-5, 52	29.43	226	50.36	20.70	28.59	48.61	28.17	28.33	1.78

Table T3. U, Th, and K concentrations in manganese nodules, Site U1366.

Core section	Acquisition time (s)	Depth (mbsf)	Th/U	U (ppm)	Th (ppm)	K (wt%)	Total mass (g)	Comments
329-U1366C-								
1H-1	1800	0.50	7.4	1.6	12.0	0.2	135.10	Outer rind remained in core
1H-3	1800	3.67	7.4	2.0	14.9	0.3	226.20	
1H-CC	1800	4.50	7.4	2.3	16.6	0.3	178.21	Two nodules together
2H-3	7200	10.02	5.9	0.9	5.5	0.2	38.20	

Table T4. Electrical conductivity measurements of surface seawater, Site U1366.

Measurement number	Electrical conductivity (mS/cm)	Temperature (°C)	Correction factor at 20°C (mS/cm)	Seawater electrical conductivity at 20°C (mS/cm)
1	52.17	20.8	48.71	51.30
2	51.97	20.7	48.61	51.21
3	51.51	20.7	48.61	50.75
4	51.49	20.7	48.61	50.73
5	51.40	20.7	48.61	50.64
6	51.25	20.7	48.61	50.50
7	51.19	20.5	48.40	50.65
8	51.10	20.4	48.30	50.67
9	50.93	20.4	48.30	50.50
10	50.89	20.3	48.20	50.57
11	50.81	20.4	48.30	50.38
12	50.44	20.3	48.20	50.12
13	50.79	20.4	48.30	50.36
14	50.80	20.4	48.30	50.37
15	50.82	20.4	48.30	50.39
16	50.78	20.4	48.30	50.35
17	51.21	20.7	48.61	50.46
18	51.01	21.2	49.12	49.74
19	51.62	21.1	49.02	50.44
20	51.04	20.7	48.61	50.29
21	51.40	21.1	49.02	50.22
22	51.49	21.0	48.91	50.41
23	50.94	20.7	48.61	50.19
24	51.38	20.7	48.61	50.62
25	50.93	20.6	48.51	50.29
26	50.91	20.5	48.40	50.37
27	50.79	20.3	48.20	50.47
28	50.77	20.3	48.20	50.45
29	50.97	20.3	48.20	50.65
30	50.72	20.2	48.10	50.51
31	50.76	20.2	48.10	50.54
32	50.87	20.2	48.10	50.65
33	50.71	20.1	48.00	50.60
34	50.74	20.3	48.20	50.42
35	50.74	20.2	48.10	50.52
36	50.73	20.2	48.10	50.52
37	50.68	20.3	48.20	50.36
38	50.74	20.2	48.10	50.52
39	50.70	20.2	48.10	50.49

Table T5. Dissolved oxygen concentrations determined using optodes, Holes U1366C and U1366F.

Core, section, interval (cm)	Depth (mbsf)	O ₂ (μM)	Core, section, interval (cm)	Depth (mbsf)	O ₂ (μM)
329-U1366C-			1H-2, 120	2.70	167.8
1H-1, 10	0.10	182.7	1H-2, 140	2.90	166.7
1H-1, 25	0.25	180.2	1H-3, 90	3.90	165.6
1H-1, 50	0.50	178.1	1H-3, 110	4.10	165.3
1H-1, 80	0.80	176.1	1H-3, 130	4.30	164.2
1H-1, 110	1.10	174.4	1H-4, 110	5.60	165.1
1H-1, 140	1.40	172.6	1H-4, 125	5.75	161.6
1H-2, 25	1.75	170.4	1H-4, 140	5.90	162.7
1H-2, 75	2.25	168.6	2H-1, 70	6.20	157.3
1H-2, 125	2.75	167.4	2H-1, 10	6.50	155.8
1H-3, 25	3.25	166.3	2H-1, 130	6.80	156.3
1H-3, 75	3.75	164.6	2H-2, 280	7.28	155.4
1H-3, 125	4.25	163.4	2H-2, 80	7.80	155.0
1H-4, 25	4.75	162.2	2H-2, 130	8.30	152.8
1H-4, 75	5.25	162.0	2H-4, 90	10.90	148.4
1H-4, 125	5.75	161.0	2H-4, 120	11.20	147.7
2H-1, 25	6.25	165.1	2H-5, 60	12.10	144.6
2H-1, 35	6.35	156.3	2H-5, 110	12.60	145.3
2H-1, 75	6.75	153.3	2H-5, 140	12.90	143.4
2H-1, 125	7.25	152.6	2H-6, 80	13.80	141.8
2H-2, 25	7.75	151.4	3H-1, 110	15.10	150.6
2H-2, 75	8.25	151.6	3H-1, 120	15.20	143.3
2H-2, 125	8.75	150.7	3H-2, 60	16.10	139.9
2H-3, 25	9.25	149.1	3H-2, 70	16.20	140.1
2H-3, 75	9.75	148.8	3H-3, 70	17.70	135.7
2H-3, 125	10.25	147.6	3H-3, 110	18.10	136.0
2H-4, 25	10.75	146.8	3H-3, 120	18.20	132.3
2H-4, 75	11.25	145.6	3H-4, 120	19.70	128.6
2H-4, 125	11.75	145.5	3H-5, 150	20.15	127.3
2H-5, 25	12.25	144.9	3H-6, 150	21.65	126.9
2H-5, 75	12.75	143.9	3H-6, 70	22.20	129.5
2H-5, 125	13.25	142.6	3H-6, 115	22.65	126.6
2H-6, 25	13.75	142.4	3H-7, 10	23.10	127.2
2H-6, 75	14.25	141.6	4H-1, 30	23.80	131.4
2H-6, 125	14.75	141.0	4H-1, 80	24.30	134.2
3H-1, 75	16.25	145.3	4H-1, 130	24.80	120.2
3H-2, 125	16.75	146.5	4H-2, 30	25.30	119.3
3H-2, 25	17.25	136.4	4H-2, 80	25.80	118.8
3H-2, 75	17.75	138.3	4H-2, 130	26.30	118.5
3H-2, 125	18.25	134.6	4H-3, 30	26.80	117.6
3H-3, 25	18.75	132.5	4H-3, 80	27.30	117.4
3H-3, 75	19.25	132.6	4H-3, 130	27.80	114.5
3H-3, 125	19.75	132.1	4H-4, 10	28.10	115.2
3H-4, 25	20.25	133.1	4H-4, 20	28.20	114.6
3H-4, 75	20.75	133.4	4H-4, 30	28.30	114.1
3H-4, 125	21.25	133.2	4H-4, 40	28.40	113.8
3H-5, 25	21.75	132.5	4H-4, 50	28.50	113.7
3H-5, 75	22.25	133.3	4H-4, 70	28.70	113.1
3H-5, 125	22.75	131.6	4H-4, 80	28.80	113.0
3H-6, 25	23.25	131.5	4H-5, 10	29.01	113.2
3H-6, 50	23.50	133.6	4H-5, 20	29.11	112.6
3H-6, 75	23.75	132.4	4H-5, 40	29.31	111.8
3H-6, 10	24.00	131.6	4H-5, 50	29.41	110.7
3H-6, 125	24.25	133.6	4H-5, 81	29.72	110.4
3H-7, 25	24.75	132.9	4H-5, 84	29.75	94.4
3H-7, 50	25.00	133.8	4H-5, 86	29.77	59.4
329-U1366F-			4H-5, 86	29.77	57.6
1H-1, 10	0.10	186.1	4H-5, 88	29.79	110.1
1H-1, 20	0.20	182.2	4H-5, 91	29.82	112.0
1H-1, 30	0.30	180.9	4H-5, 93	29.84	111.5
1H-1, 40	0.40	183.1	4H-5, 95	29.86	83.8

Table T6. Dissolved oxygen concentrations determined using electrodes, Holes U1366B–U1366D and U1366F.

Core, section, interval (cm)	Depth (mbsf)	O ₂ (μM)	Core, section, interval (cm)	Depth (mbsf)	O ₂ (μM)	Core, section, interval (cm)	Depth (mbsf)	O ₂ (μM)
329-U1366B-			2H-1, 60	6.60	145.7	3H-6, 40	24.90	104.0
2H-1, 20	7.90	140.8	2H-1, 80	6.80	135.7	3H-6, 60	25.10	109.3
2H-1, 40	8.10	156.0	2H-1, 100	7.00	138.4	3H-6, 80	25.30	103.5
2H-1, 60	8.30	163.4	2H-1, 120	7.20	139.1	3H-6, 100	25.10	109.3
2H-1, 80	8.50	152.5	2H-2, 20	7.70	138.5	3H-6, 120	25.30	103.5
2H-1, 100	8.70	149.2	2H-2, 40	7.90	136.7	329-U1366D-		
2H-1, 120	8.90	145.9	2H-2, 60	8.10	145.2	1H-1, 15	0.15	148.2
2H-2, 20	9.40	147.2	2H-2, 80	8.30	135.4	1H-2, 15	1.15	139.3
2H-2, 40	9.60	141.6	2H-2, 100	8.50	137.3	1H-2, 115	2.55	143.7
2H-2, 60	9.80	147.9	2H-2, 120	8.70	134.8	1H-3, 15	3.45	134.5
2H-2, 80	10.00	143.7	2H-3, 20	9.20	148.4	1H-3, 65	3.55	137.6
2H-2, 100	10.20	146.5	2H-3, 40	9.40	133.9	1H-3, 115	4.05	134.5
2H-2, 120	10.40	144.5	2H-3, 60	9.60	139.6	1H-4, 15	4.65	134.4
2H-3, 20	10.90	139.9	2H-3, 80	9.80	131.5	1H-4, 70	5.20	195.2
2H-3, 40	11.10	139.6	2H-3, 100	10.00	141.0	1H-4, 115	5.55	138.1
2H-3, 60	11.30	137.0	2H-3, 120	10.20	130.9	1H-5, 15	6.15	132.2
2H-3, 80	11.50	137.7	2H-4, 20	10.70	142.8	1H-5, 45	6.45	132.7
2H-3, 100	11.70	136.0	2H-4, 40	10.90	133.4	1H-6, 15	7.75	130.1
2H-3, 120	11.90	136.6	2H-4, 60	11.10	138.7	1H-6, 65	8.05	133.7
2H-4, 20	12.40	137.0	2H-4, 80	11.30	129.5	1H-6, 45	8.85	126.8
2H-4, 40	12.60	135.4	2H-4, 100	11.50	137.1	1H-7, 15	9.55	122.2
2H-4, 60	12.80	133.3	2H-4, 120	11.70	130.9	2H-7, 65	10.05	122.0
2H-4, 80	13.00	134.4	2H-5, 20	12.20	141.4	2H-7, 115	10.55	129.5
2H-4, 100	13.20	133.3	2H-5, 40	12.40	126.1	2H-2, 15	11.05	130.0
2H-4, 120	13.40	132.1	2H-5, 60	12.60	135.6	2H-2, 65	11.55	124.7
2H-5, 20	13.90	131.2	2H-5, 80	12.80	128.1	2H-3, 15	12.55	122.7
2H-5, 40	14.10	131.3	2H-5, 100	13.00	138.3	2H-3, 65	13.05	120.0
2H-5, 60	14.30	133.5	2H-5, 120	13.20	126.9	2H-3, 115	13.55	119.4
2H-5, 80	14.50	129.9	2H-6, 20	13.70	151.3	2H-4, 115	14.95	123.5
2H-5, 100	14.70	130.2	2H-6, 40	13.90	133.4	2H-5, 150	15.90	122.3
2H-5, 120	14.90	129.4	2H-6, 60	14.10	146.9	2H-5, 140	16.80	120.6
2H-6, 20	15.40	129.1	2H-6, 80	14.30	129.5	329-U1366F-		
2H-6, 60	15.80	131.4	2H-6, 100	14.50	145.2	1H-1, 25	0.25	181.2
2H-6, 80	16.00	128.7	2H-6, 120	14.70	130.9	1H-2, 135	2.85	169.1
2H-6, 100	16.20	130.0	2H-7, 20	15.70	139.9	1H-3, 100	4.00	164.3
2H-6, 120	16.40	127.5	2H-7, 40	15.90	125.6	1H-3, 120	4.20	169.5
329-U1366C-			2H-7, 60	16.10	138.3	1H-3, 140	4.40	171.8
1H-1, 30	0.30	180.0	2H-7, 80	16.30	161.6	1H-4, 115	5.65	175.0
1H-1, 45	0.45	180.0	2H-7, 100	16.50	122.4	1H-4, 130	5.80	175.7
1H-1, 60	0.60	174.7	2H-7, 120	16.70	141.1	2H-1, 85	6.35	167.5
1H-1, 90	0.90	175.3	3H-1, 20	17.20	138.5	2H-1, 110	6.60	173.9
1H-1, 105	1.05	166.8	3H-1, 40	17.40	123.0	2H-1, 135	6.85	173.7
1H-1, 120	1.20	175.7	3H-1, 60	17.60	116.0	2H-2, 15	7.15	167.4
1H-1, 135	1.35	169.8	3H-1, 80	17.80	122.5	2H-2, 30	7.30	167.8
1H-2, 15	1.65	171.5	3H-1, 100	18.00	125.6	2H-2, 90	7.90	160.3
1H-2, 30	1.80	168.2	3H-1, 120	18.20	116.8	2H-2, 110	8.10	163.4
1H-2, 45	1.95	162.1	3H-2, 20	18.70	135.1	2H-2, 130	8.30	166.8
1H-2, 60	2.10	166.4	3H-2, 40	18.90	121.5	2H-4, 12	10.12	161.1
1H-2, 75	2.25	161.4	3H-2, 60	19.10	121.1	2H-4, 24	10.24	163.3
1H-2, 90	2.40	162.7	3H-2, 80	19.30	124.0	2H-4, 95	10.95	166.6
1H-2, 105	2.55	206.5	3H-2, 100	19.50	116.2	2H-4, 120	11.20	164.0
1H-2, 120	2.70	158.6	3H-2, 120	19.70	115.2	2H-4, 135	11.35	161.0
1H-2, 135	2.85	157.8	3H-2, 80	20.80	114.4	2H-5, 55	12.05	166.2
1H-2, 40	3.40	156.8	3H-2, 120	21.20	113.3	2H-5, 115	12.65	154.7
1H-2, 60	3.60	150.8	3H-4, 20	21.70	112.3	2H-5, 130	12.80	156.1
1H-2, 80	3.80	155.1	3H-4, 40	21.90	112.2	2H-6, 55	13.55	163.0
1H-2, 100	4.00	151.6	3H-4, 60	22.10	109.2	2H-6, 70	13.70	162.5
1H-2, 120	4.20	153.8	3H-4, 80	22.30	105.9	3H-1, 115	15.15	165.2
1H-4, 20	4.70	158.4	3H-4, 100	22.50	106.8	3H-2, 64	16.14	164.8
1H-4, 40	4.90	152.1	3H-4, 120	22.70	105.7	3H-3, 73	17.73	163.1
1H-4, 60	5.10	148.3	3H-5, 20	23.20	106.0	3H-3, 114	18.14	165.9
1H-4, 80	5.30	150.1	3H-5, 40	23.40	107.1	3H-4, 123	19.73	168.1
1H-4, 100	5.50	150.0	3H-5, 60	23.60	105.3	3H-4, 68	22.18	155.4
1H-4, 120	5.70	146.5	3H-5, 80	23.80	107.0	3H-4, 120	22.70	158.7
2H-1, 20	6.20	154.6	3H-5, 100	24.00	106.3	3H-7, 15	23.15	148.8
2H-1, 40	6.40	161.9	3H-5, 120	24.20	104.2			
			3H-6, 20	24.70	114.4			

Table T7. Dissolved hydrogen measured by headspace gas method, Site U1366.

Core, section	Depth (mbsf)	H ₂ (nM)	Core, section	Depth (mbsf)	H ₂ (nM)
329-U1366D-			2H-4	10.70	16.2
1H-1	0.50	BD	2H-5	12.50	6.8
1H-1	1.00	BD	2H-6	13.30	BD
1H-1	1.50	BD	3H-1	14.50	35.8
1H-2	2.00	BD	3H-1	15.00	45.3
1H-2	2.50	BD	3H-1	15.50	5.3
1H-2	3.00	BD	3H-2	16.00	45.4
1H-3	3.50	BD	3H-2	16.50	26.6
1H-3	4.00	BD	3H-2	17.00	19.8
1H-3	4.50	BD	3H-3	17.50	BD
1H-4	5.10	BD	3H-3	18.00	13.9
1H-4	5.50	BD	3H-3	18.50	10.1
1H-4	6.00	BD	3H-4	19.00	30.3
1H-5	6.50	BD	3H-4	19.50	16.9
1H-5	7.00	BD	3H-4	20.00	14.8
1H-5	7.50	BD	3H-5	20.50	41.0
1H-6	8.00	BD	3H-5	21.00	20.7
1H-6	8.50	BD	3H-5	21.50	17.8
1H-7	9.00	BD	3H-6	22.00	39.5
2H-1	9.90	BD	3H-6	22.50	18.6
2H-1	10.40	BD	3H-6	23.00	10.8
2H-1	10.90	BD	3H-7	23.40	BD
2H-2	11.40	BD	4H-1	24.00	35.9
2H-2	11.90	BD	4H-1	24.50	50.8
2H-2	12.40	BD	4H-1	25.00	36.6
2H-3	12.90	BD	4H-2	25.50	85.9
2H-3	13.40	BD	4H-2	25.80	71.8
2H-3	13.90	BD	4H-2	26.50	33.2
2H-4	14.40	29.9	4H-3	27.00	68.7
2H-4	14.90	7.2	4H-3	27.50	62.4
2H-4	15.40	6.1	4H-3	28.00	44.3
329-U1366F-			4H-4	28.10	51.7
2H-2	7.70	8.1	4H-4	28.70	59.2
2H-3	9.80	BD	4H-5	29.50	42.8

BD = below detection (<5.2 nM).



Table T8. Interstitial fluid chemistry, Site U1366. (Continued on next page.)

Core, section, interval (cm)	Depth (mbsf)	pH ISE	Alkalinity (mM) TITRAUTO	DIC (mM) TOC	Cl (mM) M-IC	SO ₄ (mM) M-IC	S/Cl (%) Calc. anom.	NO ₃ (μM) UV-VIS IC	P (μM) Spec.	Si (μM) Spec.	Ca (mM) Dx-IC	Mg (mM) Dx-IC	Na (mM) Dx-IC	K (mM) Dx-IC	Ca (mM) ICPAES	Mg (mM) ICPAES	Na (mM) ICPAES	B (μM) ICPAES	Fe (μM) ICPAES	Mn (μM) ICPAES	Sr (μM) ICPAES
329-U1366D-																					
1H-1, 30-40	0.35	7.42	2.664	2.54	553.73	27.91	-2.57	34.87	1.53	266	10.2	51.4	482	12.4	10.1	51.9	480	529	6	5	89
1H-1, 80-90	0.85	7.32	2.559	2.56	554.50	27.93	-2.63	35.22	1.87	295	10.4	51.2	482	12.2	10.0	50.7	471	555	6	6	89
1H-1, 130-140	1.35	7.39	2.578	2.58	555.70	27.94	-2.78	35.40	1.94	311	10.4	50.9	481	12.2	10.3	51.4	481	586	7	5	90
1H-2, 30-40	1.85	7.35	2.563	2.56	556.25	27.94	-2.90	35.74	1.93	248	10.4	51.3	484	12.3	10.2	50.6	474	586	7	5	89
1H-2, 80-90	2.35	7.41	2.621	2.57	555.74	27.92	-2.86	35.43	1.64	304	10.4	51.6	484	12.2	10.1	50.9	477	584	7	9	89
1H-2, 130-140	2.85	7.55	2.793	2.56	557.05	28.01	-2.79	35.91	—	—	10.4	51.7	485	12.3	10.0	50.8	477	570	6	7	89
1H-3, 30-40	3.35	7.49	2.731	2.63	557.96	28.07	-2.73	36.69	1.88	293	10.4	51.5	486	12.6	10.4	51.6	480	578	7	7	89
1H-3, 80-90	3.85	7.32	2.539	2.56	555.84	27.99	-2.66	36.06	1.53	286	10.5	52.0	485	12.3	10.1	51.0	474	591	7	5	90
1H-3, 130-140	4.35	7.36	2.544	2.54	557.15	28.00	-2.83	36.48	1.22	268	10.5	51.9	483	12.1	10.3	51.6	478	560	7	4	90
1H-4, 30-40	4.85	7.31	2.565	2.61	558.76	28.12	-2.69	36.00	1.84	272	—	—	—	—	10.2	51.5	473	529	5	5	88
1H-4, 80-90	5.35	7.43	2.641	2.60	557.20	28.05	-2.67	36.53	1.46	264	10.4	51.9	485	12.4	10.1	51.1	474	599	7	5	90
1H-4, 130-140	5.85	7.35	2.500	2.61	557.53	28.05	-2.75	36.76	1.39	253	10.2	51.3	481	12.5	10.2	51.8	481	615	8	5	90
1H-5, 30-40	6.35	7.33	2.649	2.65	557.44	28.04	-2.75	36.35	1.45	289	10.2	51.7	487	12.7	10.3	51.9	487	571	6	5	88
1H-5, 80-90	6.85	7.37	2.644	2.59	558.69	28.08	-2.84	36.73	1.30	282	10.1	51.5	484	12.5	9.7	50.0	446	567	6	5	89
1H-5, 130-140	7.35	7.39	2.568	2.57	558.29	28.07	-2.80	36.60	1.25	—	10.3	52.1	487	12.6	10.1	51.0	479	632	8	6	90
1H-6, 30-40	7.85	7.40	2.715	2.65	558.40	27.97	-3.17	36.58	1.17	266	10.4	51.6	485	12.7	10.0	50.9	474	571	6	6	89
1H-6, 80-90	8.35	7.41	2.662	2.60	558.56	27.99	-3.14	37.10	—	—	10.5	52.2	487	12.2	10.2	51.2	475	589	6	6	90
1H-7, 10-20	8.85	7.53	2.603	2.64	—	—	-2.74	37.43	1.16	270	10.6	52.7	488	12.3	10.1	50.9	477	594	6	6	89
2H-1, 30-40	9.75	7.37	2.693	2.68	559.87	27.84	-3.86	36.93	0.94	249	10.5	51.2	483	12.1	10.0	50.8	473	608	7	6	90
2H-1, 80-90	10.25	7.40	2.753	2.72	559.34	27.83	-3.82	37.27	0.88	258	10.3	51.2	482	11.9	10.5	51.8	481	579	6	6	89
2H-1, 130-140	10.75	7.37	2.720	2.69	560.19	27.67	-4.52	37.23	1.20	257	10.6	51.0	478	11.6	10.6	51.7	482	643	7	6	91
2H-2, 30-40	11.25	7.36	2.779	2.75	560.15	27.48	-5.15	37.38	1.09	269	10.5	51.1	484	11.8	10.4	51.2	477	618	9	7	90
2H-2, 80-90	11.75	7.53	2.830	2.73	563.70	27.74	-4.87	37.39	0.89	—	10.6	51.4	488	11.9	10.4	50.5	477	668	7	6	91
2H-2, 130-140	12.25	7.35	2.738	2.73	561.09	27.63	-4.79	37.96	0.99	287	10.5	50.6	480	11.6	10.2	50.8	477	617	5	7	89
2H-3, 30-40	12.75	7.35	2.743	2.73	—	—	—	37.64	1.15	249	10.5	50.4	482	11.7	10.4	51.5	484	682	7	5	90
2H-3, 80-90	13.25	7.35	2.803	2.80	563.28	27.11	-6.94	37.75	1.19	281	10.6	50.4	487	11.9	10.5	51.3	488	636	7	7	90
2H-3, 130-140	13.75	7.38	2.779	2.74	560.48	27.39	-5.51	38.14	1.01	282	10.4	51.0	482	11.5	10.5	51.4	488	692	6	5	90
2H-4, 30-40	14.25	7.39	2.806	2.75	560.62	27.10	-6.55	37.84	0.95	263	10.6	51.7	486	12.1	10.1	51.0	482	710	7	8	90
2H-4, 80-90	14.75	7.52	2.749	2.72	562.04	27.62	-5.01	37.81	—	—	10.6	51.6	485	12.3	9.7	48.9	442	615	7	4	89
2H-4, 130-140	15.25	7.40	2.796	2.78	559.67	27.40	-5.34	37.80	0.86	291	10.4	51.1	484	12.2	10.3	51.7	490	690	7	7	89
329-U1366F-																					
1H-1, 120-130*	1.25	7.49	2.607	2.60	557.81	28.08	-2.67	—	—	—	10.4	51.1	482	12.4	10.3	51.4	485	609	6	4	89
1H-3, 60-70	3.65	7.37	2.585	2.58	557.39	28.17	-2.30	35.41	1.33	297	10.2	51.7	482	12.2	10.3	49.9	476	701	7	6	91
1H-3, 70-80*	3.75	7.47	2.648	2.59	557.14	28.04	-2.70	—	—	—	10.2	51.6	484	12.2	—	—	—	—	—	—	—
2H-1, 40-50*	5.95	7.46	2.609	2.62	558.23	28.10	-2.69	—	—	—	10.5	51.4	484	12.5	10.4	52.4	492	585	6	5	88
2H-2, 50-60	7.55	7.43	2.679	2.64	559.90	27.99	-3.34	36.73	1.03	275	10.4	51.3	484	12.2	10.5	51.3	486	623	6	5	89
2H-4, 50-60	10.55	7.40	2.774	2.80	560.67	27.68	-4.54	37.21	0.74	256	10.6	50.9	487	12.0	10.2	50.8	477	686	6	6	89
2H-5, 80-90	12.35	7.51	2.784	2.71	561.22	27.09	-6.68	38.08	0.74	258	10.3	51.0	486	12.3	10.6	51.5	491	660	7	4	90
3H-5, 120-130*	21.25	7.48	2.634	2.62	—	—	—	—	—	—	10.4	52.6	487	12.0	—	—	—	—	—	—	—
2H-6, 0-10	13.05	7.53	2.809	2.71	561.49	27.51	-5.26	37.75	0.72	147	10.3	51.1	488	12.4	10.0	50.7	478	674	7	6	90
2H-6, 10-20*	13.15	7.53	2.809	2.76	560.77	27.71	-4.46	—	—	—	—	—	—	—	10.6	52.7	493	674	6	5	89
3H-1, 30-40	14.35	7.45	2.812	2.76	563.03	27.44	-5.77	31.39	0.89	249	10.6	50.7	490	12.0	9.6	49.5	437	605	6	4	89
3H-1, 80-90	14.85	7.46	2.730	2.68	563.59	27.73	-4.89	27.28	0.92	224	—	51.3	489	12.2	10.6	52.4	493	730	7	8	90
3H-1, 130-140	15.35	7.71	2.867	2.65	562.37	28.25	-2.87	38.00	1.06	217	10.3	51.6	486	12.1	10.3	51.8	489	598	7	8	89
3H-2, 30-40	15.85	7.40	2.662	2.62	562.85	28.35	-2.63	38.21	1.00	226	10.2	51.6	484	11.9	9.7	49.0	459	583	6	5	89
3H-2, 80-90	16.35	7.49	2.741	2.64	563.64	28.35	-2.74	37.68	0.81	245	10.2	52.4	488	12.4	10.4	52.3	486	636	7	8	90
3H-2, 130-140	16.85	7.36	2.696	2.70	564.96	28.14	-3.72	38.03	—	223	10.5	52.2	491	12.4	10.3	51.0	478	636	7	5	90
3H-3, 30-40	17.35	7.47	2.666	2.63	564.72	28.23	-3.37	38.35	0.75	220	10.2	52.2	489	12.0	10.4	52.1	487	612	6	5	89



Table T8 (continued).

Core, section, interval (cm)	Depth (mbsf)	pH ISE	Alkalinity (mM) TITRAUTO	DIC (mM) TOC	Cl (mM) M-IC	SO ₄ (mM) M-IC	S/Cl (%) Calc. anom.	NO ₃ (μM) UV-VIS IC	P (μM) Spec.	Si (μM) Spec.	Ca (mM) Dx-IC	Mg (mM) Dx-IC	Na (mM) Dx-IC	K (mM) Dx-IC	Ca (mM) ICPAES	Mg (mM) ICPAES	Na (mM) ICPAES	B (μM) ICPAES	Fe (μM) ICPAES	Mn (μM) ICPAES	Sr (μM) ICPAES
3H-3, 80–90	17.85	7.44	2.630	2.59	565.21	28.21	-3.51	38.96	0.63	244	10.6	52.8	488	13.3	10.4	51.9	481	633	7	4	90
3H-3, 130–140	18.35	7.41	2.621	2.59	564.95	28.09	-3.88	39.17	0.96	244	10.8	52.3	492	12.0	10.9	52.2	487	567	6	5	89
3H-4, 30–40	18.85	7.43	2.623	2.63	567.34	28.52	-2.83	39.30	1.03	246	10.7	52.6	494	12.1	10.7	52.1	487	558	6	5	89
3H-4, 80–90	19.35	7.39	2.597	2.58	567.42	28.87	-1.63	39.33	0.86	258	10.8	53.3	491	12.2	11.1	54.1	494	528	7	5	90
3H-4, 130–140	19.85	7.68	2.749	2.60	568.92	28.60	-2.80	39.26	1.00	274	10.6	52.8	491	12.1	8.0	40.0	367	545	6	4	89
3H-5, 30–40	20.35	7.49	2.635	2.62	566.66	28.38	-3.19	39.31	0.73	287	10.6	52.8	490	12.0	10.9	52.2	495	566	38	4	90
3H-5, 80–90	20.85	7.43	2.709	2.69	567.85	28.28	-3.72	38.79	0.56	235	10.5	52.4	491	12.1	10.1	51.0	478	591	7	5	90
3H-5, 130–140	21.35	7.38	2.621	2.56	567.36	28.57	—	39.65	0.80	309	10.6	52.4	488	11.8	11.0	52.8	490	532	6	4	89
3H-6, 30–40	21.85	7.88	2.760	2.71	568.86	28.38	-3.56	39.85	0.98	259	10.4	52.3	486	11.8	10.7	52.7	489	661	7	7	91
3H-6, 80–90	22.35	7.55	2.792	2.63	569.29	28.86	-2.01	39.21	0.60	212	10.6	53.3	489	11.9	10.6	53.0	485	610	7	6	91
3H-6, 130–140	22.85	7.41	2.705	2.68	569.10	28.32	-3.80	39.30	0.85	272	10.4	53.0	491	12.0	10.4	52.5	485	611	6	5	90
3H-7, 20–30	23.25	7.51	2.713	2.66	571.57	28.65	-3.10	39.38	0.58	243	10.3	53.3	491	11.9	10.3	52.5	485	594	6	5	90
4H-1, 30–40	23.85	7.54	2.662	2.58	569.63	28.64	-2.78	33.89	0.47	253	10.3	52.7	486	12.0	10.6	53.6	494	602	6	5	91
4H-1, 80–90	24.35	7.55	2.633	2.54	569.51	28.20	-4.27	25.10	0.44	230	10.3	53.2	489	12.0	10.5	52.8	480	580	6	6	90
4H-1, 130–140	24.85	7.49	2.786	2.70	569.22	27.78	-5.65	41.18	0.73	264	11.0	51.0	494	12.4	11.2	51.6	494	599	6	5	90
4H-2, 30–40	25.35	7.44	2.665	2.62	569.93	27.81	-5.66	39.65	0.72	264	10.4	50.7	487	12.0	11.3	52.4	497	661	7	5	91
4H-2, 80–90	25.85	7.46	2.720	2.66	571.25	27.95	-5.39	39.35	0.43	—	10.4	50.4	486	12.3	11.1	51.0	489	636	5	5	89
4H-2, 120–130	26.25	7.41	2.791	2.80	570.18	27.98	—	39.18	0.62	269	—	49.6	485	12.5	11.2	50.1	489	685	7	7	90
4H-2, 130–140*	26.35	7.56	2.681	2.63	—	—	—	—	—	—	10.4	51.4	493	12.1	—	—	—	—	—	—	—
4H-3, 30–40	26.85	7.38	2.593	2.62	569.44	27.95	-5.12	39.77	0.57	—	10.6	51.3	489	12.0	10.3	49.9	476	583	7	5	90
4H-3, 80–90	27.35	7.45	2.664	2.65	569.41	28.01	-4.89	39.41	—	270	10.6	51.1	490	12.0	10.7	50.4	482	595	7	5	90
4H-3, 130–140	27.85	7.48	2.723	2.59	570.73	28.06	-4.93	39.61	0.56	279	10.6	52.6	494	11.8	10.7	52.0	484	586	6	5	90
4H-4, 10–20	28.15	7.54	2.637	2.71	570.36	28.15	-4.58	39.92	0.74	257	9.9	52.2	486	11.7	10.5	52.4	485	647	7	6	91
4H-4, 70–80	28.75	7.41	2.706	2.71	569.83	28.10	—	40.03	0.57	228	9.9	52.8	494	12.6	10.2	51.7	485	649	6	4	90
4H-4, 80–90*	28.85	7.59	2.817	2.66	—	—	—	—	—	—	10.0	53.2	495	12.4	—	—	—	—	—	—	—
4H-5, 40–50	29.36	7.40	2.671	2.51	572.29	28.84	-2.56	39.38	0.54	263	10.4	53.5	496	11.9	10.8	52.7	489	597	6	5	90

* = $\delta^{14}\text{C}$ samples. ISE = ion-selective electrode, TITRAUTO = automated titration, TOC = total organic carbon analyzer, IC = ion chromatography, M-IC = Metrohm IC, Calc. anom. = calculated anomaly, UV-VIS = ultraviolet-visible, Spec. = spectrophotometry, Dx-IC = Dionex IC, ICPAES = inductively coupled plasma-atomic emission spectroscopy. BD = below detection. — = no data.

Table T9. Solid-phase carbon and nitrogen, Site U1366.

Core, section, interval (cm)	Depth (mbsf)	TC (wt%)	TN (wt%)	TOC (wt%)	TIC (wt%)	CaCO ₃ (wt%)
329-U1366D-						
1H-1, 0-1	0.01	0.20	0.044	0.20	0.01	0.12
1H-1, 10-11	0.11	0.17	0.046	0.14	0.01	0.08
1H-1, 20-21	0.21	0.12	0.039	0.09	0.02	0.13
1H-1, 30-40	0.35	0.13	0.046	0.09	0.01	0.11
1H-1, 48-49	0.49	0.15	0.045	0.09	0.01	0.12
1H-1, 80-90	0.85	0.12	0.043	0.08	0.01	0.12
1H-1, 109-110	1.10	0.12	0.038	0.07	0.03	0.23
1H-1, 130-140	1.35	0.12	0.041	0.08	0.02	0.16
1H-2, 30-40	1.85	0.10	0.036	0.06	0.02	0.16
1H-2, 80-90	2.35	0.09	0.036	0.05	0.02	0.14
1H-2, 130-140	2.85	0.08	0.032	0.05	0.02	0.13
1H-3, 130-140	4.35	0.08	0.033	0.05	0.03	0.24
1H-4, 130-140	5.85	0.07	0.023	0.04	0.02	0.19
1H-5, 130-140	7.35	0.06	0.020	0.04	0.05	0.40
1H-7, 10-20	8.85	0.09	0.022	0.04	0.05	0.45
2H-1, 130-140	10.75	0.10	0.015	0.03	0.07	0.61
2H-2, 130-140	12.25	0.10	0.008	0.02	0.07	0.59
2H-3, 130-140	13.75	0.18	0.006	0.02	0.14	1.14
2H-4, 130-140	15.25	0.17	0.006	0.02	0.13	1.12
329-U1366F-						
1H-1, 120-130	1.25	0.12	0.044	0.09	0.01	0.09
1H-3, 70-80	3.75	0.09	0.029	0.06	0.03	0.29
2H-1, 40-50	5.95	0.06	0.018	0.05	0.02	0.20
2H-6, 10-20	13.15	0.15	0.009	0.03	0.13	1.06
3H-4, 30-40	18.85	0.05	BD	0.01	0.05	0.43
3H-4, 130-140	19.85	0.04	BD	0.02	0.04	0.36
3H-5, 130-140	21.35	0.05	BD	0.02	0.08	0.68
3H-6, 130-140	22.85	0.06	BD	0.01	0.04	0.35
4H-1, 130-140	24.85	0.09	BD	0.02	0.07	0.58
4H-2, 120-130	26.25	0.08	BD	0.02	0.07	0.58
4H-3, 130-140	27.85	0.05	BD	0.02	0.05	0.45
4H-5, 40-50	29.36	0.02	BD	0.01	0.02	0.15

TC = total carbon, TN = total nitrogen, TOC = total organic carbon, TIC = total inorganic carbon. Samples from Cores 1H and 2H in both holes are catwalk samples. BD = below detection (TN < 0.001%).

Table T10. Epifluorescence microscopy cell counts for sediment, Site U1366.

Core, section, interval (cm)	Depth (mbsf)	Cell count (\log_{10} cells/cm ³)			
		Extracted		Nonextracted	
		Count 1	Count 2	Count 1	Count 2
329-U1366D-					
1H-1, 0-10	0.1				
1H-1, 40-50	0.4	3.5	3.1	BD	BD
1H-1, 90-100	0.9				
1H-1, 140-150	1.4				
1H-2, 40-50	1.9	2.5	2.9	BD	BD
1H-2, 90-100	2.4				
1H-2, 140-150	2.9				
1H-3, 40-50	3.4	2.3		BD	BD
1H-3, 90-100	3.9				
1H-3, 140-150	4.4				
1H-4, 50-60	5.0	3.3	2.7		
1H-4, 90-100	5.4				
1H-4, 140-150	5.9				
1H-5, 40-50	6.4	3.4	BD		
1H-5, 90-100	6.9				
1H-5, 140-150	7.4				
1H-6, 40-50	7.9	3.0	2.9		
1H-6, 90-100	8.4				
1H-7, 20-30	8.9				
2H-1, 40-50	9.8	3.2			
2H-1, 90-100	10.3				
2H-1, 140-150	10.8				
2H-2, 40-50	11.3	3.4	2.7		
2H-2, 90-100	11.8				
2H-2, 140-150	12.3				
2H-3, 40-50	12.8	3.4			
2H-3, 90-100	13.3				
2H-3, 140-150	13.8				
2H-4, 40-50	14.3	2.2			
2H-4, 90-100	14.8				
2H-4, 140-150	15.3				
329-U1366F-					
2H-2, 60-70	7.6				
2H-4, 60-70	10.6				
2H-5, 30-40	11.8				
2H-5, 90-100	12.4				
2H-6, 20-30	13.2				
3H-1, 40-50	14.4	BD	BD		
3H-1, 90-100	14.9				
3H-1, 140-150	15.4				
3H-2, 40-50	15.9	3.1			
3H-2, 90-100	16.4				
3H-2, 140-150	16.9				
3H-3, 40-50	17.4	BD	BD		
3H-3, 90-100	17.9				
3H-3, 140-150	18.4				
3H-4, 40-50	18.9	3.2			
3H-4, 90-100	19.4				
3H-4, 90-100	19.4				
3H-4, 140-150	19.9				
3H-5, 40-50	20.4	3.9	3.8		
3H-5, 90-100	20.9				
3H-5, 140-150	21.4				
3H-6, 40-50	21.9	3.8			
3H-6, 90-100	22.4				
3H-6, 140-150	22.9				
3H-7, 30-41	23.3				
4H-1, 40-50	23.9	2.8	BD		
4H-1, 90-100	24.4				
4H-1, 140-150	24.9				
4H-2, 40-50	25.4	2.4	2.2		
4H-2, 70-80	25.7				
4H-2, 140-150	26.4				
4H-3, 40-50	26.9	2.6	BD		
4H-3, 90-100	27.4				
4H-3, 140-150	27.9				
4H-4, 0-10	28.0	BD	BD		
4H-4, 60-70	28.6				
4H-5, 50-59	29.4				
4H-5, 87-97	29.8	BD	BD		
4H-CC, 0-7	30.1				

BD = below detection. Blank cells = no count (will be counted postexpedition).

Table T11. Abundance of virus-like particles in sediment samples by epifluorescence microscopy, Site U1366.

Core, section	Depth (mbsf)	VLP/cm ³	STD
329-U1366E- (mudline)	0	8.07E+05	7.13E+04
329-U1366F-			
1H-1	0.40	2.17E+05	1.65E+04
1H-1	0.40	1.06E+05	9.44E+03
1H-1	1.40		
1H-2	1.50	1.24E+05	1.25E+04
1H-2	1.50	5.88E+04	7.03E+03
1H-2	2.50		
1H-3	3.50		
1H-4	4.80		
2H-1	6.00		
2H-2	7.60		
2H-3	9.55	1.07E+04	4.72E+03
2H-3	9.55	3.53E+04	1.78E+03
2H-3	9.70		
2H-5	11.80		
2H-6	13.30		
3H-1	14.20		
3H-2	15.70		
3H-3	17.50		
3H-4	19.50		
3H-6	21.70		
4H-1	24.00		
4H-2	25.40		
4H-4	28.00		
4H-5	29.78		

VLP = virus-like particle, STD = standard deviation. Blank cells = no counts (samples will be analyzed postexpedition).

Table T12. List of samples and culture media used for onboard cultivation experiments, Site U1366.

Core, section	Media used for cultivation
329-U1365F-	
1H-1	SPG-JL, MA, MR2A, SLURRY
1H-2	Mmm1, Mmm2, SPG-ASW, SPG-JL, MA, MR2A, SLURRY
1H-3	SPG-JL, MA, MR2A, SLURRY
1H-4	MA, MR2A, SLURRY
2H-3	Mmm1, Mmm2, SPG-ASW, SPG-JL, MA, MR2A, SLURRY
3H-4	SPG-ASW, SPG-JL, MA, MR2A
4H-2	SPG-JL
4H-3	Mmm1, Mmm2, SPG-ASW
4H-4	MA, MR2A
4H-5	SPG-JL, MA, MR2A, SLURRY

SLURRY = slurry in artificial seawater. For more detailed information on the media, see “Microbiology” in the “Methods” chapter (Expedition 329 Scientists, 2011a).